

# Steady-State Micro-Bunching based on Transverse-Longitudinal Coupling\*

X. J. Deng,<sup>1,†</sup> A. W. Chao,<sup>1</sup> W. H. Huang,<sup>2</sup> Z. Z. Li,<sup>2</sup> Z. L. Pan,<sup>2</sup> and C. X. Tang<sup>2</sup>

<sup>1</sup>*Institute for Advanced Study, Tsinghua University, Beijing 100084, China*

<sup>2</sup>*Department of Engineering Physics, Tsinghua University, Beijing 100084, China*

In this paper, three specific scenarios of a novel accelerator light source mechanism called steady-state micro-bunching (SSMB) have been studied, i.e., longitudinal weak focusing, longitudinal strong focusing and generalized longitudinal strong focusing (GLSF). At present, GLSF is the most promising among them in realizing high-power short-wavelength coherent radiation with a mild requirement on the modulation laser power. Its essence is to exploit the ultrasmall natural vertical emittance of an electron beam in a planar storage ring for efficient microbunching formation, like a partial transverse-longitudinal emittance exchange at the optical laser wavelength range. Based on in-depth investigation of related beam physics, a solution of a GLSF SSMB storage ring which can deliver 1 kW-average-power EUV light is presented. The work in this paper, such as the generalized Courant-Snyder formalism, the analysis of theoretical minimum emittances, transverse-longitudinal coupling dynamics, and the derivation of the bunching factor and modulation strengths for laser-induced microbunching schemes, is expected to be useful not only for the development of SSMB but also for future accelerator light sources in general that demand increasingly precise electron beam phase space manipulations.

**Keywords:** Steady-state micro-bunching, extreme ultraviolet, ARPES, generalized Courant-Snyder formalism, theoretical minimum emittances, longitudinal weak focusing, longitudinal strong focusing, generalized longitudinal strong focusing, transverse-longitudinal coupling, damping wiggler

## I. INTRODUCTION

Accelerator as light source is arguably the most active driving force for accelerator development at the moment. There are presently two types of workhorses for these sources, namely storage ring-based synchrotron radiation sources and linear accelerator (linac)-based free-electron lasers (FELs). They deliver light with high repetition rate and high peak power or brilliance, respectively. What we are trying to develop is a new storage ring-based light source mechanism called steady-state micro-bunching (SSMB) [1–19], which hopefully can combine the advantages of such two kind of sources and promise both high-repetition and high-power radiation, realizing an accelerator-based fully coherent light source. The schematic layout of an SSMB storage ring and its comparison to the present synchrotron radiation source and FEL is shown in Fig. 1. In a conventional storage ring, the electron bunches are longitudinally focused by one or multiple radio-frequency (RF) cavities, while in SSMB such bunching system is replaced by one or several optical laser modulation systems. The wavelength of laser is six orders of magnitude **shorter** than that of an RF. The bunch length or structure created by laser is very short, thus the term microbunching. When a beam becomes microbunched, it can radiate coherently and strongly, like that in a laser. But note that in SSMB, there is no exponential growth of the radiation power as that in a high-gain FEL [20] or conventional quantum laser. The term laser in this context mainly reflects that the radiation is coherent, both transversely and longitudi-

nally. To ensure the electron beam property can preserve turn by turn, the SSMB radiator length is comparatively short, typically at meter level, and the peak current of electron beam in SSMB is also lower than that in a high-gain FEL. The radiation back reaction on electron beam is therefore not violent and can be balanced by radiation damping in the ring.

Once realized, such an SSMB ring can produce EUV radiation with greatly enhanced power and flux, allowing sub-meV energy resolution in angle-resolved photoemission spectroscopy (ARPES) and providing new opportunities for fundamental physics research, like revealing key electronic structures in topological materials. A kilowatt (kW)-level EUV source based on such a scheme is also promising to EUV lithography for high-volume chip manufacturing. The reward of such an SSMB ring is therefore tremendous. But one can imagine there are problems to be investigated and solved on the road of every new concept into a reality. To generate coherent EUV radiation in a storage ring, the electron bunch length should reach nm level, which is not at all a trivial task if one keeps in mind that the typical bunch length in present electron storage rings is at mm level. This paper is about our efforts in accomplishing this challenging goal.

The work in this paper is organized as follows. In Sec. II, to build the foundation for the following analysis, we first introduce the generalized Courant-Snyder formalism which applies to a 3D general coupled lattice and present its application in electron storage ring physics. In Sec. III, based on the formalism we derive the theoretical minimum longitudinal emittance in an electron storage ring to provide the basis for later investigation since SSMB is about obtaining short bunch length and small longitudinal emittance. Following this, in Sec. IV, we conduct some key analysis of three specific SSMB scenarios along the thinking of realizing nm bunch length and high-average-power EUV radiation, i.e., longitudinal weak focusing (LWF), longitudinal strong focusing (LSF) and generalized longitudinal strong focusing (GLSF). A short summary of these three schemes is: a LWF

\* Supported by the National Key Research and Development Program of China (Grant No. 2022YFA1603401), the National Natural Science Foundation of China (NSFC Grant No. 12035010 and No. 12342501), the Beijing Outstanding Young Scientist Program (No. JWZQ20240101006) and the Tsinghua University Dushi Program.

† [dengxiujie@mail.tsinghua.edu.cn](mailto:dengxiujie@mail.tsinghua.edu.cn)

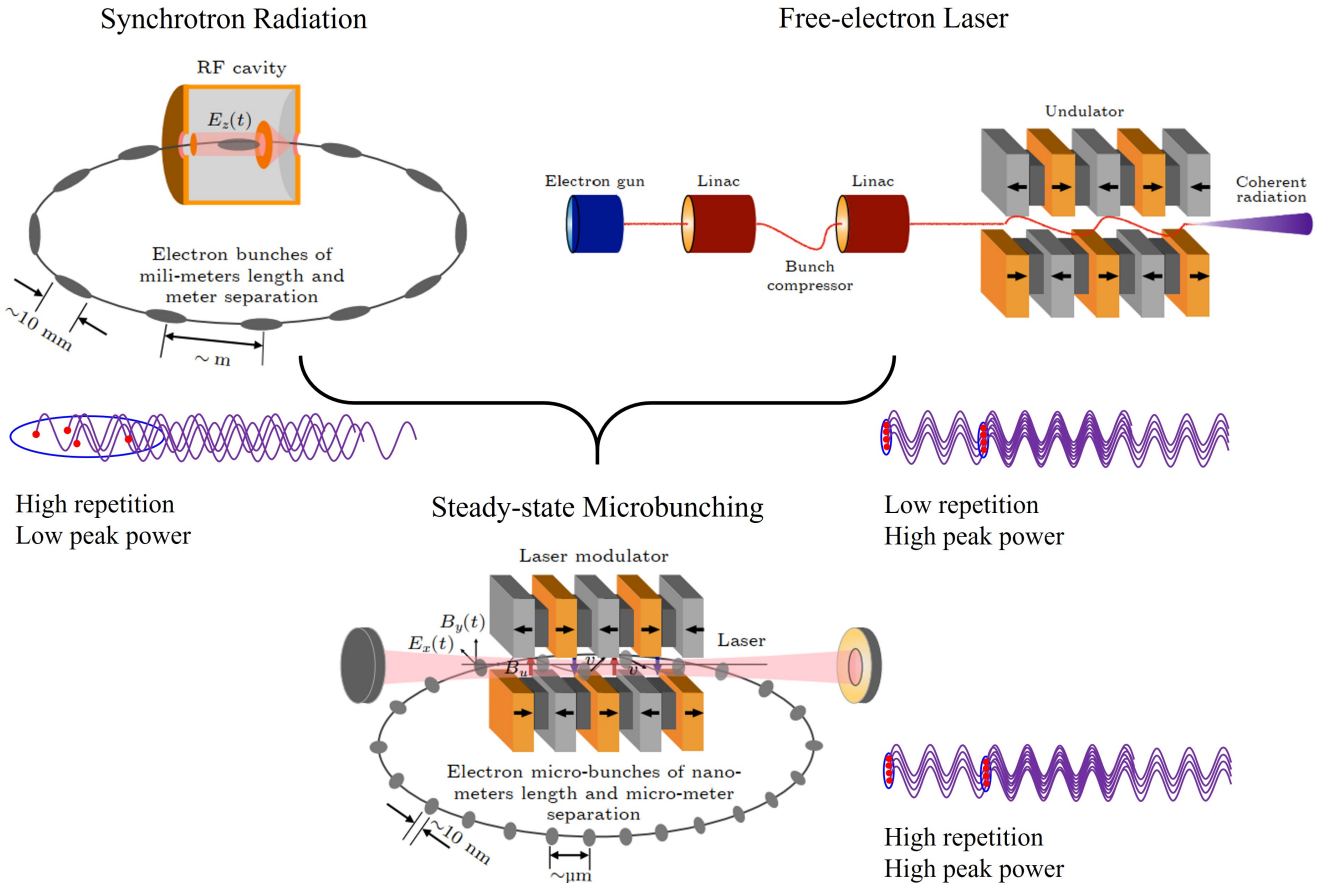


Fig. 1. A schematic layout of an SSMB storage ring, and comparison to a synchrotron radiation source and free-electron laser. (Figure adapted from Ref. [19])

66 SSMB ring can be used to generate bunches with a bunch  
 67 length of a couple of 10 nm, thus can be used to generate  
 68 coherent visible and infrared radiation. If we want to push  
 69 the bunch length to an even shorter value, the required phase  
 70 slippage factor of the LWF ring will be too small from an en-  
 71 gineering viewpoint. As a comparison, a LSF SSMB ring  
 72 can create bunches with a bunch length of nm level, thus  
 73 to generate coherent EUV radiation. However, the required  
 74 modulation laser power is at gigawatt (GW) level, and makes  
 75 the laser modulator, which typically consists of an optical en-  
 76 hancement cavity with an incident laser and an undulator and  
 77 is used to longitudinally focus the electron beam at the laser  
 78 wavelength scale, can only work at a low duty cycle pulsed  
 79 mode, thus limiting the average output EUV radiation power.  
 80 At present, a GLSF SSMB ring is the most promising among  
 81 these three to obtain nm bunch length with a mild modulation  
 82 laser power, thus allowing high-average-power radiation out-  
 83 put. The basic idea of GLSF is to exploit the ultrasmall ver-  
 84 tical emittance in a planar ring and apply partial transverse-  
 85 longitudinal emittance for bunch compression with a shallow  
 86 energy modulation strength, thus a small modulation laser  
 87 power. The backbone of such an GLSF ring is the transverse-  
 88 longitudinal coupling (TLC) dynamics, which is analyzed in  
 89 depth in this paper. Following this analysis, before going into

90 the concrete examples, we prove three theorems in Sec. V  
 91 about TLC-based bunch compression or harmonic generation  
 92 schemes. After that, we then go into the details of various  
 93 TLC schemes, with Sec. VI devoted to energy modulation-  
 94 based schemes and Sec. VII dedicated to angular modulation-  
 95 based schemes. We have derived the bunching factors and the  
 96 required modulation laser powers for them. The conclusion  
 97 from the analysis is that the energy modulation-based cou-  
 98 pling is favored for our application in GLSF SSMB. Based on  
 99 the investigations and other critical physical considerations,  
 100 an example parameter set of a 1 kW-average-power EUV light  
 101 source is finally presented in Sec. VIII. A short summary is  
 102 given in Sec. IX.

## 103 II. GENERALIZED COURANT-SNYDER FORMALISM

104 In this section, to provide the basis for the following dis-  
 105 cussions, we introduce a generalized Courant-Snyder for-  
 106 malism for storage ring physics. Particle state vector  $\mathbf{X} =$   
 107  $(x \ x' \ y \ y' \ z \ \delta)^T$  is used throughout this paper, with its com-  
 108 ponents meaning the horizontal position, horizontal angle,  
 109 vertical position, vertical angle, longitudinal position, and

110  $\delta = \Delta E/E_0$  the relative energy deviation of a particle with  
 111 respect to the reference particle, respectively.  $E_0$  is the en-  
 112 ergy of the reference particle. The superscript  $T$  means the  
 113 transpose of a vector or matrix.

144 their definitions take the real and imaginary part of  $\mathbf{E}_{ki}\mathbf{E}_{kj}^*$ ,  
 145 respectively. We use the symbol  $\hat{\cdot}$  on the top of these func-  
 146 tions to indicate ‘imaginary’. Further we can define the real  
 147 and imaginary generalized  $6 \times 6$  Twiss matrices of a storage  
 148 ring lattice corresponding to each eigen mode as

### 114 A. Generalized Beta Functions in a General Coupled Lattice

150 Inspired by Chao’s solution by linear matrix (SLIM) for-  
 151 malism [21], we introduce the definition of the generalized  
 152 beta functions in a 3D general coupled storage ring lattice as

$$153 \quad \beta_{ij}^k = 2\text{Re}(\mathbf{E}_{ki}\mathbf{E}_{kj}^*), \quad (1)$$

$$154 \quad k = \pm I, II, III,$$

$$155 \quad i, j = 1, 2, 3, 4, 5, 6,$$

156 where  $*$  means the complex conjugate, the sub or superscript  
 157  $k$  is the eigenmode index,  $\text{Re}()$  means the real component of  
 158 a complex number or matrix,  $\mathbf{E}_{ki}$  is the  $i$ -th component of the  
 159 vector  $\mathbf{E}_k$  which is the eigenvector of the  $6 \times 6$  symplectic  
 160 one-turn map  $\mathbf{M}$  of storage ring with the eigenvalue  $e^{i2\pi\nu_k}$

$$161 \quad \mathbf{M}\mathbf{E}_k = e^{i2\pi\nu_k}\mathbf{E}_k, \quad (2)$$

162 satisfying the following normalization condition

$$163 \quad \mathbf{E}_k^\dagger \mathbf{S} \mathbf{E}_k = \begin{cases} i, & k = I, II, III, \\ -i, & k = -I, -II, -III, \end{cases} \quad (3)$$

164 and

$$165 \quad \mathbf{E}_k^\dagger \mathbf{S} \mathbf{E}_j = 0 \text{ for } k \neq j, \quad (4)$$

166 where  $i$  here means the imaginary unit,  $\dagger$  means complex con-  
 167 jugate transpose, and

$$168 \quad \mathbf{S} = \begin{pmatrix} 0 & 1 & 0 & 0 & 0 & 0 \\ -1 & 0 & 0 & 0 & 0 & 0 \\ 0 & 0 & 0 & 1 & 0 & 0 \\ 0 & 0 & -1 & 0 & 0 & 0 \\ 0 & 0 & 0 & 0 & 0 & 1 \\ 0 & 0 & 0 & 0 & -1 & 0 \end{pmatrix}. \quad (5)$$

169 This normalization condition can be preserved around the  
 170 ring due to the symplecticity of the transfer matrix. Since the  
 171 one-turn map is a real symplectic matrix, for a stable motion,  
 172 we have

$$173 \quad \nu_{-k} = -\nu_k, \quad \mathbf{E}_{-k} = \mathbf{E}_k^*, \quad (6)$$

174 where  $\nu_k$  are the eigen tunes.

175 Similar to the real generalized beta function, here we define  
 176 the imaginary generalized beta functions as

$$177 \quad \hat{\beta}_{ij}^k = 2\text{Im}(\mathbf{E}_{ki}\mathbf{E}_{kj}^*), \quad (7)$$

178 where  $\text{Im}()$  means the imaginary component of a complex  
 179 number or matrix. Note that  $\hat{\beta}_{ij}^k$  as a value is actually real, just  
 180 like  $\beta_{ij}^k$ . The name ‘real’ and ‘imaginary’ here reflects that

$$149 \quad (\mathbf{T}_k)_{ij} = \beta_{ij}^k, \quad (\hat{\mathbf{T}}_k)_{ij} = \hat{\beta}_{ij}^k. \quad (8)$$

150 From their definitions we have

$$151 \quad \mathbf{T}_{-k} = \mathbf{T}_k, \quad \mathbf{T}_k^* = \mathbf{T}_k, \quad \mathbf{T}_k^T = \mathbf{T}_k, \quad (9)$$

$$152 \quad \hat{\mathbf{T}}_{-k} = -\hat{\mathbf{T}}_k, \quad \hat{\mathbf{T}}_k^* = \hat{\mathbf{T}}_k, \quad \hat{\mathbf{T}}_k^T = -\hat{\mathbf{T}}_k.$$

153 So we know that  $\mathbf{T}_k$  is a real symmetric matrix, while  $\hat{\mathbf{T}}_k$  is  
 154 a real anti-symmetric matrix. Further, we can prove that

$$155 \quad \sum_{k=I,II,III} \hat{\mathbf{T}}_k = -\mathbf{S}. \quad (10)$$

156 The generalized Twiss matrices at different places around the  
 157 ring are related to each other according to

$$158 \quad \mathbf{T}_k(s_2) = \mathbf{R}(s_2, s_1)\mathbf{T}_k(s_1)\mathbf{R}^T(s_2, s_1), \quad (11)$$

$$159 \quad \hat{\mathbf{T}}_k(s_2) = \mathbf{R}(s_2, s_1)\hat{\mathbf{T}}_k(s_1)\mathbf{R}^T(s_2, s_1).$$

160 where  $\mathbf{R}(s_2, s_1)$  is the symplectic transfer matrix of the state  
 161 vector  $\mathbf{X}$  from  $s_1$  to  $s_2$

$$162 \quad \mathbf{X}(s_2) = \mathbf{R}(s_2, s_1)\mathbf{X}(s_1), \quad (12)$$

163 and we have

$$164 \quad \mathbf{T}_k(s + C_0) = \mathbf{T}_k(s), \quad \hat{\mathbf{T}}_k(s + C_0) = \hat{\mathbf{T}}_k(s) \quad (13)$$

165 where  $C_0$  is the circumference of the ring.

166 With the help of the generalized Twiss matrices and eigen  
 167 tunes, the one-turn map  $\mathbf{M}$  can be parametrized as

$$168 \quad \mathbf{M} = e^{\mathbf{S}(\sum_{k=I,II,III} \mathbf{G}_k \Phi_k)}$$

$$169 = \left( \sum_{k=I,II,III} [\mathbf{T}_k \sin \Phi_k + \hat{\mathbf{T}}_k \cos \Phi_k] \right) \mathbf{S}, \quad (14)$$

170 where

$$171 \quad \mathbf{G}_k \equiv \mathbf{S}^T \mathbf{T}_k \mathbf{S}, \quad (15)$$

172 and  $\Phi_k = 2\pi\nu_k$  is the phase advance of the corresponding  
 173 mode in one turn. For  $\mathbf{M}^n$  we only need to replace the above  
 174  $\Phi_k$  with  $n\Phi_k$ . We can write the matrix terms of the one-turn  
 175 map more explicitly as

$$175 \quad \mathbf{M}_{ij} = (-1)^j \sum_{k=I,II,III} \left[ \beta_{i(j-(-1)^j)}^k \sin \Phi_k + \hat{\beta}_{i(j-(-1)^j)}^k \cos \Phi_k \right]. \quad (16)$$

176 Applying  $\beta_{ij}^k = \beta_{ji}^k$ ,  $\hat{\beta}_{ij}^k = -\hat{\beta}_{ji}^k$ , we have

$$\begin{aligned}
\mathbf{M}_{12} &= \sum_{k=I,II,III} \beta_{11}^k \sin \Phi_k, \\
\mathbf{M}_{21} &= - \sum_{k=I,II,III} \beta_{22}^k \sin \Phi_k, \\
\mathbf{M}_{34} &= \sum_{k=I,II,III} \beta_{33}^k \sin \Phi_k, \\
\mathbf{M}_{43} &= - \sum_{k=I,II,III} \beta_{44}^k \sin \Phi_k, \\
\mathbf{M}_{56} &= \sum_{k=I,II,III} \beta_{55}^k \sin \Phi_k, \\
\mathbf{M}_{65} &= - \sum_{k=I,II,III} \beta_{66}^k \sin \Phi_k.
\end{aligned}$$

175

Using the generalized Twiss matrices, the actions or generalized Courant-Snyder invariants of a particle are defined according to

$$J_k \equiv \frac{\mathbf{X}^T \mathbf{G}_k \mathbf{X}}{2}. \quad (18)$$

It is easy to prove that  $J_k$  are invariants of a particle when it travels around the ring, from Eqs. (11), (12), and the symplecticity of the transfer matrix

$$\mathbf{R}^T \mathbf{S} \mathbf{R} = \mathbf{S}. \quad (19)$$

For a beam with  $N_p$  particles, the three beam invariants can then be defined according to

$$\epsilon_k \equiv \langle J_k \rangle = \frac{\sum_{i=1}^{N_p} J_{k,i}}{N_p}, \quad k = I, II, III, \quad (20)$$

where  $J_{k,i}$  means the  $k$ -th mode invariant of the  $i$ -th particle. These invariants are the generalized root-mean-square (RMS) emittances of beam in the ring.

The beam emittances defined above are based on the eigen-mode motion of particles in the storage ring. Another definition of emittance is based directly on the second moments matrix of a particle beam

$$\Sigma = \langle \mathbf{X} \mathbf{X}^T \rangle, \quad (21)$$

where  $\langle \rangle$  here means particle ensemble average. The beam second moment matrix at different places are related according to

$$\Sigma(s_2) = \mathbf{R}(s_2, s_1) \Sigma(s_1) \mathbf{R}^T(s_2, s_1). \quad (22)$$

From the symplecticity of  $\mathbf{R}$ , we can prove that the eigenvalues of  $\Sigma(-i\mathbf{S})$  are unchanged with the beam transport in a linear symplectic lattice. The beam eigen emittances can thus be defined as the positive eigen values of  $\Sigma(-i\mathbf{S})$ .

When the particle beam matches the storage ring lattice, which means the beam distribution at a given location repeats itself turn by turn, we have

$$\Sigma(s + C_0) = \mathbf{M}(s) \Sigma(s) \mathbf{M}^T(s) = \Sigma(s). \quad (23)$$

It can be proven that for a matched beam the RMS emittances defined in Eq. (20) are the eigenvalues of  $\Sigma(-i\mathbf{S})$  with the eigenvector  $\mathbf{E}_k$ , i.e.,

$$\Sigma(-i\mathbf{S}) \mathbf{E}_k = \text{sgn}(k) \epsilon_k \mathbf{E}_k, \quad (24)$$

where we have used  $\epsilon_{-k} \equiv \epsilon_k$  and

$$\text{sgn}(k) = \begin{cases} 1, & k = I, II, III, \\ -1, & k = -I, -II, -III. \end{cases} \quad (25)$$

Using the generalized Twiss and second moments matrices, the eigen emittances for a matched beam can be calculated as

$$\epsilon_k = \text{Tr}(\mathbf{T}_k \mathbf{S} \Sigma \mathbf{S}^T) = \text{Tr}(\mathbf{G}_k \Sigma). \quad (26)$$

Using the generalized Twiss matrices, the actions or generalized Courant-Snyder invariants of a particle are defined according to

$$J_k \equiv \frac{\mathbf{X}^T \mathbf{G}_k \mathbf{X}}{2}. \quad (18)$$

It is easy to prove that  $J_k$  are invariants of a particle when it travels around the ring, from Eqs. (11), (12), and the symplecticity of the transfer matrix

$$\mathbf{R}^T \mathbf{S} \mathbf{R} = \mathbf{S}. \quad (19)$$

For a beam with  $N_p$  particles, the three beam invariants can then be defined according to

$$\epsilon_k \equiv \langle J_k \rangle = \frac{\sum_{i=1}^{N_p} J_{k,i}}{N_p}, \quad k = I, II, III, \quad (20)$$

where  $J_{k,i}$  means the  $k$ -th mode invariant of the  $i$ -th particle. These invariants are the generalized root-mean-square (RMS) emittances of beam in the ring.

The beam emittances defined above are based on the eigen-mode motion of particles in the storage ring. Another definition of emittance is based directly on the second moments matrix of a particle beam

$$\Sigma = \langle \mathbf{X} \mathbf{X}^T \rangle, \quad (21)$$

where  $\langle \rangle$  here means particle ensemble average. The beam second moment matrix at different places are related according to

$$\Sigma(s_2) = \mathbf{R}(s_2, s_1) \Sigma(s_1) \mathbf{R}^T(s_2, s_1). \quad (22)$$

From the symplecticity of  $\mathbf{R}$ , we can prove that the eigenvalues of  $\Sigma(-i\mathbf{S})$  are unchanged with the beam transport in a linear symplectic lattice. The beam eigen emittances can thus be defined as the positive eigen values of  $\Sigma(-i\mathbf{S})$ .

When the particle beam matches the storage ring lattice, which means the beam distribution at a given location repeats itself turn by turn, we have

$$\Sigma(s + C_0) = \mathbf{M}(s) \Sigma(s) \mathbf{M}^T(s) = \Sigma(s). \quad (23)$$

where  $\text{Tr}()$  means the trace of a matrix.

To ensure that the eigenvectors  $\mathbf{E}_k$  are uniquely defined all around the ring once they are determined at a given location, we will let

$$\mathbf{E}_k(s_2) = e^{-i \frac{s_2 - s_1}{C_0} \Phi_k} \mathbf{R}(s_2, s_1) \mathbf{E}_k(s_1). \quad (27)$$

Following this definition, we have

$$\mathbf{E}_k(s + C_0) = e^{-i \Phi_k} \Sigma(s) \mathbf{E}_k(s) = \mathbf{E}_k(s). \quad (28)$$

Using the generalized beta function, we can write the eigen-vector component in an amplitude-phase form

$$\mathbf{E}_{kj} = \sqrt{\frac{\beta_{jj}^k}{2}} e^{i \phi_j^k}. \quad (29)$$

And according to the definition we have

$$\beta_{ij}^k = \sqrt{\beta_{ii}^k \beta_{jj}^k} \cos(\phi_i^k - \phi_j^k). \quad (30)$$

Using the generalized Courant-Snyder invariants and beta functions, we can express the phase space coordinate of a particle at  $s$  as

$$\mathbf{X}_i(s) = \sum_{k=I,II,III} \sqrt{2 J_k \beta_{ii}^k(s)} \cos [\psi_i^k(s)], \quad (31)$$

with  $\psi_i^k$  determined by the initial condition of particle state.

The phase term  $\psi_i^k$  at different locations are related according to

$$\psi_i^k(s_2) = \psi_i^k(s_1) + \frac{s_2 - s_1}{C_0} \Phi_k + \phi_i^k(s_2) - \phi_i^k(s_1). \quad (32)$$

In particular, after  $n$  revolutions in the ring, we have

$$\mathbf{X}_i(s + nC_0) = \sum_{k=I,II,III} \sqrt{2 J_k \beta_{ii}^k(s)} \cos [\psi_i^k(s) + n \Phi_k]. \quad (33)$$

238

## B. Perturbations

278

## C. Application to Electron Storage Rings

239 After considering the parametrization of a general coupled  
 240 lattice and the prescribed particle motion in it, let us now  
 241 add perturbations, that from the lattice and also that from the  
 242 beam. Assume there is a perturbation  $\mathbf{K}$  to the one-turn map  
 243  $\mathbf{M}$ , i.e.,

$$244 \quad \mathbf{M}_{\text{per}} = (\mathbf{I} + \mathbf{K})\mathbf{M}_{\text{unp}}, \quad (34)$$

245 where  $\mathbf{I}$  is the identity matrix, the subscripts ‘per’ and ‘unp’  
 246 mean ‘perturbed’ and ‘unperturbed’, respectively. When the  
 247 perturbation is small, from canonical perturbation theory,  
 248 the tune shift of the  $k$ -th eigen mode can be calculated as

$$249 \quad \Delta\nu_k = -\frac{1}{4\pi} \text{Tr} \left[ \left( \text{sgn}(k)\mathbf{T}_k + i\hat{\mathbf{T}}_k \right) \mathbf{S}\mathbf{K} \right]. \quad (35)$$

250 This tune shift formula can be used to calculate the real and  
 251 imaginary tune shifts due to symplectic (for example lattice  
 252 error) and non-symplectic (for example radiation damping)  
 253 perturbations. For example, given the radiation damping ma-  
 254 trix  $\mathbf{D}$  around the ring, the damping rate of each eigen mode  
 255 per turn is

$$256 \quad \alpha_k = -\frac{1}{2} \oint \text{Tr} \left( \hat{\mathbf{T}}_k \mathbf{S}\mathbf{D} \right) ds, k = I, II, III, \quad (36)$$

257 where  $\oint$  means integration around the ring. Note that the  
 258 damping rates here are those for the corresponding eigenvec-  
 259 tors. The damping rates for particle actions or beam eigen  
 260 emittances are a factor of two larger, since they are quadratic  
 261 with respect to the phase space coordinates.

262 Apart from the radiation damping, there are also various  
 263 beam diffusion effects in the ring, like quantum excitation and  
 264 intra-beam scattering. Using Eq. (26), once we know the dif-  
 265 fusion and damping matrix  $\mathbf{N}$  around the ring, the emittance  
 266 growth per turn due to diffusion is

$$267 \quad \Delta\epsilon_k = \frac{1}{2} \oint \text{Tr} \left( \mathbf{G}_k \mathbf{N} \right) ds = -\frac{1}{2} \oint \text{Tr} \left( \mathbf{T}_k \mathbf{S}\mathbf{N}\mathbf{S} \right) ds, \quad (37)$$

268 The equilibrium eigen emittance between a balance of diffu-  
 269 sion and damping can be calculated as

$$270 \quad \epsilon_k = \frac{\Delta\epsilon_k}{2\alpha_k} = \frac{\frac{1}{2} \oint \text{Tr} \left( \mathbf{G}_k \mathbf{N} \right) ds}{-\oint \text{Tr} \left( \hat{\mathbf{T}}_k \mathbf{S}\mathbf{D} \right) ds} \quad (38)$$

$$= \frac{-\frac{1}{2} \sum_{i,j} \oint \beta_{ij}^k (\mathbf{S}\mathbf{N}\mathbf{S})_{ij} ds}{\sum_{i,j} \oint \hat{\beta}_{ij}^k (\mathbf{S}\mathbf{D})_{ij} ds}.$$

271 It can be proven that the equilibrium beam distribution in 6D  
 272 phase space given by such a balance in a linear lattice is Gaus-  
 273 sian [22], with  $\langle \mathbf{X} \rangle = 0$ . After getting the equilibrium eigen  
 274 emittances, the second moments of beam can be written as

$$275 \quad \Sigma_{ij} = \langle \mathbf{X}_i \mathbf{X}_j \rangle = \sum_{k=I,II,III} \epsilon_k \beta_{ij}^k, \quad (39)$$

276 or in matrix form as

$$277 \quad \Sigma = \sum_{k=I,II,III} \epsilon_k \mathbf{T}_k. \quad (40)$$

279 In an electron storage ring, the intrinsic diffusion and  
 280 damping are both from the emission of photons, namely the  
 281 so-called quantum excitation and radiation damping. For  
 282 quantum excitation, we have all the other components of the  
 283 diffusion matrix  $\mathbf{N}$  zero except that

$$284 \quad N_{66} = \frac{\left\langle \dot{\mathcal{N}} \frac{u^2}{E_0^2} \right\rangle}{c} = \frac{2C_L\gamma^5}{c|\rho|^3}, \quad (41)$$

285 where  $\dot{\mathcal{N}}$  is the number of photons emitted per unit time,  $u$  is  
 286 the photon energy,  $C_L = \frac{55}{48\sqrt{3}} \frac{r_e \hbar}{m_e}$  with  $r_e$  being the classical  
 287 electron radius,  $\hbar$  being the reduced Planck’s constant,  $m_e$   
 288 being the electron mass,  $\gamma$  is the Lorentz factor,  $c$  is the speed  
 289 of light in free space,  $\rho$  is the bending radius. We take the  
 290 convention that the sign of  $\rho$  is positive when the bending is  
 291 inward, and negative when the bending is outward.  $\langle \dot{\mathcal{N}} u^2 \rangle$  in  
 292 the above formula is a result of Campbell’s theorem [23, 24].

293 For damping effect, we have two sources, i.e., dipole mag-  
 294 nets and RF cavity. For a horizontal dipole, we have all the  
 295 other components of damping matrix  $\mathbf{D}$  zero except that

$$296 \quad D_{66} = -\frac{C_\gamma E_0^3}{\pi} \frac{1}{\rho^2}, \quad D_{61} = -\frac{C_\gamma E_0^3}{2\pi} \frac{1-2n}{\rho^3}, \quad (42)$$

297 where  $C_\gamma = \frac{4\pi}{3} \frac{r_e}{(m_e c^2)^3} = 8.85 \times 10^{-5} \frac{\text{m}}{\text{GeV}^2}$ ,  $n = -\frac{\rho}{B_y} \frac{\partial B_y}{\partial x}$   
 298 is the transverse field gradient index. The physical origin of  
 299  $D_{66}$  is the fact that a higher energy particle tends to radiate  
 300 more photon energy in a given magnetic field, while  $D_{61}$  is  
 301 due to the fact that a transverse displacement of particle will  
 302 affect its path length in the dipole and when there is transverse  
 303 field gradient also the magnetic field strength observed, thus  
 304 the radiation energy loss. For an RF cavity, we have all the  
 305 other damping matrix terms of  $\mathbf{D}$  zero except that

$$306 \quad D_{22} = D_{44} = -\frac{eV_{RF} \sin \phi_{RF}}{E_0} \delta(s_{RF}), \quad (43)$$

307 where  $e$  is the elementary charge and is assumed positive in  
 308 this paper,  $V_{RF}$  and  $\phi_{RF}$  are the RF voltage and phase, re-  
 309 spectively,  $\delta(s)$  means Dirac’s delta function. Here we have  
 310 assumed that the RF cavity is a zero-length one. The physical  
 311 origin of these damping terms is that the momentum boost  
 312 of a particle in the RF cavity is along the longitudinal direc-  
 313 tion, while the transverse momentums of the particle are un-  
 314 changed. Therefore, there is a damping effect on the horizon-  
 315 tal and vertical angle of the particle. We remind the readers  
 316 that if we use the horizontal and vertical particle momentum  
 317  $p_x$  and  $p_y$ , instead of  $x'$  and  $y'$ , as the phase space coordinates,  
 318 then the damping happens only at bending magnets since the  
 319 RF acceleration does not affect  $p_{x,y}$ .

320 In an electron storage ring, the RF acceleration compen-  
 321 sates the radiation energy loss of electrons. If there are  $N$   
 322 cavities in the ring, we have

$$323 \quad \sum_{i=1}^N eV_{RF,i} \sin \phi_{RF,i} = U_0, \quad (44)$$

324 where

$$325 \quad U_0 = \frac{C_\gamma E_0^4}{2\pi} I_2 \quad (45)$$

326 is the radiation energy loss per particle per turn, with

$$327 \quad I_2 = \oint \frac{1}{\rho^2} ds. \quad (46)$$

328 If the ring consists of iso-bending magnets, then  $U_0 = C_\gamma \frac{E_0^4}{\rho}$ .

329 From Eq. (42), we have

$$330 \quad \oint D_{66}(s) ds = -\frac{2U_0}{E_0}. \quad (47)$$

331 Similarly, based on Eqs. (43) and (44), we have

$$332 \quad \oint D_{22}(s) ds = \oint D_{44}(s) ds = -\frac{U_0}{E_0}. \quad (48)$$

333 Combing with Eqs. (10) and (36), it is easy to show that for

334 radiation damping, we have

$$\begin{aligned} \sum_{k=I,II,III} \alpha_k &= -\frac{1}{2} \oint \text{Tr} \left[ \left( \sum_{k=I,II,III} \hat{\mathbf{T}}_k \right) \mathbf{S} \mathbf{D} \right] ds \\ &= -\frac{1}{2} \oint \text{Tr}(\mathbf{D}) ds \\ &= -\frac{1}{2} \oint (D_{22} + D_{44} + D_{66}) ds \\ &= \frac{2U_0}{E_0}, \end{aligned} \quad (49)$$

335 which is the well-known Robinson's sum rule [25].

336 The above formulation applies for a 3D general coupled  
337 lattice. For a ring without  $x$ - $y$  coupling and when the RF  
338 cavity is placed at dispersion-free location, we can express the  
339 normalized eigenvectors using the classical Courant-Snyder  
340 functions [26]  $\alpha, \beta, \gamma$  and dispersion  $D$  and dispersion angle  
341

342  $D'$  as

$$\mathbf{E}_I = \frac{1}{\sqrt{2}} \begin{pmatrix} \sqrt{\beta_x} \\ -\alpha_x + i \\ \sqrt{\beta_x} \\ 0 \\ 0 \\ \frac{-(\alpha_x D_x + \beta_x D'_x) + i D_x}{\sqrt{\beta_x}} \\ 0 \end{pmatrix} e^{i\Psi_I}, \quad \mathbf{E}_{II} = \frac{1}{\sqrt{2}} \begin{pmatrix} 0 \\ 0 \\ \sqrt{\beta_y} \\ -\alpha_y + i \\ \sqrt{\beta_y} \\ \frac{-(\alpha_y D_y + \beta_y D'_y) + i D_y}{\sqrt{\beta_y}} \\ 0 \end{pmatrix} e^{i\Psi_{II}}, \quad \mathbf{E}_{III} = \frac{1}{\sqrt{2}} \begin{pmatrix} -\alpha_z + i \\ \sqrt{\beta_z} \\ -\alpha_z + i \\ \sqrt{\beta_z} \\ \frac{-(\alpha_z D_z + \beta_z D'_z) + i D_z}{\sqrt{\beta_z}} \\ -\alpha_z + i \\ \sqrt{\beta_z} \end{pmatrix} e^{i\Psi_{III}}, \quad (50)$$

343

344 where the subscripts  $x, y, z$  correspond to the horizontal, vertical and longitudinal dimensions, respectively, and  $\Psi_{I,II,III}$  are  
345 the phase factors of the eigenvectors. There is flexibility in choosing these phase factors as they do not affect the calculation of  
346 our defined Twiss matrices and physical quantities. But note that once they are set at one location, then their values all around  
347 the ring are determined according to Eq. (27). In this case, the real and imaginary generalized Twiss matrices can be obtained  
348 explicitly

$$\begin{aligned} \mathbf{T}_I &= \begin{pmatrix} \beta_x & -\alpha_x & 0 & 0 & -\alpha_x D_x - \beta_x D'_x & 0 \\ -\alpha_x & \gamma_x & 0 & 0 & \gamma_x D_x + \alpha_x D'_x & 0 \\ 0 & 0 & 0 & 0 & 0 & 0 \\ 0 & 0 & 0 & 0 & 0 & 0 \\ -\alpha_x D_x - \beta_x D'_x & \gamma_x D_x + \alpha_x D'_x & 0 & 0 & \mathcal{H}_x & 0 \\ 0 & 0 & 0 & 0 & 0 & 0 \end{pmatrix}, \quad \hat{\mathbf{T}}_I = \begin{pmatrix} 0 & -1 & 0 & 0 & -D_x & 0 \\ 1 & 0 & 0 & 0 & -D'_x & 0 \\ 0 & 0 & 0 & 0 & 0 & 0 \\ 0 & 0 & 0 & 0 & 0 & 0 \\ D_x & D'_x & 0 & 0 & 0 & 0 \\ 0 & 0 & 0 & 0 & 0 & 0 \end{pmatrix}, \\ \mathbf{T}_{II} &= \begin{pmatrix} 0 & 0 & 0 & 0 & 0 & 0 \\ 0 & 0 & 0 & 0 & 0 & 0 \\ 0 & 0 & \beta_y & -\alpha_y & -\alpha_y D_y - \beta_y D'_y & 0 \\ 0 & 0 & -\alpha_y & \gamma_y & \gamma_y D_y + \alpha_y D'_y & 0 \\ 0 & 0 & -\alpha_y D_y - \beta_y D'_y & \gamma_y D_y + \alpha_y D'_y & \mathcal{H}_y & 0 \\ 0 & 0 & 0 & 0 & 0 & 0 \end{pmatrix}, \quad \hat{\mathbf{T}}_{II} = \begin{pmatrix} 0 & 0 & 0 & 0 & 0 & 0 \\ 0 & 0 & 0 & 0 & 0 & 0 \\ 0 & 0 & 0 & -1 & -D_y & 0 \\ 0 & 0 & 1 & 0 & -D'_y & 0 \\ 0 & 0 & D_y & D'_y & 0 & 0 \\ 0 & 0 & 0 & 0 & 0 & 0 \end{pmatrix}, \\ \mathbf{T}_{III} &= \begin{pmatrix} \gamma_z D_x^2 & \gamma_z D_x D'_x & \gamma_z D_x D_y & \gamma_z D_x D'_y & -\alpha_z D_x & \gamma_z D_x \\ \gamma_z D_x D'_x & \gamma_z D_x'^2 & \gamma_z D'_x D_y & \gamma_z D'_x D'_y & -\alpha_z D'_x & \gamma_z D'_x \\ \gamma_z D_x D_y & \gamma_z D'_x D_y & \gamma_z D_y^2 & \gamma_z D_y D'_y & -\alpha_z D_y & \gamma_z D_y \\ \gamma_z D_x D'_y & \gamma_z D'_x D'_y & \gamma_z D_y D'_y & \gamma_z D_y'^2 & -\alpha_z D'_y & \gamma_z D'_y \\ -\alpha_z D_x & -\alpha_z D'_x & -\alpha_z D_y & -\alpha_z D'_y & \beta_z & -\alpha_z \\ \gamma_z D_x & \gamma_z D'_x & \gamma_z D_y & \gamma_z D'_y & -\alpha_z & \gamma_z \end{pmatrix}, \quad \hat{\mathbf{T}}_{III} = \begin{pmatrix} 0 & 0 & 0 & 0 & D_x & 0 \\ 0 & 0 & 0 & 0 & D'_x & 0 \\ 0 & 0 & 0 & 0 & D_y & 0 \\ 0 & 0 & 0 & 0 & D'_y & 0 \\ -D_x & -D'_x & -D_y & -D'_y & 0 & -1 \\ 0 & 0 & 0 & 0 & 1 & 0 \end{pmatrix}. \end{aligned} \quad (51)$$

349

350 Correspondingly, the generalized Courant-Snyder invariants are given by

$$\begin{aligned}
351 \quad J_I &\equiv \frac{(\mathbf{S}\mathbf{X})^T \mathbf{T}_I \mathbf{S}\mathbf{X}}{2} = \frac{(x - D_x \delta)^2 + [\alpha_x (x - D_x \delta) + \beta_x (x' - D'_x \delta)]^2}{2\beta_x}, \\
J_{II} &\equiv \frac{(\mathbf{S}\mathbf{X})^T \mathbf{T}_{II} \mathbf{S}\mathbf{X}}{2} = \frac{(y - D_y \delta)^2 + [\alpha_y (y - D_y \delta) + \beta_y (y' - D'_y \delta)]^2}{2\beta_y}, \\
J_{III} &\equiv \frac{(\mathbf{S}\mathbf{X})^T \mathbf{T}_{III} \mathbf{S}\mathbf{X}}{2} = \frac{(z + D'_x x - D_x x' + D'_y y - D_y y')^2 + [\alpha_z (z + D'_x x - D_x x' + D'_y y - D_y y') + \beta_z \delta]^2}{2\beta_z},
\end{aligned} \tag{52}$$

352 The equilibrium emittances determined by the balance of  
353 quantum excitation and radiation damping in an electron stor-  
354 age in this case reduce to the classical Sands radiation inte-  
355 grals formalism found in textbooks [27]

$$\begin{aligned}
\epsilon_x &\equiv \langle J_I \rangle = \frac{C_L \gamma^5}{2c\alpha_I} \oint \frac{\beta_{55}^I}{|\rho|^3} ds = C_q \frac{\gamma^2}{J_x} \frac{I_{5x}}{I_2}, \\
\epsilon_y &\equiv \langle J_{II} \rangle = \frac{C_L \gamma^5}{2c\alpha_{II}} \oint \frac{\beta_{55}^{II}}{|\rho|^3} ds = C_q \frac{\gamma^2}{J_y} \frac{I_{5y}}{I_2}, \\
\epsilon_z &\equiv \langle J_{III} \rangle = \frac{C_L \gamma^5}{2c\alpha_{III}} \oint \frac{\beta_{55}^{III}}{|\rho|^3} ds = C_q \frac{\gamma^2}{J_z} \frac{I_{5z}}{I_2},
\end{aligned} \tag{53}$$

357 with  $C_q = \frac{55\lambda_e}{32\sqrt{3}} = 3.8319 \times 10^{-13}$  m for electrons,  $\lambda_e =$   
358  $\frac{\lambda_e}{2\pi} = \frac{\hbar c}{m_e c^2} = 386$  fm is the reduced Compton wavelength of  
359 electron, and the radiation integrals are given by

$$\begin{aligned}
360 \quad I_2 &= \oint \frac{1}{\rho^2} ds, \quad I_{4x} = \oint D_x \left( \frac{1 - 2n}{\rho^3} \right) ds, \\
I_{5x} &= \oint \frac{\mathcal{H}_x}{|\rho|^3} ds, \quad I_{5y} = \oint \frac{\mathcal{H}_y}{|\rho|^3} ds, \quad I_{5z} = \oint \frac{\beta_z}{|\rho|^3} ds,
\end{aligned} \tag{54}$$

361 where

$$\mathcal{H}_{x,y} = \beta_{55}^{I,II} = \frac{D_{x,y}^2 + (\alpha_{x,y} D_{x,y} + \beta_{x,y} D'_{x,y})^2}{\beta_{x,y}} \tag{55}$$

363 are the horizontal and vertical dispersion invariant, and  $\beta_z =$   
364  $\beta_{55}^{III}$  is the longitudinal beta function [8]. The damping rate  
365 of three eigen modes are given by

$$\alpha_I = \frac{U_0}{2E_0} J_x, \quad \alpha_{II} = \frac{U_0}{2E_0} J_y, \quad \alpha_{III} = \frac{U_0}{2E_0} J_z, \tag{56}$$

367 where  $J_{x,y,z}$  are the damping partition numbers

$$J_x = 1 - \frac{I_{4x}}{I_2}, \quad J_y = 1, \quad J_z = 2 + \frac{I_{4x}}{I_2}. \tag{57}$$

369 The Robinson's sum rule corresponds then to

$$J_x + J_y + J_z = 4. \tag{58}$$

371 The horizontal, vertical, longitudinal radiation damping times  
372 are

$$\tau_{x,y,z} = \frac{T_0}{\alpha_{x,y,z}}, \tag{59}$$

374 where  $T_0$  is the particle revolution period time in the ring.

375 After getting the equilibrium emittance, the beam sec-  
376 ond moments can be obtained by substituting the generalized  
377 Twiss matrices from Eq. (51) into Eq. (39). For example,

$$\begin{aligned}
378 \quad \sigma_x^2 &= \langle x^2 \rangle = \epsilon_x \beta_x + \epsilon_z \gamma_z D_x^2 = \epsilon_x \beta_x + \sigma_\delta^2 D_x^2, \\
\sigma_z^2 &= \langle z^2 \rangle = \epsilon_z \beta_z + \epsilon_x \mathcal{H}_x + \epsilon_y \mathcal{H}_y.
\end{aligned} \tag{60}$$

379 We remind the readers that the generalized Courant-Snyder  
380 formalism presented in this section has been briefly reported  
381 before in Ref. [28].

### III. THEORETICAL MINIMUM EMITTANCES

383 After introducing the generalized Courant-Snyder formal-  
384 ism, we now apply it to analyze the theoretical minimum lon-  
385 gitudinal emittance in an electron storage ring. This work  
386 serves as the basis for the following investigation of SSMB,  
387 since the longitudinal weak focusing and strong focusing  
388 SSMB to be introduced soon are about lowering the equilib-  
389 rium bunch length and longitudinal emittance in an electron  
390 storage ring. For completeness, here in this section we also  
391 present the analysis of theoretical minimum transverse emit-  
392 tance since they can be treated within a single framework.

#### A. Theoretical Minimum Horizontal Emittance

394 From Eq. (53) we can see that  $\mathcal{H}_x$  and  $\beta_z$ , i.e.,  $\beta_{55}^I$  and  
395  $\beta_{55}^{III}$  as defined by us, at the bending magnets are of vital im-  
396 portance in determining the horizontal and longitudinal emit-  
397 tance, respectively. Therefore, we need to know how they  
398 evolve inside a bending magnet. The transfer matrix of the  
399 particle state vector for a sector bending magnet is

$$400 \quad \mathbf{B}(\alpha) = \begin{pmatrix} \cos \alpha & \rho \sin \alpha & 0 & 0 & 0 & \rho(1 - \cos \alpha) \\ -\frac{\sin \alpha}{\rho} & \cos \alpha & 0 & 0 & 0 & \sin \alpha \\ 0 & 0 & 1 & \rho \alpha & 0 & 0 \\ 0 & 0 & 0 & 1 & 0 & 0 \\ -\sin \alpha & -\rho(1 - \cos \alpha) & 0 & 0 & 1 & \rho \left( \frac{\alpha}{\gamma^2} - \alpha + \sin \alpha \right) \\ 0 & 0 & 0 & 0 & 0 & 1 \end{pmatrix}, \quad (61)$$

401 with  $\rho$  and  $\alpha$  being the bending radius and angle of the bend- 405 sion and dispersion angle at the dipole center where we set to  
402 ing magnet, respectively. In a planar uncoupled ring, the 406 be  $\alpha = 0$  are given by  $\alpha_{x0}, \beta_{x0}, \alpha_{z0}, \beta_{z0}, D_{x0}, D'_{x0}$ . From  
403 normalized eigenvectors of the one-turn map are given by 407 Eqs. (1), (61) and (50) we have the evolution of  $\mathcal{H}_x$  expres-  
404 Eq. (50). Assuming the Courant-Snyder functions, disper- 408 sion in the dipole

$$409 \quad \mathcal{H}_x(\alpha) \equiv \beta_{55}^I(\alpha) = 2|\mathbf{E}_{I5}(\alpha)|^2 = 2|(\mathbf{B}(\alpha)\mathbf{E}_I(0))_5|^2 \\ = \left( \sqrt{\beta_{x0}}(\sin \alpha + D'_{x0}) + \frac{\alpha_{x0}}{\sqrt{\beta_{x0}}}[D_{x0} - \rho(1 - \cos \alpha)] \right)^2 + \left( \frac{D_{x0} - \rho(1 - \cos \alpha)}{\sqrt{\beta_{x0}}} \right)^2. \quad (62)$$

410 Similarly, the evolution of  $\beta_z$  in the dipole is given by

$$411 \quad \beta_z(\alpha) \equiv \beta_{55}^{III}(\alpha) = 2|\mathbf{E}_{III5}(\alpha)|^2 = 2|(\mathbf{B}(\alpha)\mathbf{E}_{III}(0))_5|^2 \\ = \left( \sin \alpha \frac{\alpha_{z0}}{\sqrt{\beta_{z0}}} D_{x0} + \rho(1 - \cos \alpha) \frac{\alpha_{z0}}{\sqrt{\beta_{z0}}} D'_{x0} + \sqrt{\beta_{z0}} - \rho(-\alpha + \sin \alpha) \frac{\alpha_{z0}}{\sqrt{\beta_{z0}}} \right)^2 \\ + \left( -\sin \alpha \frac{1}{\sqrt{\beta_{z0}}} D_{x0} - \rho(1 - \cos \alpha) \frac{1}{\sqrt{\beta_{z0}}} D'_{x0} + \rho(-\alpha + \sin \alpha) \frac{1}{\sqrt{\beta_{z0}}} \right)^2. \quad (63)$$

412 For simplicity we have neglected the contribution of  $\frac{\rho \alpha}{\gamma^2}$  to 424 with  
413  $R_{56}$  of dipole in the above calculation of  $\beta_z$ , since we are  
414 interested in the relativistic cases. But we remind the readers  
415 that in a quasi-isochronous ring, the contribution of  $\frac{C_0}{\gamma^2}$  to the  
416 ring  $R_{56}$  or phase slippage may not be negligible.

417 With the evolution of  $\mathcal{H}_x$  and  $\beta_z$  known, now we derive the  
418 theoretical minimum emittances. For simplicity, we assume  
419 the ring consists of iso-bending-magnets, with the bending  
420 angle induced by each bending magnet being  $\theta$ , and the op-  
421 tical functions are identical in each bending magnets. Then  
422 from Eq. (53), we have

$$423 \quad \epsilon_x = C_q \frac{\gamma^2}{J_x} \frac{1}{\rho} f_x(\alpha_{x0}, \beta_{x0}, D_{x0}, D'_{x0}), \quad (64)$$

$$425 \quad f_x(\alpha_{x0}, \beta_{x0}, D_{x0}, D'_{x0}) = \frac{1}{\theta} \int_{-\frac{\theta}{2}}^{\frac{\theta}{2}} \mathcal{H}_x(\alpha) d\alpha. \quad (65)$$

426  $f_x$  can be interpreted as the average value of  $\mathcal{H}_x$  in dipoles.  
427 The lengthy explicit expression of  $f_x(\alpha_{x0}, \beta_{x0}, D_{x0}, D'_{x0})$  is  
428 omitted here. It can be obtained straightforwardly by insert-  
429 ing Eq. (62) in Eq. (65). The mathematical problem we are  
430 trying to solve is then to minimize  $f_x$ , by adjusting  $\alpha_{x0}, \beta_{x0},$   
431  $D_{x0}, D'_{x0}$ . From Eq. (65) we have

$$432 \quad \frac{\partial f_x}{\partial \alpha_{x0}} = \alpha_{x0} \frac{2D_{x0} \left( D_{x0} - 2\rho + 2\rho \frac{\sin \frac{\theta}{2}}{\frac{\theta}{2}} \right) + \rho^2 \left( 3 - 4 \frac{\sin \frac{\theta}{2}}{\frac{\theta}{2}} + \frac{\sin \theta}{\theta} \right)}{\beta_{x0}} + D'_{x0} 2 \left( D_{x0} - \rho + \rho \frac{\sin \frac{\theta}{2}}{\frac{\theta}{2}} \right), \\ \frac{\partial f_x}{\partial D'_{x0}} = \alpha_{x0} 2 \left( D_{x0} - \rho + \rho \frac{\sin \frac{\theta}{2}}{\frac{\theta}{2}} \right) + D'_{x0} 2 \beta_{x0}. \quad (66)$$

433 We notice that the requirement of  $\frac{\partial f_x}{\partial \alpha_{x0}} = 0$  and  $\frac{\partial f_x}{\partial D'_{x0}} = 0$  434 leads to  $\alpha_{x0} = 0$  and  $D'_{x0} = 0$ . Under the above conditions,

435 then

$$436 \quad \frac{\partial f_x}{\partial D_{x0}} = \frac{2 \left( D_{x0} - \rho + \rho \frac{\sin \frac{\theta}{2}}{\frac{\theta}{2}} \right)}{\beta_{x0}}.$$

437 The requirement of  $\frac{\partial f_x}{\partial D_{x0}} = 0$  leads to

$$438 \quad D_{x0} = \rho \left( 1 - \frac{\sin \frac{\theta}{2}}{\frac{\theta}{2}} \right) \approx \frac{\rho \theta^2}{24}.$$

439 Under the above conditions, then

$$440 \quad \frac{\partial f_x}{\partial \beta_{x0}} = \frac{\theta(\theta - \sin \theta) - \frac{\rho^2(\theta^2 + \theta \sin \theta + 4 \cos \theta - 4)}{\beta_{x0}^2}}{2\theta^2}.$$

441 The requirement of  $\frac{\partial f_x}{\partial \beta_{x0}} = 0$  leads to

$$442 \quad \beta_{x0} = \rho \sqrt{\frac{(\theta^2 + \theta \sin \theta + 4 \cos \theta - 4)}{\theta(\theta - \sin \theta)}} \approx \frac{\rho \theta}{2\sqrt{15}}.$$

443 Summarizing, the extreme value of  $f_x$  is realized when

$$444 \quad \alpha_{x0} = 0, \beta_{x0} \approx \frac{\rho \theta}{2\sqrt{15}}, D_{x0} \approx \frac{\rho \theta^2}{24}, D'_{x0} = 0,$$

445 which means

$$446 \quad \mathcal{H}_{x0} = \rho \frac{\left( 1 - \frac{\sin \frac{\theta}{2}}{\frac{\theta}{2}} \right)^2}{\sqrt{\frac{(\theta^2 + \theta \sin \theta + 4 \cos \theta - 4)}{\theta(\theta - \sin \theta)}}} \approx \frac{5\rho\theta^3}{96\sqrt{15}}, \quad (72)$$

447 and

$$448 \quad f_{x,\min} = \rho \left( 1 - \frac{\sin \theta}{\theta} \right) \sqrt{\frac{(\theta^2 + \theta \sin \theta + 4 \cos \theta - 4)}{\theta(\theta - \sin \theta)}} \approx \frac{\rho \theta^3}{12\sqrt{15}}. \quad (73)$$

449 One can check that this is the minimum value of  $f_x$ . Note that 450  $f_{x,\min} = \frac{8}{5} \mathcal{H}_{x0}$ . Under these conditions we get the minimum

451 horizontal emittance

$$452 \quad \epsilon_{x,\min} = C_q \frac{\gamma^2}{J_x} \frac{\theta^3}{12\sqrt{15}}. \quad (74)$$

453 The above results are consistent with the classical results of 454 Teng [29]. For practical use, and considering nominally  $J_x \approx 455 1$ , the above scaling can be written as

$$456 \quad \epsilon_{x,\min} [\text{nm}] = 31.6 E_0^2 [\text{GeV}] \theta^3 [\text{rad}]. \quad (75)$$

457 For example, if  $E_0 = 6$  GeV and  $\theta = \frac{2\pi}{300}$  rad, we have 458  $\epsilon_{x,\min} = 10.4$  pm.

## B. Theoretical Minimum Longitudinal Emittance

459

460 Now we analyze the theoretical minimum longitudinal 461 emittance. Similar to the horizontal direction, we have

$$462 \quad \epsilon_z = C_q \frac{\gamma^2}{J_z} \frac{1}{\rho} f_z(\alpha_{z0}, \beta_{z0}, D_{x0}, D'_{x0}), \quad (76)$$

463 with

$$464 \quad f_z(\alpha_{z0}, \beta_{z0}, D_{x0}, D'_{x0}) = \frac{1}{\theta} \int_{-\frac{\theta}{2}}^{\frac{\theta}{2}} \beta_z(\alpha) d\alpha, \quad (77)$$

465 which can be interpreted as the average value of  $\beta_z$  in dipoles. 466 Then

$$467 \quad \begin{aligned} \frac{\partial f_z}{\partial \alpha_{z0}} &= \alpha_{z0} \mathcal{G}(\rho, \theta, D_{x0}, D'_{x0}, \beta_{z0}) + D'_{x0} 2\rho \left( 1 - \frac{\sin \frac{\theta}{2}}{\frac{\theta}{2}} \right), \\ \frac{\partial f_z}{\partial D'_{x0}} &= \alpha_{z0} 2\rho \left( 1 - \frac{\sin \frac{\theta}{2}}{\frac{\theta}{2}} \right) \\ &+ D'_{x0} \frac{(1 + \alpha_{z0}^2) \rho^2 \left( 3 - 4 \frac{\sin \frac{\theta}{2}}{\frac{\theta}{2}} + \frac{\sin \theta}{\theta} \right)}{\beta_{z0}}, \end{aligned} \quad (78)$$

468 where the lengthy explicit expression of 469  $\mathcal{G}(\rho, \theta, D_{x0}, D'_{x0}, \beta_{z0})$  is omitted here. Similar to the 470 analysis of transverse minimum emittance, we notice again 471 that the requirement of  $\frac{\partial f_z}{\partial \alpha_{z0}} = 0$  and  $\frac{\partial f_z}{\partial D'_{x0}} = 0$  leads to 472  $\alpha_{z0} = 0$  and  $D'_{x0} = 0$ . Under the above conditions, then

$$473 \quad \frac{\partial f_z}{\partial D_{x0}} = \frac{D_{x0} \left( 1 - \frac{\sin \theta}{\theta} \right) - \rho \left( 1 - \frac{\sin \theta}{\theta} - 2 \frac{\sin \frac{\theta}{2}}{\frac{\theta}{2}} + 2 \cos \frac{\theta}{2} \right)}{\beta_{z0}}. \quad (79)$$

474 The requirement of  $\frac{\partial f_z}{\partial D_{x0}} = 0$  leads to

$$475 \quad D_{x0} = \frac{\rho \left( 1 - \frac{\sin \theta}{\theta} - 2 \frac{\sin \frac{\theta}{2}}{\frac{\theta}{2}} + 2 \cos \frac{\theta}{2} \right)}{1 - \frac{\sin \theta}{\theta}} \approx -\frac{\rho \theta^2}{40}. \quad (80)$$

476 Under the above conditions, then

$$477 \quad \frac{\partial f_z}{\partial \beta_{z0}} = 1 - \frac{\rho^2 (\theta^4 - 12\theta^2 - (\theta^2 - 48)\theta \sin \theta - 12(\theta^2 - 4)\cos \theta - 48)}{12\theta(\theta - \sin \theta)\beta_{z0}^2}. \quad (81)$$

478 The requirement of  $\frac{\partial f_z}{\partial \beta_{z0}} = 0$  leads to

$$479 \quad \beta_{z0} = \rho \sqrt{\frac{(\theta^4 - 12\theta^2 - (\theta^2 - 48)\theta \sin \theta - 12(\theta^2 - 4)\cos \theta - 48)}{12\theta(\theta - \sin \theta)}} \approx \frac{\rho\theta^3}{120\sqrt{7}}, \quad (82)$$

480 Summarizing, the extreme value of  $f_z$  is realized when

$$481 \quad \alpha_{z0} = 0, \beta_{z0} \approx \frac{\rho\theta^3}{120\sqrt{7}}, D_{x0} \approx -\frac{\rho\theta^2}{40}, D'_{x0} = 0, \quad (83)$$

482 and

$$483 \quad f_{z,\min} = \rho \sqrt{\frac{(\theta^4 - 12\theta^2 - (\theta^2 - 48)\theta \sin \theta - 12(\theta^2 - 4)\cos \theta - 48)}{3\theta(\theta - \sin \theta)}} \approx \frac{\rho\theta^3}{60\sqrt{7}}. \quad (84)$$

484 One can check that this is the minimum value of  $f_z$ . Note that  
485  $f_{z,\min} = 2\beta_{z0}$ . Under these conditions we get the minimum  
486 longitudinal emittance

$$487 \quad \epsilon_{z,\min} = C_q \frac{\gamma^2}{J_z} \frac{\theta^3}{60\sqrt{7}}. \quad (85)$$

488 The above result has also been given in Ref. [7]. For practical  
489 use, and considering nominally  $J_z \approx 2$ , the above scaling can  
490 be written as

$$491 \quad \epsilon_{z,\min} [\text{nm}] = 4.62 E_0^2 [\text{GeV}] \theta^3 [\text{rad}]. \quad (86)$$

492 For example, if  $E_0 = 600 \text{ MeV}$  and  $\theta = \frac{2\pi}{50} \text{ rad}$ , we have  
493  $\epsilon_{z,\min} = 3.3 \text{ pm}$ .

494 Here we remind the readers that in reality it may not be  
495 easy to reach the optimal conditions Eq. (83) for all the  
496 dipoles in a ring. This is based on the observation that when  
497 we realize Eq. (83) at the dipole center, the dipole as a whole  
498 will have a nonzero  $R_{56}$  or more accurately a nonzero phase  
499 slippage. So to make the longitudinal optics identical in dif-  
500 ferent dipoles, there should be RF or laser modulator kicks  
501 between neighboring dipoles, otherwise the required drift  
502 space between each two dipoles will be very long to com-  
503 pensate this nonzero phase slippage [7]. It may not be easy  
504 to apply too many RF cavities or laser modulators in a ring to  
505 manipulate the longitudinal optics, while in the transverse di-  
506 mension it is straightforward to implement many quadrupoles  
507 to manipulate the transverse optics. Instead, we may choose  
508 a more practical strategy to realize small longitudinal emit-  
509 tance, which is letting each half of the bending magnet be  
510 isochronous, and the longitudinal optics for each dipole can  
511 then be identical. This can be realized by requiring

$$512 \quad \alpha_{z0} = 0, \beta_{z0} \approx \frac{\rho\theta^3}{12\sqrt{210}}, D_{x0} \approx -\frac{\rho\theta^2}{24}, D'_{x0} = 0. \quad (87)$$

513 In this case, we still have  $f_z = 2\beta_{z0}$ . Under such conditions,  
514 the minimum longitudinal emittance is [17]

$$515 \quad \epsilon_{z,\min,ISO} = C_q \frac{\gamma^2}{J_z} \frac{\theta^3}{6\sqrt{210}}. \quad (88)$$

516 The emittance given in Eq. (88) is larger than the real theo-  
517 retical minimum Eq. (86), but offers a more practical refer-  
518 ence. For practical use, and considering nominally  $J_z \approx 2$ ,  
519 the above scaling can be written as

$$520 \quad \epsilon_{z,\min,ISO} [\text{nm}] = 8.44 E_0^2 [\text{GeV}] \theta^3 [\text{rad}]. \quad (89)$$

521 Based on this emittance and  $\beta_{z0}$ , we can know the bunch  
522 length at the dipole center contributed from the longitudinal  
523 emittance. We remind the readers that the bunch length can in  
524 principle be even smaller than this value, by pushing  $\beta_{z0}$  to an  
525 even smaller value, although the longitudinal emittance will  
526 actually grow then since  $\beta_z$  will diverge faster when going  
527 away from the dipole center. If the ring works in a longitu-  
528 dinal weak focusing regime to be introduced in next section,  
529 there is actually a lower limit of bunch length in this pro-  
530 cess, which is a factor of  $\sqrt{2}$  smaller than the bunch length  
531 given by conditions of Eqs. (89) and (87). The energy spread  
532 will diverge when we push the bunch length to this limit [30].  
533 Putting in the numbers, we have this lower limit of bunch  
534 length in a longitudinal weak focusing ring [17]

$$535 \quad \sigma_{z,\min,ISO} [\mu\text{m}] = 4.93 \rho^{\frac{1}{2}} [\text{m}] E_0 [\text{GeV}] \theta^3 [\text{rad}]. \quad (90)$$

536 For example, if  $E_0 = 600 \text{ MeV}$ ,  $\theta = \frac{2\pi}{50} \text{ rad}$  and  $\rho = 1.5 \text{ m}$   
537 which corresponds to a bending field strength  $B_0 = 1.33 \text{ T}$ ,  
538 then  $\sigma_{z,\min,ISO} = 7.2 \text{ nm}$ .

### C. Application of Transverse Gradient Bend

540 The previous analysis assumes that the transverse gradient  
541 of the bending field is zero. Now we consider the applica-  
542 tion of transverse gradient bending (TGB) magnets to lower  
543 the horizontal and longitudinal emittances. For simplicity, we  
544 will consider the case of a constant gradient. The transfer  
545 matrix of a sector bending magnet with a constant transverse  
546 gradient  $n = -\frac{\rho}{B_y} \frac{\partial B_y}{\partial x}$  is

$$\mathbf{B}_{\text{TGB}}(\alpha) = \begin{pmatrix}
\cos(\sqrt{1-n}\alpha) & \frac{\rho}{\sqrt{1-n}} \sin(\sqrt{1-n}\alpha) & 0 & 0 \\
-\frac{\sqrt{1-n}}{\rho} \sin(\sqrt{1-n}\alpha) & \cos(\sqrt{1-n}\alpha) & 0 & 0 \\
0 & 0 & \cos(\sqrt{n}\alpha) & \frac{\rho}{\sqrt{n}} \sin(\sqrt{n}\alpha) \\
0 & 0 & -\frac{\sqrt{n}}{\rho} \sin(\sqrt{n}\alpha) & \cos(\sqrt{n}\alpha) \\
-\frac{1}{\sqrt{1-n}} \sin(\sqrt{1-n}\alpha) & -\frac{\rho}{1-n} (1 - \cos(\sqrt{1-n}\alpha)) & 0 & 0 \\
0 & 0 & 0 & 0 \\
0 & \frac{\rho}{1-n} (1 - \cos(\sqrt{1-n}\alpha)) & 0 & 0 \\
0 & \frac{1}{\sqrt{1-n}} \sin(\sqrt{1-n}\alpha) & 0 & 0 \\
0 & 0 & 0 & 0 \\
1 & \frac{\rho\alpha}{\gamma^2} + \frac{\rho}{(1-n)^{\frac{3}{2}}} (-\sqrt{1-n}\alpha + \sin(\sqrt{1-n}\alpha)) & 0 & 0 \\
0 & 1 & 0 & 0
\end{pmatrix}. \quad (91)$$

547

548

### 1. Horizontal Emittance

549 Following similar steps presented in the above analysis, we  
550 find the minimum value of  $f_x$  in Eq. (65) is now realized when

$$\begin{aligned}
\alpha_{x0} &= 0, \beta_{x0} \approx \frac{\rho\theta}{2\sqrt{15}} \left[ 1 + \frac{(1-n)\theta^2}{140} \right] + \mathcal{O}(\theta^6), \\
D_{x0} &\approx \frac{\rho\theta^2}{24} \left[ 1 - \frac{(1-n)\theta^2}{48} \right] + \mathcal{O}(\theta^6), D'_{x0} = 0,
\end{aligned} \quad (92)$$

552 where  $\mathcal{O}(\theta^n)$  means terms of order  $\theta^n$  and higher, which  
553 means

$$\mathcal{H}_{x0} = \frac{D_{x0}^2}{\beta_{x0}} \approx \frac{5\rho\theta^3}{96\sqrt{15}} \left[ 1 - \frac{9(1-n)\theta^2}{280} \right] + \mathcal{O}(\theta^7), \quad (93)$$

555 and

$$f_{x,\min} \approx \frac{\rho\theta^3}{12\sqrt{15}} \left[ 1 - \frac{3(1-n)\theta^2}{70} \right] + \mathcal{O}(\theta^7). \quad (94)$$

557 So we have

$$\epsilon_{x,\min,\text{TGB}} = C_q \frac{\gamma^2}{J_x} \frac{\theta^3}{12\sqrt{15}} \left[ 1 - \frac{3(1-n)\theta^2}{70} \right]. \quad (95)$$

559 Therefore, the impact of the transverse gradient on the theo-  
560 retical minimum emittance is on the higher order of the bend-  
561 ing angle of each magnet. However, we should recognize that  
562  $n$  can be a quite large value in practice. So its impact may  
563 actually be not small. In addition, a transverse gradient bend  
564 can also affect the damping partition, whose details we do not  
565 go into here.

566

### 2. Longitudinal Emittance

567 Similarly, using TGB, the minimum value of  $f_z$  in Eq. (77)  
568 is realized when

$$\begin{aligned}
\alpha_{z0} &= 0, \beta_{z0} \approx \frac{\rho\theta^3}{120\sqrt{7}} \left[ 1 + \frac{(1-n)\theta^2}{90} \right] + \mathcal{O}(\theta^7), \\
D_{x0} &\approx -\frac{\rho\theta^2}{40} \left[ 1 + \frac{19(1-n)\theta^2}{1680} \right] + \mathcal{O}(\theta^6), D'_{x0} = 0,
\end{aligned} \quad (96)$$

569 and

$$f_{z,\min} \approx \frac{\rho\theta^3}{60\sqrt{7}} \left[ 1 + \frac{(1-n)\theta^2}{90} \right] + \mathcal{O}(\theta^7). \quad (97)$$

572 Note that  $f_{z,\min} = 2\beta_{z0}$  still holds here. So we have

$$\epsilon_{z,\min,\text{TGB}} = C_q \frac{\gamma^2}{J_z} \frac{\theta^3}{60\sqrt{7}} \left[ 1 + \frac{(1-n)\theta^2}{90} \right]. \quad (98)$$

## D. Application of Longitudinal Gradient Bend

573 We can also apply longitudinal gradient bends (LGBs) to  
574 lower the transverse and longitudinal emittance. For simplic-  
575 ity, we will study the case of a LGB consisting of several  
576 sub-dipoles with each a constant bending radius. Further, we  
577 will assume each sub-dipole is a sector dipole. The analysis  
578 for the case of rectangular dipoles is similar, as long as the  
579 impact of edge angles on transfer matrix and damping parti-  
580 tion have been properly handled. Now we investigate the case  
581 of sector sub-dipoles. For example, we may choose to let the  
582 LGB has a symmetric structure

$$(\rho_2, \theta_2), (\rho_1, \theta_1), (\rho_0, 2\theta_0), (\rho_1, \theta_1), (\rho_2, \theta_2) \quad (99)$$

585 The total bending angle of such a LGB is  $\theta_T = 2(\theta_0 + \theta_1 +$   
586  $\theta_2)$ , and the total length is  $2(\rho_0\theta_0 + \rho_1\theta_1 + \rho_2\theta_2)$ . Note that  
587  $\rho_i\theta_i \geq 0$ . We use this structure as an example for the analysis.  
588 The presented method however applies also to a more general  
589 setup.

### 1. Horizontal Emittance

592 Now we calculate the theoretical minimum horizontal  
593 emittance by invoking LGBs with each the structure given  
594 in Eq. (99). Still we assume all the LGB setup in the ring and  
595 optical functions in each LGB are identical, then

$$\epsilon_x = C_q \frac{\gamma^2}{J_x} I_{5x}(\alpha_{x0}, \beta_{x0}, D_{x0}, D'_{x0}) \quad (100)$$

597 with

598

$$I_{5x}(\alpha_{x0}, \beta_{x0}, D_{x0}, D'_{x0}) = \frac{1}{2 \left( \frac{\theta_0}{\rho_0} + \frac{\theta_1}{\rho_1} + \frac{\theta_2}{\rho_2} \right)} \int_{-(\rho_0\theta_0 + \rho_1\theta_1 + \rho_2\theta_2)}^{(\rho_0\theta_0 + \rho_1\theta_1 + \rho_2\theta_2)} \frac{\mathcal{H}_x(s)}{|\rho(s)|^3} ds. \quad (101)$$

599 Note that the dimension of  $I_{5x}$  here is equivalent to  $\frac{f_x}{\rho}$  given 603 that given in Eq. (62), but note that here for different part 600 in previous sections. The mathematical problem is then to 604 (sub-dipole) of the LGBs, we should apply the transfer ma- 605 trix from the middle point of the LGB to the corresponding 606 location. Following similar procedures, we find that to get 607 the minimum emittance, we still need  $\alpha_{x0} = 0$  and  $D'_{x0} = 0$ . 608 Then we have  $\mathcal{H}_x(-s) = \mathcal{H}_x(s)$ , which means

609

$$I_{5x} = \frac{1}{\left( \frac{\theta_0}{\rho_0} + \frac{\theta_1}{\rho_1} + \frac{\theta_2}{\rho_2} \right)} \left( \int_0^{\rho_0\theta_0} \frac{\mathcal{H}_x(s)}{|\rho_0|^3} ds + \int_{\rho_0\theta_0}^{\rho_0\theta_0 + \rho_1\theta_1} \frac{\mathcal{H}_x(s)}{|\rho_1|^3} ds + \int_{\rho_0\theta_0 + \rho_1\theta_1}^{\rho_0\theta_0 + \rho_1\theta_1 + \rho_2\theta_2} \frac{\mathcal{H}_x(s)}{|\rho_2|^3} ds \right). \quad (102)$$

610 We find a general analytical discussion of the combination 611 of  $\rho_i$  and  $\theta_i$  cumbersome. Here for simplicity and to get a 612 concrete feeling, we first consider one specific case:  $\rho_i = 613 \rho_0 2^i$ . The physical consideration behind this choice is that 614  $\mathcal{H}_x$  will be smaller in the central part of the bending magnet, 615 and larger at the entrance and exit. So we make the bending 616 field in the center stronger and smaller at the entrance and 617 exit region, such that to minimize the quantum excitation of 618 horizontal emittance. For example, we may choose

619

$$\left( 4\rho, \frac{\theta}{8} \right), \left( 2\rho, \frac{\theta}{8} \right), \left( \rho, \frac{\theta}{4} \right), \left( \rho, \frac{\theta}{4} \right), \left( 2\rho, \frac{\theta}{8} \right), \left( 4\rho, \frac{\theta}{8} \right). \quad (103)$$

620 The total length of such a LGB is  $2\rho\theta$ . The minimum value of 621  $I_{5x}$  and horizontal emittance  $\epsilon_x$  in this case is realized when

622

$$\alpha_{x0} = 0, \beta_{x0} \approx \frac{\sqrt{\frac{35977}{133755}} \rho \theta}{4}, D_{x0} \approx \frac{127 \rho \theta^2}{7104}, D'_{x0} = 0, \quad (104)$$

623 which means

624

$$\mathcal{H}_{x0} = \frac{D_{x0}^2}{\beta_{x0}} \approx 0.183 \times \frac{5}{96\sqrt{15}} \rho \theta^3, \quad (105)$$

625 and

626

$$I_{5x,\min} \approx 0.344 \times \frac{\theta^3}{12\sqrt{15}}, \quad (106)$$

627 which compared to Eq. (74) means the theoretical minimum 628 horizontal emittance can now become about one third of the 629 case with no longitudinal gradient. So application of LGB is 630 quite effective in lowering the transverse emittance.

631 The next question is: what is the optimal combination of 632  $\theta_{0,1,2}$  and  $\rho_{0,1,2}$ ? This question is not straightforward to 633 answer by analytical method. Here we refer to numerical 634 method to do the optimization directly.  $\alpha_{x0}$  and  $D'_{x0}$  are set 635 to be zero in the optimization. The variables in the numer- 636 ical optimization are  $(\theta_0, \theta_1, \theta_2, \rho_0, \rho_1, \rho_2, \beta_{x0}, D_{x0})$ . Two

637 optimization goals are  $\frac{\epsilon_{x,LGB}}{\epsilon_{x,UB}}$  and the length of a LGB  $L_{LGB}$ , 638 where  $\epsilon_{x,UB}$  is the theoretical minimum emittance of applying 639 bending magnet without longitudinal gradient. We require 640  $\rho_i \theta_i > 0$ . In the optimization, we keep the total bending an- 641 gle of a LGB a constant value. The optimization result of one 642 specific case where  $\theta_T = 2(\theta_0 + \theta_1 + \theta_2) = \frac{\pi}{10}$  is presented 643 in Fig. 2, from which we can see that in this case by applying 644 LGBs, in principle we can lower the horizontal emittance by 645 a factor of five with a reasonable length of the LGB. Note that 646 in this optimization and the one in the following section, we 647 have assumed that  $\rho_i > 0$ . But the formalism applies also to 648 the case with anti-bends.

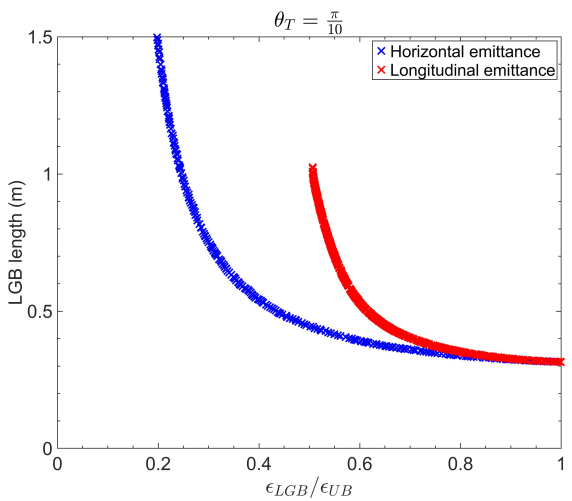


Fig. 2. Application of LGB to minimize horizontal (blue) and longitudinal (red) emittance, respectively. The subscripts “LGB” and “UB” represent longitudinal gradient bend and uniform bend, respectively.

649

## 2. Longitudinal Emittance

652 with

650

Similarly, for the longitudinal emittance we have

651

$$\epsilon_z = C_q \frac{\gamma^2}{J_z} I_{5z}(\alpha_{z0}, \beta_{z0}, D_{x0}, D'_{x0}) \quad (107)$$

653

$$I_{5z}(\alpha_{z0}, \beta_{z0}, D_{x0}, D'_{x0}) = \frac{1}{2 \left( \frac{\theta_0}{\rho_0} + \frac{\theta_1}{\rho_1} + \frac{\theta_2}{\rho_2} \right)} \oint_{-(\rho_0\theta_0 + \rho_1\theta_1 + \rho_2\theta_2)}^{(\rho_0\theta_0 + \rho_1\theta_1 + \rho_2\theta_2)} \frac{\beta_z(s)}{|\rho(s)|^3} ds. \quad (108)$$

654 For example, if we still choose the setup given in Eq. (103),  
 655 the minimum value of  $I_{5z}$  and longitudinal emittance in this  
 656 case is realized when

657

$$\alpha_{z0} = 0, \beta_{z0} \approx \frac{\sqrt{\frac{36233641}{62419}} \rho \theta^3}{7680}, \quad (109)$$

$$D_{x0} \approx -\frac{169 \rho \theta^2}{9640}, D'_{x0} = 0,$$

658 and

659

$$F_{z,\min} \approx 0.838 \times \frac{\theta^3}{60\sqrt{7}}, \quad (110)$$

660 which compared with Eq. (85) means the theoretical mini-  
 661 mum longitudinal emittance now can become a bit smaller  
 662 than the case of applying a constant bending field.

663 Similar to what presented just now about lowering trans-  
 664 verse emittance, we also apply the numerical optimization to  
 665 choose a better combination of  $\rho_i$  and  $\theta_i$  in lowering longitu-  
 666 dinal emittance. Presented in Fig. 2 is the result of one spe-  
 667 cific case where  $\theta_T = 2(\theta_0 + \theta_1 + \theta_2) = \frac{\pi}{10}$ , from which we  
 668 can see that in this case by applying LGBs, in principle we  
 669 can lower the longitudinal emittance by a factor of two with  
 670 a reasonable length of the LGB. So generally, LGB is more  
 671 effective in lowering the horizontal emittance, compared to  
 672 lowering the longitudinal emittance.

673

## IV. STEADY-STATE MICRO-BUNCHING STORAGE RINGS

674

675 In this section, based on the theoretical minimum emittance  
 676 derived in the last section, we conduct some key analysis of  
 677 three specific SSMB scenarios along the thinking of realiz-  
 678 ing nm bunch length and high-average-power EUV radiation,

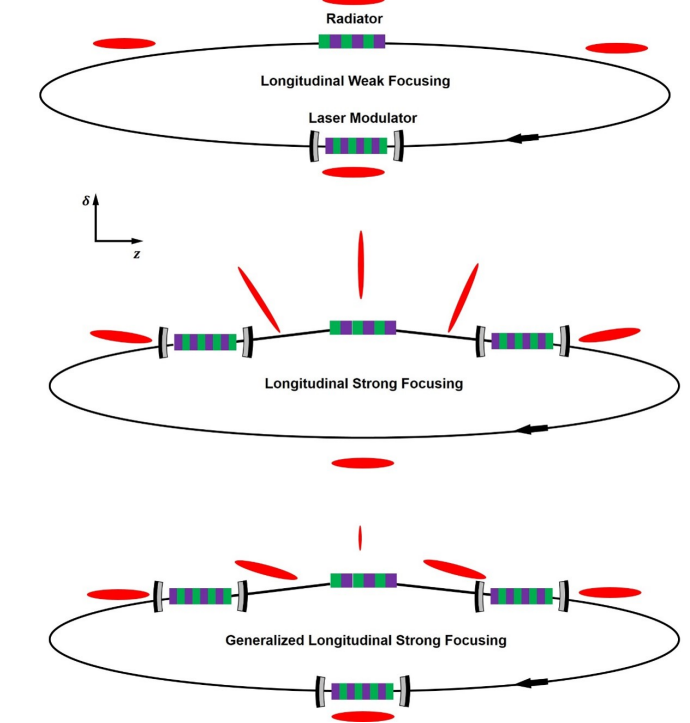


Fig. 3. Schematic layout of longitudinal weak focusing (LWF), longitudinal strong focusing (LSF), generalized longitudinal strong focusing (GLSF) SSMB storage rings. The red ellipses illustrate the beam distribution in longitudinal phase space. To realize the same bunch length compression ratio, the required energy chirp strength in the GLSF scheme is much smaller than that of LSF.

679 i.e., longitudinal weak focusing (LWF), longitudinal strong  
 680 focusing (LSF) and generalized longitudinal strong focusing  
 681 (GLSF). The analysis aims to answer the question why GLSF  
 682 SSMB is our present choice in realizing high-average-power  
 683 EUV radiation. Before going into the details, here first we use  
 684 Table 1 and Fig. 3 to briefly summarize the characteristics of  
 685 these three scenarios. Note that in Fig. 3, the beam distri-  
 686 bution in longitudinal phase space are all of the microbunch,  
 687 whose length is at the laser wavelength range. We also re-  
 688 mind the readers that in the figure, the energy chirp strength  
 689 in GLSF is much smaller than that of LSF. The physical rea-  
 690 son should be clear with the analysis in this section unfolded.

TABLE 1. Main characteristics of LWF, LSF and GLSF SSMB storage rings.

LWF	$\nu_s \ll 1$	$\frac{\beta_{z,\max}}{\beta_{z,\min}} \approx 1$	2D phase space dynamics
LSF	$\nu_s \sim 1$	$\frac{\beta_{z,\max}}{\beta_{z,\min}} \gg 1$	2D phase space dynamics
GLSF	-	$\frac{\sigma_{z,\max}}{\sigma_{z,\min}} \gg 1$	4D or 6D phase space dynamics

In all the example calculations to be shown in the following part of this paper, we set the electron energy to be  $E_0 = 600$  MeV, and modulation laser wavelength to be  $\lambda_L = 1064$  nm. The choice of this beam energy is because it is an appropriate energy for EUV generation using an undulator as radiator. On one hand, it is not too high, otherwise the laser modulation will become more difficult, which means more laser power is needed to imprint a given modulation strength. On the other hand, it is not too low otherwise intra-beam scattering (IBS) could become too severe. Actually as we will see in Sec. VIII, IBS is a fundamental issue in SSMB storage rings which require at least one of the three eigen emittances to be small. The reason for choosing this laser wavelength is due to the fact that it is the common wavelength range for high-power optical enhancement cavity, which is used together with an undulator to form the laser modulator of SSMB.

### A. Longitudinal Weak Focusing

Now we start the quantitative analysis. We start from the longitudinal weak focusing (LWF) SSMB ring. In a LWF ring with a single laser modulator (LM) as shown in Fig. 3, the single-particle longitudinal dynamics turn by turn is modeled as

$$\begin{aligned} \delta_{n+1} &= \delta_n + \frac{h}{k_L} \sin(k_L z_n), \\ z_{n+1} &= z_n - \eta C_0 \delta_{n+1}, \end{aligned} \quad (111)$$

where the subscripts  $n, n+1$  means the number of revolutions,  $h$  is the energy chirp strength around the zero-crossing phase,  $k_L = \frac{2\pi}{\lambda_L}$  is the wavenumber of the modulation laser and  $\lambda_L$  is the laser wavelength,  $C_0$  is the ring circumference, and

$$\eta = \frac{\Delta T/T_0}{\Delta E/E_0} = \frac{1}{C_0} \oint \left( \frac{D_x}{\rho} - \frac{1}{\gamma^2} \right) ds \quad (112)$$

is the phase slippage factor of the ring. Note that in the above model, we have assumed that the radiation energy loss in an SSMB storage ring will be compensated by other system instead of the laser modulators, so the microbunching will be formed around the laser zero-crossing phase. The laser in principle can also be used for energy compensation, but is not a cost-effective choice and will also limit the output radiation power. We can use induction linacs or RF cavities to supply the radiation energy loss. Linear stability of Eq. (111) around the zero-crossing phase requires that  $0 < h\eta C_0 < 4$ . To avoid strong chaotic dynamics which may destroy the regular longitudinal phase space structure, an empirical criterion is

$$0 < h\eta C_0 \lesssim 0.1. \quad (113)$$

In a LWF ring, when the synchrotron tune  $|\nu_s| \approx \sqrt{h\eta C_0}/2\pi \ll 1$ , the longitudinal beta function at the center of laser modulator is [17]

$$\beta_{zM} \approx \sqrt{\frac{\eta C_0}{h}}. \quad (114)$$

Note that in this paper, we will use subscript 'M' to represent modulator, and 'R' to represent radiator. From Eq. (113) we then require

$$|\eta C_0| \lesssim \frac{\beta_{zM}}{\sqrt{10}}. \quad (115)$$

Now we can use the previous analysis of theoretical minimum longitudinal emittance, more specifically Eq. (90), and the above result to do some evaluation for a LWF ring. If  $E_0 = 600$  MeV, the bending radius of dipoles in the ring  $\rho_{ring} = 1.5$  m which corresponds to a bending field strength  $B_{ring} = 1.33$  T, and if our desired bunch length is  $\sigma_z = 50$  nm ( $\sigma_z \lesssim \lambda_L/20$  for microbunches to be safely stored in the optical microbuckets for  $\lambda_L = 1064$  nm), then we may need  $\sigma_{z,min,ISO} \leq 50/\sqrt{2}$  nm to avoid significant energy widening when we reach the desired bunch length. From Eq. (90) we then need  $\theta \leq \frac{2\pi}{30}$  rad. Therefore, we need at least 30 bending magnets in the ring. Assuming the length of each isochronous cell containing a bending magnet is 3 m, then the arc section of such a storage ring has a length of about 90 m. Considering the straight section for beam injection/extraction, radiation energy loss compensation, and insertion device for radiation generation, the circumference of such a ring could be 100 m to 120 m.

To reach the desired bunch length, according to Eq. (87) we need  $\beta_{zM} = \beta_{z0} = \rho\theta^3/12\sqrt{210}$ . In our present example case, if  $\rho = 1.5$  m,  $\theta = \frac{2\pi}{30}$ , then this value we need is  $\beta_{zM} = 79.2$   $\mu$ m. Then from Eq. (115) we have

$$|\eta C_0| \lesssim 25 \mu\text{m}. \quad (116)$$

If  $C_0 = 100$  m, then it means we need a phase slippage factor  $|\eta| \lesssim 2.5 \times 10^{-7}$ , which is a quite small value. If we want a bunch length even smaller than 50 nm at a beam energy of 600 MeV, then the required phase slippage will be too demanding to be realized using present technology. More details on the lattice design of an LWF SSMB ring which can store microbunches with a couple of 10 nm bunch length can be found in Ref. [16].

### B. Longitudinal Strong Focusing

After discussing the LWF SSMB ring, we now start the analysis of LSF. First we observe that the above analysis of LWF SSMB considers the case with only a single LM. When there are multiple LMs, for the longitudinal dynamics, it is similar to implementing multiple quadrupoles in the transverse dimension, and the beam dynamics can have more possibilities. Longitudinal strong focusing scheme for example can be invoked, not unlike its transverse counterpart which is the foundation of modern high-energy accelerators. Here we use a setup with two LMs for SSMB as an example to show the scheme of manipulating  $\beta_z$  around the ring using the strong focusing regime. The schematic layout of the ring is shown in Fig. 4. The treatment of cases with more LMs is similar.

We divide the ring into five sections from the transfer ma-

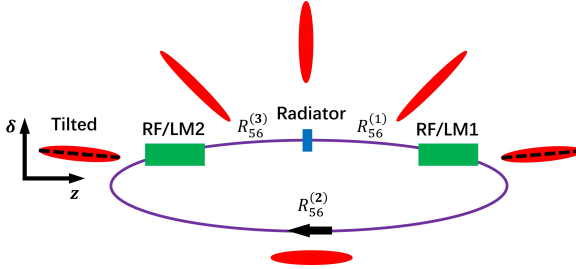


Fig. 4. A schematic layout of a storage ring using two RF systems for longitudinal strong focusing and an example beam distribution evolution in longitudinal phase space. (Figure from Ref. [8])

789 trix viewpoint, i.e., three longitudinal drifts ( $R_{56}$ ) and two  
790 LM kicks ( $h$ ), with the linear transfer matrices of the state  
791 vector in longitudinal ( $z, \delta$ )<sup>T</sup> given by

$$\begin{aligned} \mathbf{T}_{D1} &= \begin{pmatrix} 1 & R_{56}^{(1)} \\ 0 & 1 \end{pmatrix}, \quad \mathbf{T}_{LM1} = \begin{pmatrix} 1 & 0 \\ h_1 & 1 \end{pmatrix}, \\ \mathbf{T}_{D2} &= \begin{pmatrix} 1 & R_{56}^{(2)} \\ 0 & 1 \end{pmatrix}, \quad \mathbf{T}_{LM2} = \begin{pmatrix} 1 & 0 \\ h_2 & 1 \end{pmatrix}, \\ \mathbf{T}_{D3} &= \begin{pmatrix} 1 & R_{56}^{(3)} \\ 0 & 1 \end{pmatrix}. \end{aligned} \quad (117)$$

793 Then the one-turn map at the radiator center is

$$794 \quad \mathbf{M}_R = \mathbf{T}_{D3} \mathbf{T}_{LM2} \mathbf{T}_{D2} \mathbf{T}_{LM1} \mathbf{T}_{D1}.$$

795 For the generation of coherent radiation, we usually want the  
796 bunch length to reach its minimum at the radiator, then we  
797 need  $\alpha_z = 0$  at the radiator.

798 With the primary goal of presenting the principle, instead  
799 of a detailed design, here for simplicity we focus on one spe-  
800 cial case:  $R_{56}^{(1)} = R_{56}^{(3)}$ ,  $h_1 = h_2 = h$ . Denote

$$801 \quad \zeta_1 \equiv 1 + R_{56}^{(1)} h, \quad \zeta_2 \equiv 1 + \frac{R_{56}^{(2)}}{2} h,$$

802 we then have

$$803 \quad \mathbf{M}_R = \begin{pmatrix} 2\zeta_1\zeta_2 - 1 & 2\frac{\zeta_1\zeta_2 - \zeta_1}{h} \\ 2h\zeta_2 & 2\zeta_1\zeta_2 - 1 \end{pmatrix}. \quad (120)$$

804 The linear stability requires  $|2\zeta_1\zeta_2 - 1| < 1$  which means  
805  $0 < \zeta_1\zeta_2 < 1$ .

806 We remind the readers that the analysis above in this sub-  
807 section about LSF has been presented before in Ref. [17] and  
808 is presented here again for completeness. Now we try to go  
809 further to gain more insight. The longitudinal beta function at  
810 the radiator is

$$811 \quad \beta_{zR} = \frac{2\frac{\zeta_1^2\zeta_2 - \zeta_1}{h}}{\sin \Phi_z} = \frac{1}{|h|} \sqrt{\frac{\zeta_1(1 - \zeta_1\zeta_2)}{\zeta_2}}, \quad (121)$$

812 where  $\Phi_z = 2\pi\nu_s$  is the synchrotron phase advance per turn.

813 The longitudinal beta function at the opposite of the radiator,  
814 from where to LM2 has an  $R_{56}^{(2)} = \frac{R_{56}^{(2)}}{2}$ , is

$$815 \quad \beta_{zRO} = \frac{1}{|h|} \sqrt{\frac{\zeta_2(1 - \zeta_1\zeta_2)}{\zeta_1}}, \quad (122)$$

816 which can be obtained by switching  $\zeta_1$  and  $\zeta_2$  in the expres-  
817 sion of  $\beta_{zR}$  in Eq. (121). So we have

$$818 \quad \frac{\beta_{zRO}}{\beta_{zR}} = \frac{\zeta_2}{\zeta_1}. \quad (123)$$

819 The longitudinal beta function at the LM1 and LM2 (here we  
820 name them as modulators) is

$$821 \quad \beta_{zM} = \beta_{zR} + \frac{R_{56}^{(1)}}{\beta_{zR}}. \quad (124)$$

822 For efficient bunch compression from the place of modulator  
823 to the place of radiator, we have  $|\zeta_1| \ll 1$ . Then

$$824 \quad \frac{\beta_{zM}}{\beta_{zR}} = \frac{\zeta_1 - 2\zeta_1\zeta_2 + \zeta_2}{\zeta_1(1 - \zeta_1\zeta_2)} \approx \frac{\zeta_2}{\zeta_1(1 - \zeta_1\zeta_2)} = \frac{1}{h^2\beta_{zR}^2}, \quad (125)$$

825 from which we have the required energy chirp strength

$$826 \quad |h| \approx \frac{1}{\sqrt{\beta_{zR}\beta_{zM}}}. \quad (126)$$

827 This relation is similar to the theorems to be presented in  
828 Sec. V about transverse-longitudinal coupling-based bunch  
829 compression schemes which are the backbone of the GLSF  
830 scheme. The relation can also be casted as

$$831 \quad |h| \approx \frac{\sqrt{\epsilon_z/\beta_{zM}}}{\sqrt{\epsilon_z\beta_{zR}}} = \frac{\sqrt{\epsilon_z/\beta_{zM}}}{\sigma_{zR}}, \quad (127)$$

832 with  $\sigma_{zR} = \sqrt{\epsilon_z\beta_{zR}}$  being the bunch length at the radiator.

833 We now investigate the required energy chirp strength and  
834 modulation laser power based on the analysis. We assume  
835 that in a LSF ring, the longitudinal emittance is dominantly  
836 from the quantum excitation in ring dipoles. This assumption  
837 will be justified later to see if it is really the case. Further,  
838 we assume that the average longitudinal beta function at the  
839 dipoles equals that at the modulator, i.e.,  $\langle \beta_z \rangle = \beta_{zM}$ . Then  
840 the equilibrium longitudinal emittance given by the balance of  
841 quantum excitation and radiation damping in a ring consisting  
842 of iso-bending-magnets has the scaling

$$843 \quad \epsilon_{z,LSF} = C_q \frac{\gamma^2}{J_z} \frac{I_{5z}}{I_2} = C_q \frac{\gamma^2}{J_z} \frac{\frac{\langle \beta_z \rangle}{\rho_{ring}^3} 2\pi\rho_{ring}}{\frac{1}{\rho_{ring}^2} 2\pi\rho_{ring}} \propto \gamma^2 \frac{\beta_{zM}}{\rho_{ring}}, \quad (128)$$

844 which combining with Eq. (127) gives

$$845 \quad |h| \propto \frac{\gamma}{\sigma_{zR}\sqrt{\rho_{ring}}}. \quad (129)$$

846 Here,  $\sigma_{zR}$  is determined by our desired radiation wavelength.

847 Therefore, given the beam energy and desired bunch length,  
848 to lower the required energy chirp strength in LSF, we should  
849 use as large  $\rho_{ring}$  as possible which means as weak as bending  
850 magnet as possible. But note that the total length of the bend-  
851 ing magnets should be within a reasonable range. Also note

852 that when the bending magnets in the ring are very weak, the  
 853 assumption that the longitudinal emittance in a LSF ring is  
 854 dominantly from them will fail, since the quantum excitation  
 855 in the bending magnets will become weaker, while there are  
 856 other contributions like quantum excitation at the laser mod-  
 857 ulators.

858 We have mentioned in the introduction section that a short  
 859 bunch can generate coherent radiation. The parameter used to  
 860 quantify the capability of beam for coherent radiation gener-  
 861 ation is called bunching factor, and in the 1D case is defined  
 862 as

$$863 \quad b(\omega) = \int_{-\infty}^{\infty} \psi(z) e^{-i\frac{\omega}{c}z} dz, \quad (130)$$

864 with  $\omega$  the radiation frequency,  $\psi(z)$  the longitudinal  
 865 charge density distribution satisfying the normalization  
 866  $\int_{-\infty}^{\infty} \psi(z) dz = 1$ . We will present more indepth discussion  
 867 of bunching factor in Sec. VI A. The coherent radiation power  
 868 of a beam with  $N_p$  particles at frequency  $\omega$  is related to the  
 869 radiation of a single particle according to

$$870 \quad P_{\text{beam}}(\omega) = N_e^2 b^2(\omega) P_{\text{single}}(\omega). \quad (131)$$

871 For a Gaussian bunch with an RMS bunch length of  $\sigma_z$ , we  
 872 have  $b(\omega) = \exp\left[-\left(\frac{\omega}{c}\sigma_z\right)^2/2\right]$ . For significant 13.5 nm-  
 873 wavelength coherent EUV radiation generation, we may need  
 874  $\sigma_{zR} \lesssim 4$  nm which corresponds to  $b_{13.5 \text{ nm}} \gtrsim 0.18$ . To in-  
 875 crease the radiation power, we may need the radiator, which  
 876 is assumed to be an undulator, has a large period number  
 877  $N_u$  (for example  $N_u \approx 300$ ). To avoid significant bunch  
 878 lengthening from the energy spread and the undulator  $R_{56} =$   
 879  $2N_u\lambda_R$ , we then need  $N_u\lambda_R\sigma_{\delta} \lesssim \sigma_{zR}$ , which then requires  
 880 the energy spread at the radiator  $\sigma_{\delta R} \lesssim 1 \times 10^{-3}$ . So we  
 881 need  $\epsilon_z = \sigma_{zR}\sigma_{\delta R} \lesssim 4$  pm. Since in a LSF ring, as explained  
 882 we cannot make the optimal conditions Eq. (83) be satisfied  
 883 in all the bending magnets, a reasonable argument is that the  
 884 real longitudinal emittance should be at least a factor of two  
 885 larger than the true theoretical minimum, which then requires

$$886 \quad \epsilon_{z,\min} \lesssim 2 \text{ pm}. \quad (132)$$

887 Then according to Eq. (86), if  $E_0 = 600$  MeV, we need  
 888  $\theta \lesssim \frac{2\pi}{59}$ , which means 59 bending magnets are needed. As-  
 889 suming the length of each isochronous cell containing a bend-  
 890 ing magnet is 3 m, then the arc section of such a ring has  
 891 a length of about 177 m. Considering the straight section  
 892 for beam injection/extraction, radiation energy loss compen-  
 893 sation, and longitudinal strong focusing section, the circum-  
 894 ference of such a ring is about 200 m.

895 If  $\epsilon_z = 4$  pm, to get  $\sigma_{zR} \lesssim 4$  nm, we then need

$$896 \quad \beta_{zR} = \frac{\sigma_{zR}^2}{\epsilon_z} \lesssim 4 \text{ } \mu\text{m}. \quad (133)$$

897 From Eq. (126), given  $\beta_{zR}$ , we should apply as large  $\beta_{zM}$   
 898 as possible to decrease the energy chirp strength  $h$ . Since  
 899  $\beta_{z0} \propto \rho$  with  $\theta$  given, we will choose a reasonable large  
 900 bending radius for the dipoles in the ring. If  $\rho = 10$  m

901 which corresponds to  $B_0 = 0.2$  T and a total bending mag-  
 902 net length of 62.8 m, then the longitudinal beta function at  
 903 the dipole center required to reach the practical theoretical  
 904 minimum longitudinal emittance (see Eqs. (89) and (87)) is  
 905  $\beta_{z0} = \rho\theta^3/12\sqrt{210} = 69.5 \text{ } \mu\text{m}$ . Then we may let

$$906 \quad \beta_{zM} \approx 2\beta_{z0} \approx 139 \text{ } \mu\text{m}. \quad (134)$$

907 Then from Eqs. (126), (133) and (134), the energy chirp  
 908 strength required in such a LSF SSMB ring is

$$909 \quad |h| \approx \frac{1}{\sqrt{\beta_{zR}\beta_{zM}}} \gtrsim 4.24 \times 10^4 \text{ m}^{-1}. \quad (135)$$

910 According to Eq. (221) to be presented later about the laser  
 911 modulator induced energy chirp strength, if  $E_0 = 600$  MeV,  
 912 and for a modulator undulator with period  $\lambda_{uM} = 8$  cm  
 913 ( $B_{0M} = 1.13$  T), length  $L_{uM} = 1.6$  m, and for a laser with  
 914 wavelength  $\lambda_L = 1064$  m, to introduce the required energy  
 915 chirp strength, we need a laser power  $P_L \approx 1$  GW. This is a  
 916 large value and is three orders of magnitude higher than the  
 917 average stored laser power reachable in an optical enhance-  
 918 ment cavity at the moment [31], which is at the level of one  
 919 megawatt (MW). This makes the optical enhancement cavity  
 920 only work in a low duty cycle pulsed mode, thus limiting the  
 921 filling factor of the microbunched electron beam in the ring,  
 922 and thus limiting the average output EUV power.

923 We remind the readers that there is a subtle point in a LSF  
 924 SSMB ring if we take the nonlinear sinusoidal modulation  
 925 waveform into account, since the dynamical system is then  
 926 strongly chaotic and requires careful analysis to ensure a large  
 927 enough stable region for particle motion in the longitudinal  
 928 phase space. More details in this respect can be found in  
 929 Ref. [18].

930 Now for completeness of discussion, let us evaluate the  
 931 contribution of modulator undulators to longitudinal emit-  
 932 tance in our above example case, since there is also quantum  
 933 excitation at the modulators. The quantum excitation contri-  
 934 butions of two modulators to  $\epsilon_z$  in a LSF ring are

$$935 \quad \begin{aligned} \Delta\epsilon_{zM} &= C_q \frac{\gamma^2}{J_z} \frac{\Delta I_{5zM}}{I_2} \\ &= C_q \frac{\gamma^2}{J_z} \frac{1}{I_2} \times 2 \int_{-\frac{L_{uM}}{2}}^{\frac{L_{uM}}{2}} \frac{\beta_{zM}}{|\rho(s)|^3} ds \\ &= C_q \frac{\gamma^2}{J_z} \frac{1}{I_2} \times 2 \frac{\beta_{zM}}{\rho_{0M}^3} \frac{4}{3\pi} L_{uM}, \end{aligned} \quad (136)$$

936 where  $\Delta I_{5zM}$  is the contribution of two modulators to  $I_{5z}$  de-  
 937 fined in Eq. (54),  $\rho_{0M}$  is the bending radius at the peak mag-  
 938 netic field of the modulator. Put in the numbers, and taking  
 939 the approximation  $I_2 \approx \frac{2\pi}{\rho_{\text{ring}}}$  which means the radiation loss  
 940 is mainly from dipoles in the ring,  $J_z \approx 2$ , we have

$$941 \quad \Delta\epsilon_{zM} [\text{nm}] = 8.9 B_{\text{ring}}^{-1} [\text{T}] B_{0M}^3 [\text{T}] \beta_{zM} [\text{m}] L_{uM} [\text{m}]. \quad (137)$$

942 In our example case,  $B_{\text{ring}} = 0.2$  T,  $B_{0M} = 1.13$  T,  $\beta_{zM} =$   
 943  $139 \text{ } \mu\text{m}$ ,  $L_{uM} = 1.6$  m, we have

$$944 \quad \Delta\epsilon_{zM} = 14.3 \text{ pm}, \quad (138)$$

945 which is even larger than the desired 4 pm longitudinal emit-  
946 tance, and therefore is unacceptable.

947 The above evaluation of longitudinal emittance contribu-  
948 tion means we need to use a weaker or shorter modulator.  
949 Since our desired longitudinal emittance is  $\epsilon_z \lesssim 4$  pm, we  
950 need to control the contribution from two modulators to be  
951  $\Delta\epsilon_{zM} \lesssim 1$  pm since the ring dipoles will also contribute lon-  
952 gitudinal emittance with a theoretical minimum about 2 pm.  
953 For example, we may choose to weaken the modulator field  
954 by more than a factor of two. If  $\lambda_{uM} = 0.15$  m and  $B_{0M} =$   
955 0.435 T,  $L_{uM} = 1.5$  m, then the contribution of two modula-  
956 tors to longitudinal emittance is

$$957 \Delta\epsilon_{zM} = 0.76 \text{ pm}, \quad (139)$$

958 which should be acceptable for a target total longitudinal  
959 emittance of 4 pm. But then to introduce the desired energy  
960 chirp strength, we now need  $P_L \approx 2$  GW.

961 Note that in this updated parameter choice, there is still one  
962 issue we need take care. In the evaluation of quantum excita-  
963 tion contribution of modulators to longitudinal emittance, we  
964 have implicitly assumed that the longitudinal beta function  
965 does not change inside it. This is not true strictly speaking.  
966 The undulator itself has an  $R_{56} = 2N_u\lambda_0$ , with  $\lambda_0$  the funda-  
967 mental resonance wavelength of the undulator and in our case  
968 is the modulation laser wavelength. And the criterion whether  
969 the thin-lens approximation applies is to evaluate whether or  
970 not  $|hR_{56}| \ll 1$ , where  $R_{56}$  is that of the undulator. Here in  
971 this updated example, we have  $hR_{56} = h2N_u\lambda_L = 0.9$  for  
972 the modulator, which means that the thin-lens kick approxi-  
973 mation actually does not apply here. So more accurately we  
974 should use the thick-lens map of the modulator [17] to calcu-  
975 late the evolution of longitudinal beta function in the modu-  
976 lator, and then evaluate the contribution to longitudinal emit-  
977 tance.

978 With all the subtle points carefully handled, LSF as an-  
979 alyzed above in principle can realize the desired nm bunch  
980 length and thus generate coherent EUV radiation. The main  
981 issue of such an EUV source is the required modulation laser  
982 power (GW level) is too high and makes the optical enhance-  
983 ment cavity can only work in a low duty cycle pulsed mode,  
984 thus limiting the average EUV output power.

### 985 C. Generalized Longitudinal Strong Focusing

986 The previous analysis of LWF and LSF leads us to con-  
987 sider the generalized longitudinal strong focusing (GLSF)  
988 scheme [9]. The basic idea of GLSF is to take advantage  
989 of the ultrasmall natural vertical emittance in a planar elec-  
990 tron storage ring. More specifically, we will apply a par-  
991 tial transverse-longitudinal emittance exchange at the opti-  
992 cal laser wavelength range to achieve efficient microbunch-  
993 ing generation. As shown in Fig. 3, the schematic setup of  
994 a GLSF ring is very similar to that of a LSF ring. But as  
995 stressed before, the energy chirp strength required in GLSF is  
996 much smaller than that in the LSF scheme, which means the  
997 required modulation laser power can also be smaller. A sharp  
998 reader may also notice that in Fig. 3, the longitudinal phase

999 space area of beam is not conserved in the bunch compression  
1000 or harmonic generation section of a GLSF ring. The funda-  
1001 mental physical law like Liouville's theorem of course cannot  
1002 be violated in a symplectic system. The reason for this ap-  
1003 parent "contradiction" is that GLSF invokes 4D or 6D phase  
1004 space dynamics as summarized in Tab. 1, and what conserved  
1005 are the eigen emittances, instead of the projected emittances.  
1006 One may also note that in the plot, the phase space rotation di-  
1007 recton in the GLSF scheme is reversed after the radiator com-  
1008 pared to that before the radiator, while in the LSF scheme this  
1009 is not the case. In other words, in GLSF, we choose to make  
1010 the upstream and downstream modulations cancel each other.  
1011 In this sense, this setup is a special case of the reversible  
1012 seeding scheme of SSMB [32]. The reason of doing this is  
1013 that we want to make the system transverse-longitudinal cou-  
1014 pled only in a limited local region in the ring, the so called  
1015 GLSF section, such that we can maintain  $\mathcal{H}_y = 0$  being at  
1016 the majority places of the ring to minimize the quantum exci-  
1017 tation and IBS contribution to vertical emittance, thus keep-  
1018 ing the small vertical emittance of a planar uncoupled ring.  
1019 Further, this cancellation of nonlinear sinusoidal modulation  
1020 waveforms will make the nonlinear dynamics of the ring eas-  
1021 ier to handle. To make the modulations perfectly cancel, we  
1022 need the lattice between the upstream and down stream mod-  
1023 ulator to be an isochronous achromat. This reversible seeding  
1024 setup makes the following decoupling of the system straight-  
1025 forward. All we need to do is to make the GLSF section  
1026 an achromat, as the section from the upstream modulator to  
1027 downstream modulator is transparent to the longitudinal dy-  
1028 namics. Another advantage of this reversible seeding setup is  
1029 that it makes the bunch length at the modulator more flexible.  
1030 It can be a short microbunched beam as shown in Fig. 3. It can  
1031 also be a conventional RF-bunched beam, or even a coasting  
1032 beam. A coasting beam in this context means the beam is  
1033 not pre-microbunched, and its length is much longer than the  
1034 modulation laser wavelength, or even longer than that of an  
1035 RF bunch. Actually in our present design to be presented in  
1036 Sec. VIII, we actually use an RF-bunched beam in the ring.  
1037 So the third laser modulator of such a GLSF ring is actually  
1038 an RF system. Having explained the reason why we choose  
1039 this reversible seeding setup for GLSF, we remind the read-  
1040 ers that this however is not the only possible way to realize  
1041 the GLSF scheme [9]. For example, a symmetric lattice setup  
1042 with respect to the radiator is also possible, although the non-  
1043 linear dynamics might be challenging.

1044 After this general introduction of the GLSF scheme, we  
1045 now appreciate in a more physical way why GLSF could be  
1046 favored compared to LSF, in lowering the required modula-  
1047 tion laser power. The key is that LSF has contribution of  $\epsilon_z$   
1048 from both the LSF section and the ring dipoles, while GLSF  
1049 has only contribution of  $\epsilon_y$  from the GLSF section, since  $\mathcal{H}_y$   
1050 outside the GLSF section is zero as just explained. This is the  
1051 key physical argument from the single-particle dynamics per-  
1052 spective that why GLSF may require a smaller energy mod-  
1053 ulation compared to LSF, to realize the same desired bunch  
1054 length at the radiator. Actually if the longitudinal emittance in  
1055 LSF is only from the quantum excitation of LSF modulators,  
1056 and the vertical emittance in GLSF is only from the quantum

1057 excitation of GLSF modulators, then GLSF and LSF are ac- 1099  
 1058 tually equivalent in essence (only a factor of two difference in  
 1059 damping rates) concerning the requirement on energy modu-  
 1060 lation strength from the single-particle dynamics perspective.

1061 Now we explain the above argument more clearly using  
 1062 formulas. As we will show in the following section, more  
 1063 specifically Eq. (150), in GLSF at best case we have

$$1064 \quad |h| = \frac{1}{\sqrt{\mathcal{H}_{yR}\mathcal{H}_{yM}}} = \frac{\sqrt{\epsilon_y/\mathcal{H}_{yM}}}{\sqrt{\epsilon_y\mathcal{H}_{yR}}} = \frac{\sqrt{\epsilon_y/\mathcal{H}_{yM}}}{\sigma_{zR}}, \quad (140)$$

1065 where  $\mathcal{H}_y = \beta_{55}^{II}$  is defined in Sec. II and quantifies the con-  
 1066 tribution of vertical emittance to the bunch length. Note that  
 1067 we have used  $\sigma_{zR} = \sqrt{\epsilon_y\mathcal{H}_{yR}}$ , which means the bunch length  
 1068 at the radiator in GLSF scheme is solely determined by the  
 1069 beam vertical emittance. One can appreciate the similarity of  
 1070 the above formula with Eq. (127) for the case of LSF. There-  
 1071 fore, GLSF will be advantageous to LSF in lowering the re-  
 1072 quired energy modulation strength if

$$1073 \quad \frac{\epsilon_{y, \text{GLSF}}}{\mathcal{H}_{yM, \text{GLSF}}} < \frac{\epsilon_{z, \text{LSF}}}{\beta_{zM, \text{LSF}}}. \quad (141)$$

1074 Now we compare the two schemes in a more quantitative  
 1075 way. We assume that the two schemes work at the same beam  
 1076 energy. As we will show in Sec. VIII C, in a GLSF SSMB ring  
 1077 and if we consider only single-particle dynamics, the domi-  
 1078 nant contribution of vertical emittance is from the quantum  
 1079 excitation of two modulators in the GLSF section, and we  
 1080 have

$$1081 \quad \epsilon_{y, \text{GLSF}} \approx C_q \frac{\gamma^2}{J_y} \frac{1}{I_2} \times 2 \frac{\mathcal{H}_{yM, \text{GLSF}}}{\rho_{0M}^3} \frac{4}{3\pi} L_{uM, \text{GLSF}}. \quad (142)$$

1082 While in LSF, we assume that the longitudinal emittance is  
 1083 mainly from the quantum excitation in dipoles of the ring, and  
 1084 the average longitudinal beta function around the ring dipoles  
 1085 is the same as that at the modulators  $\langle \beta_z \rangle \approx \beta_{zM}$ . Taking  
 1086 the approximation  $I_2 \approx \frac{2\pi}{\rho_{\text{ring}}}$  which means in both rings the  
 1087 radiation loss is mainly from the dipoles in the ring,  $J_z \approx$   
 1088 2,  $J_x \approx 1$ , and combining with Eq. (128), Eq. (141) then  
 1089 corresponds to

$$1090 \quad 4\rho_{\text{ring, GLSF}} \frac{\frac{4}{3\pi} L_{uM, \text{GLSF}}}{\rho_{0M, \text{GLSF}}^3} < \rho_{\text{ring, LSF}} \frac{2\pi\rho_{\text{ring, LSF}}}{\rho_{\text{ring, LSF}}^3}. \quad (143)$$

1091 The above condition should be straightforward to fulfill in  
 1092 practice. For example, if the bending magnet strengths are  
 1093 the same in both schemes, i.e., if  $\rho_{\text{ring, GLSF}} = \rho_{\text{ring, LSF}} = \rho_{\text{ring}}$ ,  
 1094 the above relation corresponds to

$$1095 \quad L_{uM, \text{GLSF}} < \frac{3\pi^2}{8} \frac{\rho_{0M, \text{GLSF}}^3}{\rho_{\text{ring}}^2}, \quad (144)$$

1096 which is easy to satisfy in practice. So GLSF can be favored  
 1097 compared to LSF in lowering the required modulation laser  
 1098 power.

## D. Short Summary

1100 From the analysis in this section our tentative conclusion  
 1101 is: a LWF SSMB ring can be used to generate bunches with  
 1102 a couple of 10 nm bunch length, thus to generate coherent  
 1103 visible and infrared radiation. If we want to push the bunch  
 1104 length to an even shorter range, the required phase slippage  
 1105 factor of the ring will be too small from an engineering view-  
 1106 point. A LSF SSMB ring can create bunches with a bunch  
 1107 length at nm level, thus to generate coherent EUV radiation.  
 1108 However, the required modulation laser power is at GW level,  
 1109 and makes the optical enhancement cavity can only work at  
 1110 a low duty cycle pulsed mode, thus limiting the average out-  
 1111 put EUV radiation power. At present, a GLSF SSMB ring  
 1112 is the most promising among these three schemes to realize  
 1113 nm bunch length with a smaller modulation laser power com-  
 1114 pared to LSF SSMB, thus allowing a higher average power  
 1115 EUV radiation generation.

## V. TRANSVERSE-LONGITUDINAL COUPLING FOR BUNCH COMPRESSION AND HARMONIC GENERATION

1116 In the following sections, we will go into more details  
 1117 of the GLSF scheme, more specifically we will investigate  
 1118 the backbone of a GLSF SSMB storage ring, the transverse-  
 1119 longitudinal phase space coupling dynamics, in a systematic  
 1120 way. As the first step, in this section we present three theo-  
 1121 rems or inequalities that dictate such TLC-based bunch com-  
 1122 pression or harmonic generation schemes. If the initial bunch  
 1123 is longer than the modulation RF or laser wavelength, then  
 1124 compression of bunch or microbunch can just be viewed as  
 1125 a harmonic generation scheme. Therefore, in this paper, we  
 1126 will treat bunch compression and harmonic generation as the  
 1127 same thing in essence. We remind the readers that the theo-  
 1128 rems presented here are the generalization of that presented in  
 1129 Refs. [17, 33] from 4D phase space to 6D phase space. These  
 1130 formal mathematical relations will be useful in our later more  
 1131 detailed study for a GLSF SSMB light source.

## A. Problem Definition

1135 Let us first define the problem we are trying to solve. We  
 1136 assume  $\epsilon_y$  is the small eigen emittance we want to exploit.  
 1137 The case of using  $\epsilon_x$  is similar. The schematic layout of a  
 1138 TLC-based bunch compression section is shown in Fig. 5.  
 1139 Suppose the beam at the entrance of the bunch compression  
 1140 section is  $x$ - $y$ - $z$  decoupled, with its second moments matrix  
 1141 given by



Fig. 5. A schematic layout of applying TLC dynamics for bunch compression. (Figure adapted from Ref. [33]).

$$1142 \quad \Sigma_i = \langle \mathbf{X} \mathbf{X}^T \rangle_i = \begin{pmatrix} \epsilon_x \beta_{xi} & -\epsilon_x \alpha_{xi} & 0 & 0 & 0 & 0 \\ -\epsilon_x \alpha_{xi} & \epsilon_x \gamma_{xi} & 0 & 0 & 0 & 0 \\ 0 & 0 & \epsilon_y \beta_{yi} & -\epsilon_y \alpha_{yi} & 0 & 0 \\ 0 & 0 & -\epsilon_y \alpha_{yi} & \epsilon_y \gamma_{yi} & 0 & 0 \\ 0 & 0 & 0 & 0 & \epsilon_z \beta_{zi} & -\epsilon_z \alpha_{zi} \\ 0 & 0 & 0 & 0 & -\epsilon_z \alpha_{zi} & \epsilon_z \gamma_{zi} \end{pmatrix}, \quad (145)$$

1143 where  $\alpha$ ,  $\beta$  and  $\gamma$  are the Courant-Snyder functions, the sub- 1165  
 1144 script  $i$  means initial, and  $\epsilon_x$ ,  $\epsilon_y$  and  $\epsilon_z$  are the eigen emit- 1166  
 1145 tances of the beam corresponding to the horizontal, vertical 1167  
 1146 and longitudinal mode, respectively. Note that the eigen emit- 1168  
 1147 tances are beam invariants with respect to linear symplectic 1169  
 1148 transport. For the application of TLC for bunch compression, 1170  
 1149 it means that the final bunch length at the exit or radiator  $\sigma_{zR}$  1171  
 1150 depends only on the vertical emittance  $\epsilon_y$ , and neither on the 1172  
 1151 horizontal one  $\epsilon_x$  and nor on the longitudinal one  $\epsilon_z$ . 1173

1152 We divide such a bunch compression section into three 1172  
 1153 parts, with their symplectic transfer matrices given by 1173

$$1173 \quad \mathbf{M}_1 = \begin{pmatrix} r_{11} & r_{12} & r_{13} & r_{14} & 0 & r_{16} \\ r_{21} & r_{22} & r_{23} & r_{24} & 0 & r_{26} \\ r_{31} & r_{32} & r_{33} & r_{34} & 0 & r_{36} \\ r_{41} & r_{42} & r_{43} & r_{44} & 0 & r_{46} \\ r_{51} & r_{52} & r_{53} & r_{54} & 1 & r_{56} \\ 0 & 0 & 0 & 0 & 0 & 1 \end{pmatrix},$$

1154  $\mathbf{M}_2$  = modulation kick map,

$$1176 \quad \mathbf{M}_3 = \begin{pmatrix} R_{11} & R_{12} & R_{13} & R_{14} & 0 & R_{16} \\ R_{21} & R_{22} & R_{23} & R_{24} & 0 & R_{26} \\ R_{31} & R_{32} & R_{33} & R_{34} & 0 & R_{36} \\ R_{41} & R_{42} & R_{43} & R_{44} & 0 & R_{46} \\ R_{51} & R_{52} & R_{53} & R_{54} & 1 & R_{56} \\ 0 & 0 & 0 & 0 & 0 & 1 \end{pmatrix},$$

1155 with  $\mathbf{M}_1$  representing “from entrance to modulator”,  $\mathbf{M}_2$  rep- 1166  
 1156 resenting “modulation kick” and  $\mathbf{M}_3$  representing “modula- 1167  
 1157 tor to radiator”. Note that  $\mathbf{M}_1$  and  $\mathbf{M}_3$  are in their general 1168  
 1158 thick-lens form, and do not necessarily need to be  $x$ - $y$  decou- 1169  
 1159 pled. The transfer matrix from the entrance to the radiator is 1170  
 1160 then 1180

$$1176 \quad (146) \quad h^2 \mathcal{H}_{yM} \mathcal{H}_{yR} \geq 1, \quad (150)$$

1177 where the subscripts M and R represent the place of modula- 1178  
 1178 tor and radiator, respectively.

1179 **Theorem two:** If

$$1180 \quad \mathbf{M}_2 = \begin{pmatrix} 1 & 0 & 0 & 0 & 0 & 0 \\ 0 & 1 & 0 & 0 & 0 & 0 \\ 0 & 0 & 1 & 0 & 0 & 0 \\ 0 & 0 & 0 & 1 & 0 & 0 \\ 0 & 0 & 0 & 0 & 1 & 0 \\ 0 & 0 & 0 & 0 & 0 & 1 \end{pmatrix}, \quad (151)$$

1181 which corresponds to the case of a transverse deflecting (in 1182  
 1182  $y$ -dimension) RF or a  $\text{TEM}_{01}$  mode laser modulator or other 1183  
 1183 schemes for angular modulation, then

$$1184 \quad g^2 \beta_{yM} \mathcal{H}_{yR} \geq 1. \quad (152)$$

$$1161 \quad \mathbf{O} = \mathbf{M}_3 \mathbf{M}_2 \mathbf{M}_1. \quad (147) \quad 1185 \quad \text{Theorem three: If}$$

$$1186 \quad \mathbf{M}_2 = \begin{pmatrix} 1 & 0 & 0 & 0 & 0 & 0 \\ 0 & 1 & 0 & 0 & 0 & 0 \\ 0 & 0 & 1 & 0 & q & 0 \\ 0 & 0 & 0 & 1 & 0 & 0 \\ 0 & 0 & 0 & 0 & 1 & 0 \\ 0 & 0 & 0 & -q & 0 & 1 \end{pmatrix}, \quad (153)$$

$$1164 \quad O_{51} = 0, O_{52} = 0, O_{55} = 0, O_{56} = 0. \quad (148)$$

1162 From the problem definition, for  $\sigma_{zR}$  to be independent of  $\epsilon_x$  1163  
 1163 and  $\epsilon_z$ , we need

1187 then

1188 
$$q^2 \gamma_{yM} \mathcal{H}_{yR} \geq 1. \quad (154)$$

1194

2. Proof

1189 There is no commonly used single element realizing the kick

1190 map Eq. (153) directly. Instead, it takes the combination of 1195 Here we present the details for the proof of Theorem one. 1191 several elements to realize such a map, making its applica- 1196 The proof of the other two is just similar. From the problem 1192 tion less straightforward compared to the cases correspond to 1197 definition, for  $\sigma_{zR}$  to be independent of  $\epsilon_x$  and  $\epsilon_z$ , we need

---


$$\begin{aligned} O_{51} &= r_{11}R_{51} + r_{21}R_{52} + r_{31}R_{53} + r_{41}R_{54} + r_{51}(hR_{56} + 1) = 0, \\ O_{52} &= r_{12}R_{51} + r_{22}R_{52} + r_{32}R_{53} + r_{42}R_{54} + r_{52}(hR_{56} + 1) = 0, \\ O_{55} &= hR_{56} + 1 = 0, \\ O_{56} &= r_{16}R_{51} + r_{26}R_{52} + r_{36}R_{53} + r_{46}R_{54} + r_{56}(hR_{56} + 1) + R_{56} = 0. \end{aligned} \quad (155)$$

1199 Under the above conditions, we have

1200 
$$\mathbf{O} = \begin{pmatrix} \mathbf{A} & \mathbf{B} & \mathbf{C} \\ \mathbf{D} & \mathbf{E} & \mathbf{F} \\ \mathbf{G} & \mathbf{H} & \mathbf{I} \end{pmatrix}, \quad (156)$$

1201 with  $\mathbf{A} \sim \mathbf{I}$  being  $2 \times 2$  submatrices of  $\mathbf{T}$ , and

1202 
$$\begin{aligned} \mathbf{G} &= \begin{pmatrix} 0 & 0 \\ r_{51}h & r_{52}h \end{pmatrix}, \\ \mathbf{H} &= \begin{pmatrix} r_{13}R_{51} + r_{23}R_{52} + r_{33}R_{53} + r_{43}R_{54} & r_{14}R_{51} + r_{24}R_{52} + r_{34}R_{53} + r_{44}R_{54} \\ r_{53}h & r_{54}h \end{pmatrix}, \\ \mathbf{I} &= \begin{pmatrix} 0 & 0 \\ h & r_{56}h + 1 \end{pmatrix}. \end{aligned} \quad (157)$$

1203 Note that  $\mathbf{I}$  in this subsection does not mean the identity matrix. The bunch length squared at the modulator and the radiator are 1204 obtained as that given in Eq. (60) with the evolution of generalized beta functions properly handled according to Eq. (11) and 1205 the results are

1206 
$$\begin{aligned} \sigma_{zM}^2 &= \epsilon_x \frac{(\beta_{xi}r_{51} - \alpha_{xi}r_{52})^2 + r_{52}^2}{\beta_{xi}} + \epsilon_y \frac{(\beta_{yi}r_{53} - \alpha_{yi}r_{54})^2 + r_{54}^2}{\beta_{yi}} + \epsilon_z (\beta_{zi} - 2\alpha_{zi}r_{56} + \gamma_{zi}r_{56}^2) \\ &= \epsilon_x \mathcal{H}_{xM} + \epsilon_y \mathcal{H}_{yM} + \epsilon_z \beta_{zM}, \\ \sigma_{zR}^2 &= \epsilon_y \frac{(\beta_{yi}O_{53} - \alpha_{yi}O_{54})^2 + O_{54}^2}{\beta_{yi}} = \epsilon_y \mathcal{H}_{yR}. \end{aligned} \quad (158)$$

1207 According to the Cauchy-Schwarz inequality, we have

1208 
$$\begin{aligned} h^2 \mathcal{H}_{yM} \mathcal{H}_{yR} &= h^2 \frac{[(\beta_{yi}r_{53} - \alpha_{yi}r_{54})^2 + r_{54}^2]}{\beta_{yi}} \frac{[(\beta_{yi}O_{53} - \alpha_{yi}O_{54})^2 + O_{54}^2]}{\beta_{yi}} \\ &\geq \frac{h^2}{\beta_{yi}^2} [-(\beta_{yi}r_{53} - \alpha_{yi}r_{54})O_{54} + r_{54}(\beta_{yi}O_{53} - \alpha_{yi}O_{54})]^2 \\ &= (O_{53}r_{54}h - O_{54}r_{53}h)^2 = (O_{53}O_{64} - O_{54}O_{63})^2 = |\text{Det}(\mathbf{H})|^2, \end{aligned} \quad (159)$$

1209 where  $\text{Det}()$  means the determinant of the matrix. The equality holds when  $\frac{-(\beta_{yi}r_{53} - \alpha_{yi}r_{54})}{O_{54}} = \frac{r_{54}}{(\beta_{yi}O_{53} - \alpha_{yi}O_{54})}$ . The symple- 1210 ticity of  $\mathbf{O}$  requires that  $\mathbf{O} \mathbf{S} \mathbf{O}^T = \mathbf{S}$ , where  $\mathbf{S} = \begin{pmatrix} \mathbf{J} & 0 & 0 \\ 0 & \mathbf{J} & 0 \\ 0 & 0 & \mathbf{J} \end{pmatrix}$  and  $\mathbf{J} = \begin{pmatrix} 0 & 1 \\ -1 & 0 \end{pmatrix}$ , so we have

1211 
$$\begin{pmatrix} \mathbf{AJA}^T + \mathbf{BJB}^T + \mathbf{CJC}^T & \mathbf{AJD}^T + \mathbf{BJE}^T + \mathbf{CJF}^T & \mathbf{AJG}^T + \mathbf{BJH}^T + \mathbf{CJI}^T \\ \mathbf{DJA}^T + \mathbf{EJB}^T + \mathbf{FJC}^T & \mathbf{DJD}^T + \mathbf{EJE}^T + \mathbf{FJF}^T & \mathbf{DJG}^T + \mathbf{EJH}^T + \mathbf{FJI}^T \\ \mathbf{GJA}^T + \mathbf{HJB}^T + \mathbf{IJC}^T & \mathbf{GJD}^T + \mathbf{HJE}^T + \mathbf{IJF}^T & \mathbf{GJG}^T + \mathbf{HJH}^T + \mathbf{IJI}^T \end{pmatrix} = \mathbf{S}. \quad (160)$$

1212 According to Eq. (157), we have

$$1213 \quad \mathbf{GJG}^T = \begin{pmatrix} 0 & 0 \\ 0 & 0 \end{pmatrix}, \quad \mathbf{IJI}^T = \begin{pmatrix} 0 & 0 \\ 0 & 0 \end{pmatrix}. \quad (161)$$

1214 Therefore,

$$1215 \quad \mathbf{HJH}^T = \mathbf{J}, \quad (162)$$

1216 which means  $\mathbf{H}$  is also a symplectic matrix. So we have <sup>1250</sup> **Theorem one:** If  $\mathbf{M}_2$  is as shown in Eq. (149), then  
1217  $\text{Det}(\mathbf{H}) = 1$ . The theorem is thus proven.

### 1218 C. Dragt's Minimum Emittance Theorem

1219 Theorem one in Eq. (150) can also be expressed as

$$1220 \quad |h| \geq \frac{\epsilon_y}{\sqrt{\epsilon_y \mathcal{H}_{yM}} \sqrt{\epsilon_y \mathcal{H}_{yR}}} = \frac{\epsilon_y}{\sigma_{zyM} \sigma_{zR}}. \quad (163)$$

1221 Note that in the above formula,  $\sigma_{zyM}$  means the bunch length  
1222 at the modulator contributed from the vertical emittance  $\epsilon_y$ .  
1223 So given a fixed  $\epsilon_y$  and desired  $\sigma_{zR}$ , a smaller  $h$ , i.e., a  
1224 smaller RF acceleration gradient or modulation laser power  
1225 ( $P_L \propto |h|^2$ ), means a larger  $\mathcal{H}_{yM}$ , thus a larger  $\sigma_{zyM}$ , is  
1226 needed. As  $|h|\sigma_{zM}$  quantifies the energy spread introduced  
1227 by the modulation kick, we thus also have

$$1228 \quad \sigma_{zR} \sigma_{\delta R} \geq \epsilon_y. \quad (164)$$

1229 Similarly for Theorem two and three, we have

$$1230 \quad |g| \geq \frac{\epsilon_y}{\sigma_{y\beta M} \sigma_{zR}}, \quad (165)$$

1231 and

$$1232 \quad |q| \geq \frac{\epsilon_y}{\sigma_{y'\beta M} \sigma_{zR}}, \quad (166)$$

1233 respectively, and also Eq. (164). Note that in the above for-  
1234 mulas, the vertical beam size or divergence at the modulator  
1235 contains only the vertical betatron part, i.e., that from the ver-  
1236 tical emittance  $\epsilon_y$ .

1237 Equation (164) is actually a manifestation of the classical  
1238 uncertainty principle [34], which states that

$$1239 \quad \begin{aligned} \Sigma_{11} \Sigma_{22} &\geq \epsilon_{\min}^2, \\ \Sigma_{33} \Sigma_{44} &\geq \epsilon_{\min}^2, \\ \Sigma_{55} \Sigma_{66} &\geq \epsilon_{\min}^2, \end{aligned} \quad (167)$$

1240 where  $\epsilon_{\min}$  is the minimum one among the three eigen emit-  
1241 tances  $\epsilon_{I,II,III}$ . In our bunch compression case, we assume  
1242 that  $\epsilon_y$  is the smaller one compared to  $\epsilon_z$ .

1243 Actually there is a stronger inequality compared to the clas-  
1244 sical uncertainty principle, i.e., the minimum emittance theo-  
1245 rem [34], which states that the projected emittance cannot be  
1246 smaller than the minimum one among the three eigen emit-  
1247 tances,

$$1248 \quad \begin{aligned} \epsilon_{x,\text{pro}}^2 &= \Sigma_{11} \Sigma_{22} - \Sigma_{12}^2 \geq \epsilon_{\min}^2, \\ \epsilon_{y,\text{pro}}^2 &= \Sigma_{33} \Sigma_{44} - \Sigma_{34}^2 \geq \epsilon_{\min}^2, \\ \epsilon_{z,\text{pro}}^2 &= \Sigma_{55} \Sigma_{66} - \Sigma_{56}^2 \geq \epsilon_{\min}^2. \end{aligned} \quad (168)$$

## D. Theorems Cast in Another Form

1249 <sup>1250</sup> As another way to appreciate the result, here we cast the  
1251 theorems in a form using the generalized beta functions as  
1252 introduced in Sec. II. According to definition, we have

$$1253 \quad \beta_y \equiv \beta_{33}^{II}, \quad \gamma_y \equiv \beta_{44}^{II}, \quad \mathcal{H}_y \equiv \beta_{55}^{II}. \quad (169)$$

1255 <sup>1256</sup> where  $M_{2,65}$  is the <sub>65</sub> matrix term of  $\mathbf{M}_2$ , i.e.,  $h$ . The su-  
1257 perscript 2 of  $M_{2,65}^2$  means the square of  $M_{2,65}$ . For better  
1258 visualization, in this subsection, we use brackets to denote  
1259 the location, with Ent, Mod and Rad meaning entrance, mod-  
1260 ulator and radiator, respectively.

1261 **Theorem two:** If  $\mathbf{M}_2$  is as shown in Eq. (151), then

$$1262 \quad M_{2,63}^2(\text{Mod}) \beta_{33}^{II}(\text{Mod}) \beta_{55}^{II}(\text{Rad}) \geq 1. \quad (170)$$

1263 **Theorem three:** If  $\mathbf{M}_2$  is as shown in Eq. (153), then

$$1264 \quad M_{2,64}^2(\text{Mod}) \beta_{44}^{II}(\text{Mod}) \beta_{55}^{II}(\text{Rad}) \geq 1. \quad (171)$$

$$1265 \quad \mathbf{T}_I(\text{Ent}) = \begin{pmatrix} \beta_{xi} & -\alpha_{xi} & 0 & 0 & 0 & 0 \\ -\alpha_{xi} & \gamma_{xi} & 0 & 0 & 0 & 0 \\ 0 & 0 & 0 & 0 & 0 & 0 \\ 0 & 0 & 0 & 0 & 0 & 0 \\ 0 & 0 & 0 & 0 & 0 & 0 \\ 0 & 0 & 0 & 0 & 0 & 0 \end{pmatrix}, \quad (173)$$

1266 and similar expressions for  $\mathbf{T}_{II,III}(\text{Ent})$ , with  $x$  replaced by  
1267  $y, z$  and the location of the  $2 \times 2$  matrix shifted in the diagonal  
1268 direction. Then

$$1269 \quad \beta_{33}^{II}(\text{Mod}) = \frac{(\beta_{yi} r_{33} - \alpha_{yi} r_{34})^2 + r_{34}^2}{\beta_{yi}}, \quad (174)$$

$$1270 \quad \beta_{44}^{II}(\text{Mod}) = \frac{(\beta_{yi} r_{43} - \alpha_{yi} r_{44})^2 + r_{44}^2}{\beta_{yi}}, \quad (175)$$

$$1271 \quad \beta_{55}^{II}(\text{Mod}) = \frac{(\beta_{yi} r_{53} - \alpha_{yi} r_{54})^2 + r_{54}^2}{\beta_{yi}}, \quad (176)$$

$$1272 \quad \beta_{55}^I(\text{Rad}) = \frac{(\beta_{xi} O_{51} - \alpha_{xi} O_{52})^2 + O_{52}^2}{\beta_{xi}}, \quad (177)$$

$$1273 \quad \beta_{55}^{II}(\text{Rad}) = \frac{(\beta_{yi} O_{53} - \alpha_{yi} O_{54})^2 + O_{54}^2}{\beta_{yi}}, \quad (178)$$

$$1274 \quad \beta_{55}^{III}(\text{Rad}) = \frac{(\beta_{zi} O_{55} - \alpha_{zi} O_{56})^2 + O_{56}^2}{\beta_{zi}}. \quad (179)$$

1275 For  $\sigma_{zR}$  to be independent of  $\epsilon_x$  and  $\epsilon_z$ , we need  $\beta_{55}^I(\text{Rad}) = 0$  and  $\beta_{55}^{III}(\text{Rad}) = 0$ , which then lead to Eq. (148). And the  
1276 following proof procedures are the same as that shown in the  
1277 above Sec. V B 2.

1286 **VI. ENERGY MODULATION-BASED COUPLING  
1287 SCHEMES**

1288 After introducing the three formal theorems, now we con- 1289 duct more detailed analysis of the TLC-based bunch compres- 1290 sion or microbunching generation schemes. We group these 1291 schemes into two categories, i.e., energy modulation-based 1292 and angular modulation-based schemes. They corresponds 1293 to the case of Theorem One and Two presented in last sec- 1294 tion. In this section, we focus on energy modulation-based 1295 schemes, and next section is dedicated to angular modulation- 1296 based schemes. The physical realization corresponding to the 1297 case of Theorem Three is not that straightforward compared 1298 to the cases of Theorem One and Two, and we do not expand 1299 its discussion in this paper.

1300 **A. Form Function and Bunching Factor**

1301 *1. General Formula*

1302 For coherent radiation generation, a parameter of vital im- 1303 portant is the bunching factor of the electron beam. Here first 1304 we derive the bunching factor of the energy-modulation based 1305 TLC microbunching schemes. The mathematical model is 1306 formulated as follows.

1307 6D particle state vector:

$$1308 \mathbf{X} \equiv (x \ x' \ y \ y' \ z \ \delta)^T. \quad (180)$$

1309 6D spectral vector:

$$1310 \mathbf{K} \equiv (k_x \ k_{x'} \ k_y \ k_{y'} \ k_z \ k_\delta). \quad (181)$$

1311 Normalized particle density distribution in phase space  $\psi(\mathbf{X})$ :

$$1312 \int \psi(\mathbf{X}) d\mathbf{X} = 1, \psi(\mathbf{X}) \geq 0, \quad (182)$$

1313 where  $\int d\mathbf{X}$  means  $\int_{-\infty}^{\infty} \int_{-\infty}^{\infty} \int_{-\infty}^{\infty} \int_{-\infty}^{\infty} \int_{-\infty}^{\infty} \int_{-\infty}^{\infty} dx dx' dy$   
1314  $dy' dz d\delta$ . Here we introduce the form function (FF) of beam  
1315 as:

$$1316 \mathcal{F}(\mathbf{K}) \equiv \int \psi(\mathbf{X}) e^{-i\mathbf{K}\mathbf{X}} d\mathbf{X}. \quad (183)$$

1317  $\psi(\mathbf{X})$  and  $\mathcal{F}(\mathbf{K})$  then forms a Fourier transform pair

$$1318 \psi(\mathbf{X}) = \frac{1}{2\pi} \int \mathcal{F}(\mathbf{K}) e^{i\mathbf{K}\mathbf{X}} d\mathbf{K}, \quad (184)$$

1319 where  $\int d\mathbf{K}$  means  $\int_{-\infty}^{\infty} \int_{-\infty}^{\infty} \int_{-\infty}^{\infty} \int_{-\infty}^{\infty} \int_{-\infty}^{\infty} dk_x dk_{x'}$   
1320  $dk_y dk_{y'} dk_z dk_\delta$ . This form function is another complete de-  
1321 scription of beam distribution and can offer complementary  
1322 insight for beam dynamics study. More details on this respect  
1323 will be reported elsewhere.

1324 The classical 1D bunching factor or form factor used in  
1325 literature is a specific point in our defined FF, i.e., with  $\mathbf{K} =$   
(0, 0, 0, 0,  $k_z$ , 0),

$$1327 b(k_z) = \mathcal{F}(0, 0, 0, 0, k_z, 0) = \int_{-\infty}^{\infty} \psi(z) e^{-ik_z z} dz, \quad (185)$$

1288 After introducing the three formal theorems, now we con- 1289 duct more detailed analysis of the TLC-based bunch compres- 1290 sion or microbunching generation schemes. We group these 1291 schemes into two categories, i.e., energy modulation-based 1292 and angular modulation-based schemes. They corresponds 1293 to the case of Theorem One and Two presented in last sec- 1294 tion. In this section, we focus on energy modulation-based 1295 schemes, and next section is dedicated to angular modulation- 1296 based schemes. The physical realization corresponding to the 1297 case of Theorem Three is not that straightforward compared 1298 to the cases of Theorem One and Two, and we do not expand 1299 its discussion in this paper.

1288 where  $\psi(z) = \int_{-\infty}^{\infty} \int_{-\infty}^{\infty} \int_{-\infty}^{\infty} \int_{-\infty}^{\infty} \int_{-\infty}^{\infty} \int_{-\infty}^{\infty} \psi(\mathbf{X}) dx dx' dy dy' d\delta$   
1289 is the normalized longitudinal distribution of particles. Here  
1290 in this paper, we will use  $\mathcal{F}$  to denote the 6D form function,  
1291 and  $b$  the classical 1D bunching factor.

1292 Now we derive the form function and bunching factor  
1293 for a single-stage energy modulation-based microbunching  
1294 schemes. A lumped description of the laser-induced energy  
1295 modulation can be written as:

$$1336 \delta = \delta + A \sin(k_L z), \quad (186)$$

1337 where  $k_L = \frac{2\pi}{\lambda_L}$  is the laser wavenumber and  $A$  is the modu-  
1338 lation strength. After the modulation, the particle state vector  
1339 evolves according to:

$$1340 \mathbf{X}_f = \mathbf{R} \mathbf{X}_i, \quad (187)$$

1341 where  $\mathbf{R}$  is the linear  $6 \times 6$  symplectic transfer matrix of the  
1342 magnet lattice, which could be a single-pass one like a linear  
1343 accelerator or a multi-pass one like a storage ring. In this pa-  
1344 per we only consider the case that the magnet lattice is linear.  
1345 Denote:

$$1346 \begin{aligned} \mathbf{A} &\equiv (0, 0, 0, 0, 0, A)^T, \\ \mathbf{U}_p &\equiv (0 \ 0 \ 0 \ pk_L \ 0), \\ \mathbf{M}_p &\equiv \mathbf{K} \mathbf{R} - \mathbf{U}_p, \end{aligned} \quad (188)$$

1347 with  $p$  being an integer. Then the final FF is

$$1348 \begin{aligned} \mathcal{F}(\mathbf{K}) &= \int \psi_f(\mathbf{X}) e^{-i\mathbf{K}\mathbf{X}} d\mathbf{X} \\ &= \int \psi_{m+}(\mathbf{X}) e^{-i\mathbf{K}\mathbf{R}\mathbf{X}} d\mathbf{X} \\ &= \int \psi_0(\mathbf{X}) e^{-i(\mathbf{K}\mathbf{R}\mathbf{X} + \mathbf{K}\mathbf{R}\mathbf{A} \sin(k_L z))} d\mathbf{X} \\ &= \sum_{p=-\infty}^{\infty} J_p(-\mathbf{K}\mathbf{R}\mathbf{A}) \int \psi_0(\mathbf{X}) e^{-i(\mathbf{K}\mathbf{R}\mathbf{X} - pk_L z)} d\mathbf{X} \\ &= \sum_{p=-\infty}^{\infty} J_p(-\mathbf{K}\mathbf{R}\mathbf{A}) \int \psi_0(\mathbf{X}) e^{-i\mathbf{M}_p \mathbf{X}} d\mathbf{X} \\ &= \sum_{p=-\infty}^{\infty} J_p(-\mathbf{K}\mathbf{R}\mathbf{A}) \mathcal{F}_0(\mathbf{M}_p), \end{aligned} \quad (189)$$

1349 where  $\psi_0(\mathbf{X})$ ,  $\psi_{m+}(\mathbf{X})$ , and  $\psi_f(\mathbf{X})$  mean the beam distri-  
1350 bution at the beginning, right after the energy modulation  
1351 and the final point, respectively.  $J_p$  is the  $p$ -th order Bessel  
1352 function of the first kind. Jacobi-Anger identity  $e^{ix \sin y} =$   
1353  $\sum_{n=-\infty}^{\infty} e^{iny} J_n[x]$  has been used in the above derivation.  
1354 Note that we have also used the fact that for a symplectic  
1355 matrix  $\mathbf{R}$  we have  $\text{Det}(\mathbf{R}) = 1$ .  $\mathcal{F}_0(\mathbf{K})$  is the initial FF.

1356 The above formula is general and applies for arbitrary ini-  
1357 tial beam distribution. If the initial beam distribution is Gaus-  
1358 sian in 6D phase space:

$$1359 \quad \psi_0(\mathbf{X}) = \frac{1}{(2\pi)^3 \sqrt{\text{Det}(\Sigma_0)}} \exp\left(-\frac{1}{2} \mathbf{X}^T \Sigma_0^{-1} \mathbf{X}\right) \quad (190)$$

1360 with  $\Sigma_0$  being the initial second moments of the beam, the  
1361 initial FF is then

$$1362 \quad \mathcal{F}_0(\mathbf{K}) = \exp\left(-\frac{\mathbf{K} \Sigma_0 \mathbf{K}^T}{2}\right). \quad (191)$$

1363 The final FF is then

$$1364 \quad \mathcal{F}(\mathbf{K}) = \sum_{p=-\infty}^{\infty} J_p(-\mathbf{K} \mathbf{R} \mathbf{A}) \exp\left(-\frac{\mathbf{M}_p \Sigma_0 \mathbf{M}_p^T}{2}\right), \quad (192)$$

1365

## 2. HGHG

1366 In many applications, the classical 1D bunching factor suf-  
1367 fices. With  $\mathbf{K} = (0 \ 0 \ 0 \ 0 \ k_z \ 0)$ , then

$$\mathbf{K} \mathbf{R} \mathbf{A} = k_z R_{56} A,$$

$$1368 \quad \mathbf{M}_p = k_z \left( R_{51} \ R_{52} \ R_{53} \ R_{54} \ R_{55} - \frac{p k_L}{k_z} \ R_{56} \right). \quad (193)$$

1369 If further  $R_{51} = 0$ ,  $R_{52} = 0$ ,  $R_{53} = 0$ ,  $R_{54} = 0$  and  $R_{55} = 1$ ,  
1370 and the initial beam is transverse-longitudinal decoupled and  
1371 upright in the longitudinal phase space, which corresponds  
1372 to the case of high-gain harmonic-generation (HGHG) [35],  
1373 then

$$1374 \quad b(k_z) = \sum_{p=-\infty}^{\infty} J_p(-k_z R_{56} A) \exp\left(-\frac{k_z^2}{2} \left[ \left(1 - \frac{p k_L}{k_z}\right)^2 \sigma_{z0}^2 + (R_{56} \sigma_{\delta0})^2 \right]\right), \quad (194)$$

1375 where  $\sigma_{z0}$  and  $\sigma_{\delta0}$  are the initial RMS bunch length and en-  
1376 ergy spread, respectively. If the initial bunch length is much  
1377 longer than the laser wavelength, i.e.,  $k_L \sigma_{z0} \gg 1$ , the above  
1378 exponential terms will be non-zero only when  $k_z = p k_L$ ,  
1379 which means there is only bunching at the laser harmonics.  
1380 In this case, we have the bunching factor at the  $n$ -th ( $n$  being  
1381 integer) laser harmonic

$$b_n = b(k_z = n k_L)$$

$$1382 \quad = J_n(-n k_L R_{56} A) \exp\left[-\frac{(n k_L R_{56} \sigma_{\delta0})^2}{2}\right]. \quad (195)$$

1383 For  $n > 4$ , the maximal value of the Bessel function  $J_n$  is  
1384 about  $0.67/n^{1/3}$  and is achieved when its argument is equal  
1385 to  $n + 0.81n^{1/3}$ . For large  $n$ , this argument corresponds to  
1386  $k_L R_{56} A \sim 1$ . Then to make sure the exponential term in  
1387 Eq. (195) not too small, we need  $A \sim n \sigma_{\delta0}$ . So generally  
1388 if we want to realize  $n$ -th harmonic bunching in HGHG, we  
1389 need an energy modulation strength a factor of  $n$  larger than  
1390 the initial energy spread.

## 3. TLC-based Microbunching

1391 Now let us consider the case of nonzero  $R_{51,52,53,54}$ , which  
1392 corresponds to transverse-longitudinal coupling (TLC)-based  
1393 microbunching. Below we use  $y$ - $z$  coupling as an example  
1394 for the analysis and ignore the  $x$ -dimension. The analysis for  
1395  $x$ - $z$  coupling is similar. If  $\mathbf{K} \equiv (0 \ 0 \ 0 \ 0 \ k_z \ 0)$ ,  $R_{51} = 0$ ,  
1396  $R_{52} = 0$ ,  $R_{55} = 1$ ,  $R_{66} = 1$ , then  
1397

$$1398 \quad \mathbf{K} \mathbf{R} \mathbf{A} = k_z R_{56} A, \quad (196)$$

$$\mathbf{M}_p = k_z \left( 0 \ 0 \ R_{53} \ R_{54} \ 1 - \frac{p k_L}{k_z} \ R_{56} \right).$$

1399 Using the real and imaginary generalized beta functions and  
1400 Twiss matrices introduced in Sec. II, the bunching factor at  
1401 the  $n$ -th laser harmonic can be expressed as

$$1402 \quad b_n = \sum_{p=-\infty}^{\infty} J_p(-n k_L R_{56} A) \exp\left[-\frac{(\epsilon_{II} \mathbf{M}_p \mathbf{T}_{II} \mathbf{M}_p^T + \epsilon_{III} \mathbf{M}_p \mathbf{T}_{III} \mathbf{M}_p^T)}{2}\right], \quad (197)$$

1403 where  $\mathbf{T}_{II,III}$  are the real generalized Twiss matrices right before the modulation. We then require

$$1404 \quad \mathbf{M}_p \mathbf{T}_{III} \mathbf{M}_p^T \Big|_{p=n} = (n k_L)^2 (\mathbf{R} \mathbf{T}_{III} \mathbf{R}^T - 2 \mathbf{R} \mathbf{T}_{III} + \mathbf{T}_{III})_{55} = 0. \quad (198)$$

1405 The physical reason of this requirement is that for  $p = n$ , we want the longitudinal emittance does not contribute to the bunching  
1406 factor. By doing this, the bunching factor will be mainly determined by the vertical emittance, which is assumed to be a small  
1407 value. Therefore, we can realize high harmonic bunching with a shallow energy modulation strength  $A$ . The above relation can  
1408 be written more specifically using the generalized beta functions and the matrix terms of  $\mathbf{R}$  as

$$1409 \quad R_{53}^2 \beta_{33}^{III} + R_{54}^2 \beta_{44}^{III} + R_{56}^2 \beta_{66}^{III} + 2 R_{53} R_{54} \beta_{34}^{III} + 2 R_{53} R_{56} \beta_{36}^{III} + 2 R_{54} R_{56} \beta_{46}^{III} = 0. \quad (199)$$

1410 If the generalized Twiss matrices of the eigenmode  $II$  and  $III$  right before the modulation are given by Eq. (51), and further  
1411 assuming that at the modulation point we have  $D_x = 0$  and  $D'_x = 0$ , then Eq. (199) can be casted into

$$1412 \quad R_{53} D_y + R_{54} D'_y + R_{56} = 0. \quad (200)$$

1413 This relation means that the final coordinate  $z$  does not depend on the initial energy deviation  $\delta$  in linear approximation. Under  
 1414 the above condition, we have

1415

$$\mathbf{M}_p \mathbf{T}_{III} \mathbf{M}_p^T = (nk_L)^2 \left(1 - \frac{p}{n}\right)^2 \beta_{zM}, \quad (201)$$

1416 and

1417

$$\mathbf{M}_p \mathbf{T}_{II} \mathbf{M}_p^T = (nk_L)^2 \left[ \mathcal{H}_{yR} + \left(1 - \frac{p}{n}\right)^2 \mathcal{H}_{yM} + 2 \left(1 - \frac{p}{n}\right) (\gamma_y R_{54} D_y - \alpha_y R_{53} D_y + \alpha_y R_{54} D'_y - \beta_y R_{53} D'_y) \right]. \quad (202)$$

1418 Then the bunching factor at the  $n$ -th laser harmonic at the final point which in our context means the radiator is

1419

$$b_n = \sum_{p=-\infty}^{\infty} J_p (-nk_L R_{56} A) \exp \left[ -\frac{(nk_L)^2}{2} \epsilon_y \mathcal{H}_{yR} \right] \exp \left[ -\frac{k_L^2}{2} (n-p)^2 (\epsilon_y \mathcal{H}_{yM} + \epsilon_z \beta_{zM}) \right] \exp \left[ -\frac{k_L^2}{2} 2n(n-p) \epsilon_y (\gamma_y R_{54} D_y - \alpha_y R_{53} D_y + \alpha_y R_{54} D'_y - \beta_y R_{53} D'_y) \right]. \quad (203)$$

1420 Here we remind the readers that there is an extra factor in wavelength, then there is only one term non-vanishing in the  
 1421 Eq. (203) compared to the result in our previous publications above summation, i.e., the term with  $p = n$ . Then  
 1422 in Refs. [17, 33], i.e.,

1423

$$b_n = \sum_{p=-\infty}^{\infty} J_p (-nk_L R_{56} A) \exp \left[ -\frac{(nk_L)^2}{2} \epsilon_y \mathcal{H}_{yR} \right] \quad (204) \quad \begin{aligned} 1447 \quad b_n = J_n (-nk_L R_{56} A) \exp \left[ -\frac{(nk_L)^2}{2} \epsilon_y \mathcal{H}_{yR} \right]. \quad (206) \\ 1448 \quad \text{Here we make a short comment that our derivation of} \\ 1449 \quad \text{bunching factor, and also most of that found in literature, ne-} \\ 1450 \quad \text{glects the collective interactions between the electron beam} \\ 1451 \quad \text{and the co-propagation electromagnetic field. Such a collec-} \\ 1452 \quad \text{tive interaction may disturb the modulation performance. Al-} \\ 1453 \quad \text{though not much work on this subject, the interested readers} \\ 1454 \quad \text{may refer to a recent relevant work [41].} \end{aligned}$$

1424 We conclude that the Eq. (203) here is rigorously more accurate than Eq. (204). We have proven in last section there is  
 1425 rate.

1426 If the modulation waveform is linear, according to Eq. (158), the RMS bunch length at the modulator and radiator are given by

1429

$$\sigma_{zM}^2 = \epsilon_z \beta_{zM} + \epsilon_y \mathcal{H}_{yM}, \quad (205) \quad \begin{aligned} 1456 \quad \text{After deriving the bunching factor, now we derive the for-} \\ 1457 \quad \text{mula of modulation strength, given the laser, electron and un-} \\ 1458 \quad \text{dulator parameters. This is a necessary work for quantitative} \\ 1459 \quad \text{analysis and comparison.} \end{aligned}$$

1430 So in this paper, we call  $\sigma_{zR} = \sqrt{\epsilon_y \mathcal{H}_{yR}}$  the linear bunch length at the radiator. We have proven in last section there is

1431 a fundamental inequality dictating the energy chirp strength  $h$  and  $\mathcal{H}_y$  at the modulator and radiator, respectively, i.e.,

1433  $h^2 \mathcal{H}_{yM} \mathcal{H}_{yR} \geq 1$ . Basically, given the vertical emittance and

1435 desired  $\sigma_{zR}$ , to lower the energy chirp strength, we need to lengthen the bunch at the modulator. If the initial bunch is shorter than the modulation laser wavelength, considering the actual laser modulation waveform is sinusoidal, then according to Eq. (203), a bunch lengthening at the modulator means a bunching factor drop at the radiator as can be seen from the second exponential term. For more discussions on this point, the readers are referred to Refs. [17, 33].

1443 When  $k_L^2 (\epsilon_y \mathcal{H}_{yM} + \epsilon_z \beta_{zM}) \gg 1$  which means the bunch length at the modulation point is much longer than the laser

## B. Modulation Strength

### I. A Normally Incident Laser

1444 length at the modulation point which in our context means the radiator is much longer than the laser. The most common method of imprinting energy modulation on an electron beam at the laser wavelength is to use a TEM<sub>00</sub> mode laser to resonate with the electrons in an undulator. Below we use a planar undulator as the modulator. A helical undulator can also be applied for energy modulation, but since we want to preserve the ultrasmall vertical emittance, we need to avoid  $x$ - $y$  coupling as much as possible, and thus a planar undulator might be preferred. The electro-

1445 magnetic field of a TEM<sub>00</sub> mode Gaussian laser polarized in the horizontal plane is [36].

1471

$$\begin{pmatrix} E_x \\ E_y \\ E_z \\ cB_x \\ cB_y \\ cB_z \end{pmatrix} = E_{x0} e^{ik_L s - i\omega_L t + i\phi_0} (-iZ_R Q) \exp \left[ i \frac{k_L Q}{2} (x^2 + y^2) \right] \begin{pmatrix} 1 \\ 0 \\ -Qx \\ -Q^2 xy \\ Q^2 x^2 - \frac{iQ}{k_L} + 1 \\ -Qy \end{pmatrix}, \quad (207)$$

1472 where  $E_{x,y,z}$  and  $B_{x,y,z}$  are the horizontal, vertical and longi- 1499 with  $\beta = \sqrt{1 - \frac{1}{\gamma^2}}$ , and  
 1473 tudinal electric and magnetic field, respectively,  $s$  is the lon-  
 1474 gitudinal global path length variable,  $t$  is the time variable,  $c$   
 1475 is the speed of light in free space,  $\omega_L = k_L c$ ,  $Z_R = \pi w_0^2 / \lambda_L$   
 1476 is the Rayleigh length,  $w_0$  the beam waist radius, and

$$1477 Q = \frac{i}{Z_R \left( 1 + i \frac{s}{Z_R} \right)} \quad (208)$$

1478 with  $i$  here being the imaginary unit. We remind the readers  
 1479 that it has been implicitly assumed that all the fields will take  
 1480 the real part of their complex expressions.

1481 The relationship between the peak electric field  $E_{x0}$  and 1506  
 1482 the laser peak power  $P_L$  is given by

$$1483 P_L = \frac{E_{x0}^2 Z_R \lambda_L}{4 Z_0}, \quad (209)$$

1484 in which  $Z_0 = 376.73 \Omega$  is the impedance of free space. The 1509 Note that since the longitudinal coordinate of electron will  
 1485 prescribed wiggling motion of electron in a planar undulator 1510 affect the laser phase observed, so we need to calculate its  
 1486 is 1511 precision to the order of  $\frac{1}{\gamma^2}$ , while for the horizontal coordi-  
 1512 nate  $x$ , we only need to calculate it to the order of  $\frac{1}{\gamma}$ . In the  
 1513 following, we will adopt the approximation  $\beta \approx 1$  since we  
 1514 are interested in relativistic cases.

1488 with  $\gamma$  being the Lorentz factor,

$$1489 K = \frac{e B_0 \lambda_u}{2 \pi m_e c} = 0.934 \cdot B_0 [\text{T}] \cdot \lambda_u [\text{cm}] \quad (211)$$

1490 being the dimensionless undulator parameter, where  $B_0$  is 1519 the energy transfer from the laser to the electron. Note that  
 1491 the peak magnetic field,  $\lambda_u$  is the undulator period, and 1520 in this manuscript  $e$  represents the elementary charge and is  
 1492  $k_u = 2\pi/\lambda_u$  being the undulator wavenumber. The resonant 1521 assumed to be positive. Assuming that the laser beam waist is  
 1493 condition of laser-electron interaction inside a planar undula- 1522 in the middle of the undulator, whose length is  $L_u$ , and when  
 1494 tor is 1523 the electron transverse coordinates are much smaller than the  
 1524 laser beam waist  $x, y \ll w_0$ , which is true in most of the cases  
 1525 under consideration, we drop the factor  $\exp \left[ i \frac{k_L Q}{2} (x^2 + y^2) \right]$   
 1526 in the laser electric field. Further, when the transverse dis-  
 1527 placement of electron is much smaller than the Rayleigh  
 1528 length  $x \ll Z_R$  which is also usually the case, we can also  
 1529 drop the contribution from  $E_z$  on the energy modulation. As-  
 1530 suming the relative phase of laser field to the electron hori-  
 1531 zontal velocity  $v_x$  at the undulator center is  $\phi_0$ , the integrated  
 1532 modulation voltage induced by the laser on the electron beam  
 1533 in a planar undulator is then

$$1495 \lambda_L = \frac{1 + \frac{K^2}{2}}{2\gamma^2} \lambda_u. \quad (212)$$

1496 From the prescribed motion we can calculate the electron hor-  
 1497 izontal and longitudinal velocity

$$1498 v_x(s) \approx \frac{\beta c K}{\gamma} \cos(k_u s),$$

$$v_z(s) = \sqrt{v^2 - v_x^2} \approx \bar{v}_z - \frac{c K^2}{4\gamma^2} \cos(2k_u s), \quad (213)$$

1534 
$$V_L \approx \operatorname{Re} \left[ \int_{-\frac{L_u}{2}}^{\frac{L_u}{2}} v_x E_x \frac{ds}{c} \right] \approx E_{x0} \frac{K}{\gamma} \operatorname{Re} \left[ e^{i\phi_0} \int_{-\frac{L_u}{2}}^{\frac{L_u}{2}} \frac{1}{1 + i \frac{s}{Z_R}} \sum_{n=-\infty}^{\infty} J_n(-\chi) e^{in2k_u s} \frac{1 + e^{-i2k_u s}}{2} ds \right], \quad (219)$$

1535 where  $\operatorname{Re}()$  means taking the real component of the complex 1561 0.8 m ( $N_u = 10$ ),  $Z_R = 0.359L_u$ , then the induced energy 1536 number. When  $L_u \gg \lambda_u$ , which means the undulator period 1562 chirp strength with  $P_L = 1$  MW is  $h = 955 \text{ m}^{-1}$ . 1537 number  $N_u \gg 1$ , in the above integration, only the term with 1538  $n = 0$  and  $n = 1$  will give notable non-vanishing value. 1539 Denote  $[JJ] \equiv J_0(\chi) - J_1(\chi)$ , we then have 1563

$$\begin{aligned} V_L &= E_{x0} \frac{K}{\gamma} \frac{[JJ]}{2} \operatorname{Re} \left[ e^{i\phi_0} \int_{-\frac{L_u}{2}}^{\frac{L_u}{2}} \frac{1 - i \frac{s}{Z_R}}{1 + \left( \frac{s}{Z_R} \right)^2} ds \right] \\ &= E_{x0} \frac{K}{\gamma} [JJ] Z_R \tan^{-1} \left( \frac{L_u}{2Z_R} \right) \cos \phi_0. \end{aligned} \quad (220)$$

1541 We want the energy modulation strength as large as possible, 1542 so we choose  $\phi_0 = 0$ . Put in the expression of peak electric 1543 field from Eq. (209), the linear energy chirp strength around 1544 the zero-crossing phase is therefore

$$\begin{aligned} h &= \frac{eV_L}{E_0} k_L \\ &= \frac{ek_L K [JJ]}{\gamma^2 m_e c^2} \sqrt{\frac{2P_L Z_0}{\lambda_L}} \frac{\tan^{-1} \left( \frac{L_u}{2Z_R} \right)}{\sqrt{\frac{L_u}{2Z_R}}} \sqrt{L_u}. \end{aligned} \quad (221)$$

1546 Once the modulator length is given, we can optimize the laser 1547 Rayleigh length to maximize the energy modulation. Figure 6 1548 is a plot of  $f(x) = \frac{\tan^{-1}(x)}{\sqrt{x}}$  as a function of  $x$ . The 1549 maximum value of  $f(x)$  is 0.8034 and is realized when  $x = 1.392$ . 1550 So when  $Z_R = \frac{L_u}{2 \times 1.392} = 0.359L_u$ , the energy modulation 1551 reaches the maximum value. Note that when  $Z_R$  is within a 1569 induced by single laser with a laser power four times larger. 1552 small range close to the optimal value, the impact of Rayleigh 1570 Our calculation shows that indeed dual-tilted-laser (DTL) can 1553 length on the energy modulation strength is not very sensitive. 1571 induce a larger energy modulation compared to that of a sin- 1554 Therefore, for easy of remembering, the optimal condition 1572 gle laser, but the issue is that the required crossing angle (less 1555 can be expressed as 1573 than 2 mrad) is too small from an engineering viewpoint. We 1574 remind the readers that we can boost the bunching factor and 1575 thus radiation power by adding a third-harmonic modulation 1576 in addition to the fundamental-frequency modulation, as dis- 1577 cussed in Ref. [33]. Here in this paper we focus on the case 1578 of using a fundamental-frequency modulation only.

## 2. Dual-Tilted-Laser for Energy Modulation

1564 Now with a hope to increase the energy modulation 1565 strength with a given laser power, we may use a configuration 1566 of crossing two lasers for energy modulation. The basic idea 1567 is that if two crossing lasers can double the energy modula- 1568 tion strength of that of a single laser, then the effect is like that

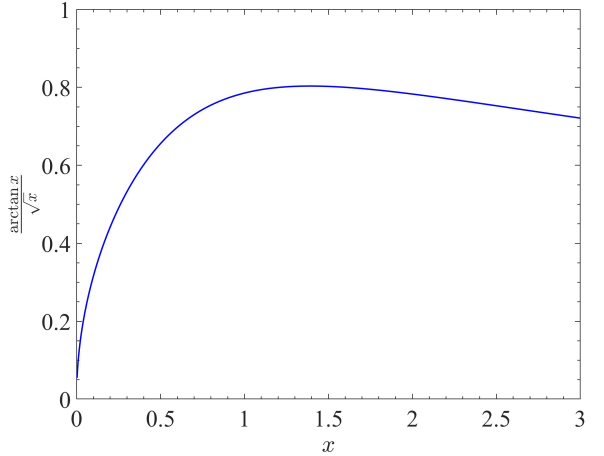


Fig. 6.  $f(x) = \frac{\tan^{-1}(x)}{\sqrt{x}}$  vs.  $x$ . This curve describes the laser induced energy modulation strength as a function of the laser Rayleigh length, with the laser power and modulator length given.

1556  $Z_R \approx \frac{L_u}{3}$ . 1569 induced by single laser with a laser power four times larger. 1570 Our calculation shows that indeed dual-tilted-laser (DTL) can 1571 induce a larger energy modulation compared to that of a sin- 1572 gle laser, but the issue is that the required crossing angle (less 1573 than 2 mrad) is too small from an engineering viewpoint. We 1574 remind the readers that we can boost the bunching factor and 1575 thus radiation power by adding a third-harmonic modulation 1576 in addition to the fundamental-frequency modulation, as dis- 1577 cussed in Ref. [33]. Here in this paper we focus on the case 1578 of using a fundamental-frequency modulation only.

1557 From Eq. (221), we can see that under the optimal condition, 1579 Now we present the analysis. First we consider the case 1558 we have  $h \propto \sqrt{P_L L_u}$ . Using Eq. (221) we can also do some 1580 of two lasers crossing in the  $y$ - $z$  plane. The laser field of an 1559 example calculation to get a more concrete feeling. If  $E_0 = 1581$  oblique TEM<sub>00</sub> laser is given by first replacing the physical 1560 600 MeV,  $\lambda_L = 1064$  nm,  $\lambda_u = 8$  cm ( $B_0 = 1.13$  T),  $L_u = 1582$  coordinate with the rotated coordinates

1583  $x \rightarrow x, y \rightarrow y_1 = y \cos \theta + s \sin \theta, s \rightarrow s_1 = -y \sin \theta + s \cos \theta, t \rightarrow t,$  1584 (223)

1584 with  $\theta$  in this section and below being the tilted angle of the incident laser instead of the dipole bending angle in Sec. III. We 1585 hope their difference is clear from context. The resulting field expression according to Eq. (207) is

1586

$$\begin{pmatrix} E_x \\ E_y \\ E_z \\ cB_x \\ cB_y \\ cB_z \end{pmatrix}_{\text{rot}} = E_{x0} e^{ik_L s_1 - i\omega_L t} \frac{\exp \left[ -\frac{k_L(x^2 + y_1^2)}{2(Z_R + is_1)} \right]}{1 + i \frac{s_1}{Z_R}} \begin{pmatrix} 1 \\ 0 \\ -i \frac{x}{Z_R + is_1} \\ \frac{x y_1}{(Z_R + is_1)^2} \\ -\frac{x^2}{(Z_R + is_1)^2} - \frac{1}{k_L(Z_R + is_1)} + 1 \\ -i \frac{y_1}{Z_R + is_1} \end{pmatrix}. \quad (224)$$

1587 Note however, in the above expression,  $x, y, s$  of the electromagnetic fields are defined according to the oblique laser propagating direction. To get the expression back in the original coordinate system, i.e., undulator axis as the  $z$  axis, we need to rotate 1588 the laser field as,

1590  $E_x \rightarrow E_{x\text{rot}}, E_y \rightarrow E_y = E_{y\text{rot}} \cos \theta - E_{z\text{rot}} \sin \theta, E_z \rightarrow E_z = E_{y\text{rot}} \sin \theta + E_{z\text{rot}} \cos \theta, t \rightarrow t,$  (225)

1591 and for the electric field the result is

1592 
$$\begin{pmatrix} E_x \\ E_y \\ E_z \end{pmatrix}_{\text{unrot}} = E_{x0} e^{ik_L s_1 - i\omega_L t} \frac{\exp \left[ -\frac{k_L(x^2 + y_1^2)}{2(Z_R + is_1)} \right]}{1 + i \frac{s_1}{Z_R}} \begin{pmatrix} 1 \\ -i \frac{x}{Z_R + is_1} \sin \theta \\ -i \frac{x}{Z_R + is_1} \cos \theta \end{pmatrix}. \quad (226)$$

1593 Assuming that the two crossing lasers are in-phase and have the same amplitude. In addition, we assume that  $\theta_2 = -\theta_1 = -\theta$ , 1594 and the two lasers have the same Rayleigh length. Then the superimposed field is

1595 
$$\begin{pmatrix} E_x \\ E_y \\ E_z \end{pmatrix}_{\text{unrot}} = E_{x0} e^{ik_L(-y \sin \theta + s \cos \theta) - i\omega_L t} \frac{\exp \left[ -\frac{k_L(x^2 + (y \cos \theta + s \sin \theta)^2)}{2(Z_R + i(-y \sin \theta + s \cos \theta))} \right]}{1 + i \frac{(-y \sin \theta + s \cos \theta)}{Z_R}} \begin{pmatrix} 1 \\ -i \frac{x}{Z_R + i(-y \sin \theta + s \cos \theta)} \sin \theta \\ -i \frac{x}{Z_R + i(-y \sin \theta + s \cos \theta)} \cos \theta \end{pmatrix} \\ + E_{x0} e^{ik_L(y \sin \theta + s \cos \theta) - i\omega_L t} \frac{\exp \left[ -\frac{k_L(x^2 + (y \cos \theta - s \sin \theta)^2)}{2(Z_R + i(y \sin \theta + s \cos \theta))} \right]}{1 + i \frac{(y \sin \theta + s \cos \theta)}{Z_R}} \begin{pmatrix} 1 \\ i \frac{x}{Z_R + i(y \sin \theta + s \cos \theta)} \sin \theta \\ -i \frac{x}{Z_R + i(y \sin \theta + s \cos \theta)} \cos \theta \end{pmatrix}. \quad (227)$$

1596 As before here we focus on the impact of  $E_x$  on laser-electron 1612 or  
1597 interaction, and ignore the contribution from  $E_z$ . When  $\theta$  is  
1598 very small, the superimposed  $E_x$  can be approximated as

1613 
$$E_x = 2E_{x0} \frac{\exp \left[ ik_L s \cos \theta - i\omega t - \frac{k_L(x^2 + s^2 \sin^2 \theta)}{2(Z_R + is \cos \theta)} \right]}{1 + i \frac{is \cos \theta}{Z_R}} \\ \approx 2E_{x0} e^{ik_L s \cos \theta - i\omega_L t} \frac{\exp \left[ -\frac{k_L s^2 \theta^2}{2(Z_R + is)} \right]}{1 + i \frac{s}{Z_R}}. \quad (228)$$

1599 Note that in the final approximated expression, we have kept 1616 Note that  $\chi$  now depends on  $\theta$ , more specifically,  
1600  $s \cos \theta$  in the laser phase term. The reason is that the laser  
1602 phase is of key importance in laser-electron interaction and  
1603 the accuracy requirement is high. In addition, we have also  
1604 kept the  $s^2 \theta^2$  in the intensity decay term, this is because  $L_u \theta$   
1605 may not be small compared to the laser beam waist radius  $w_0$ . 1618 Assume that the laser beam waists are in the middle of the  
1606 The expression of  $E_x$  for the case of crossing in  $x$ - $z$  plane 1619 undulator, whose length is  $L_u$ , and denote  
1607 is similar. So the difference of crossing in  $x$ - $z$  plane and  $y$ - $z$   
1608 plane is not much in inducing energy modulation.

1609 For effective laser-electron interaction, the off-axis reso- 1620  $v \equiv \frac{k_L Z_R \theta^2}{2} = \left( \frac{Z_R \theta}{w_0} \right)^2$ , (233)  
1610 nance condition now is

1611  $c \frac{\lambda_u}{\bar{v}_z} - \lambda_u \cos \theta = \lambda_L,$

1621 the integrated modulation voltage induced by the DTL in a  
1622 planar undulator is then

$$\chi = \frac{K^2 k_L}{8\gamma^2 k_u} \approx \frac{K^2}{4 + 2K^2 + 4\gamma^2 \theta^2}. \quad (232)$$

$$\begin{aligned}
1623 \quad V_L &\approx \operatorname{Re} \left[ \int_{-\frac{L_u}{2}}^{\frac{L_u}{2}} v_x E_x \frac{ds}{c} \right] \\
1624 \quad &\approx E_{x0} \frac{K[JJ]}{\gamma} Z_R \int_{-\frac{L_u}{2Z_R}}^{\frac{L_u}{2Z_R}} \frac{\exp \left( -v \frac{u^2}{1+u^2} \right)}{1+u^2} \left[ \cos \left( v \frac{u^3}{1+u^2} \right) + u \sin \left( v \frac{u^3}{1+u^2} \right) \right] du \cos \phi_0.
\end{aligned} \tag{234}$$

1624 To maximize the energy modulation, we choose  $\phi_0 = 0$ . Put in the expression of  $E_{x0}$  from Eq. (209), the linear energy chirp  
1625 strength around the zero-crossing phase is therefore

$$1626 \quad h = \frac{eV_L}{E_0} k_L = \frac{ek_L K[JJ]}{\gamma^2 m_e c^2} \sqrt{\frac{2P_L Z_0}{\lambda_L}} F_{\text{DTL-E}} \left( \frac{L_u}{2Z_R}, \frac{k_L Z_R \theta^2}{2} \right) \sqrt{L_u}, \tag{235}$$

1627 where

$$1628 \quad F_{\text{DTL-E}}(x, v) = \frac{1}{\sqrt{x}} \int_{-x}^x \frac{\exp \left( -v \frac{u^2}{1+u^2} \right)}{1+u^2} \left[ \cos \left( v \frac{u^3}{1+u^2} \right) + u \sin \left( v \frac{u^3}{1+u^2} \right) \right] du. \tag{236}$$

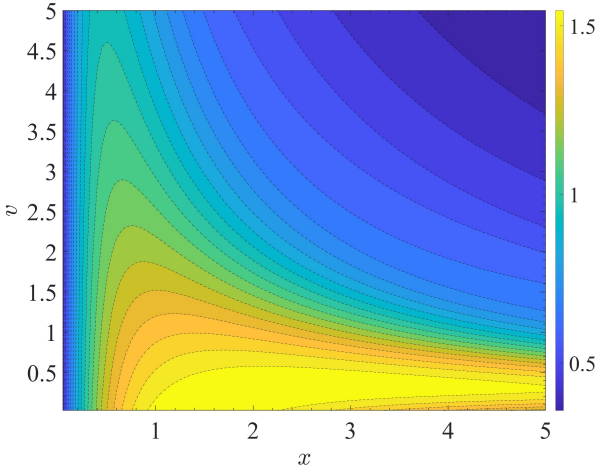


Fig. 7. Contour plot of  $F_{\text{DTL-E}}(x, v)$  given by Eq. (236).

1629 A flat contour plot of  $F_{\text{DTL-E}}(x, v)$  is given in Fig. 7.

1630 Now we can use the derived formula to calculate the energy  
1631 chirp strength induced by DTL. First we consider the case of  
1632 keeping  $\lambda_u$  fixed when changing  $\theta$ , then the off-axis resonant  
1633 condition leads to the undulator parameter as a function of  $\theta$   
1634 given by

$$1635 \quad K_\theta = \sqrt{2} \sqrt{2\gamma^2 \left( 1 - \frac{1}{\frac{\lambda_L}{\lambda_u} + \cos \theta} \right) - 1}. \tag{237}$$

1636 With the increase of  $\theta$ ,  $K_\theta$  will decrease. Note that in this case  
1637  $K_\theta \propto B_{0\theta}$ , so the magnetic field strength  $B_{0\theta}$  also decreases  
1638 with the increase of  $\theta$ . An example calculation of  $K_\theta$  vs.  $\theta$  is  
1639 given in Fig. 8. The corresponding contour plot of the energy  
1640 chirp strength normalized by the largest energy chirp induced  
1641 by a single normally incident laser, vs.  $\theta$  and  $Z_R/L_u$ , is given  
1642 in Fig. 9.

1643 The previous calculation assumes  $\lambda_u$  is kept unchanged

1644 when we adjust the incident angle  $\theta$ . This will result in a  
1645 limited region of  $\theta$  to fulfill the resonant condition as shown  
1646 in Fig. 8. Now we conduct the calculation by assuming the  
1647 peak magnetic field  $B_0$  unchanged when we adjust  $\theta$ . Put the  
1648 expression of undulator parameter Eq. (211) in the off-axis  
1649 resonant condition Eq. (230), we have

$$1650 \quad \frac{1}{2} \left( \frac{eB_0}{2\pi m_e c} \right)^2 \lambda_u^3 + (1 + \gamma^2 \theta^2) \lambda_u - 2\gamma^2 \lambda_L = 0, \tag{238}$$

1651 from which we get

$$1652 \quad \lambda_u = \frac{2\pi^{2/3} \sqrt[3]{\mathcal{D}}}{3^{2/3} B_0^2 e^2} - \frac{4\pi^{4/3} c^2 (\gamma^2 \theta^2 + 1) m_e^2}{\sqrt[3]{3} \sqrt[3]{\mathcal{D}}}, \tag{239}$$

1653 with

$$\begin{aligned}
1654 \quad \mathcal{D} = & \sqrt{3B_0^6 c^4 e^6 m_e^4 \left( 27B_0^2 \gamma^4 e^2 \lambda_L^2 + 8\pi^2 c^2 (\gamma^2 \theta^2 + 1)^3 m_e^2 \right)} \\
1655 & + 9B_0^4 c^2 \gamma^2 e^4 m_e^2 \lambda_L.
\end{aligned} \tag{240}$$

1656 For example, if  $\lambda_L = 1064$  nm and  $B_0 = 1.2$  T, then  $\lambda_u$  as  
1657 a function of  $\theta$  for the case of  $E_0 = 600$  MeV is shown in  
1658 Fig. 10. Note that in this case  $K_\theta \propto \lambda_u$  which depends on  $\theta$ ,  
1659 so the undulator parameter also decreases with the increase of  
1660  $\theta$ . But the decrease is not that fast compared to that presented  
1661 in Fig. 8. The corresponding contour plot of the energy chirp  
1662 strength induced by DTL normalized by the largest energy  
1663 chirp induced by a single normally incident laser, vs.  $\theta$  and  
1664  $Z_R/L_u$ , is given in Fig. 11.

1665 As can be seen from the calculation results in Figs. 9 and  
1666 11, DTL indeed can induce a larger energy modulation com-  
1667 pared to a single normally incident laser. But the required  
1668 crossing angle (less than 2 mrad) is too small for engineering.  
1669 So the usual setup of a single normally incident TEM<sub>00</sub> mode  
laser is still the preferred choice in practical application.

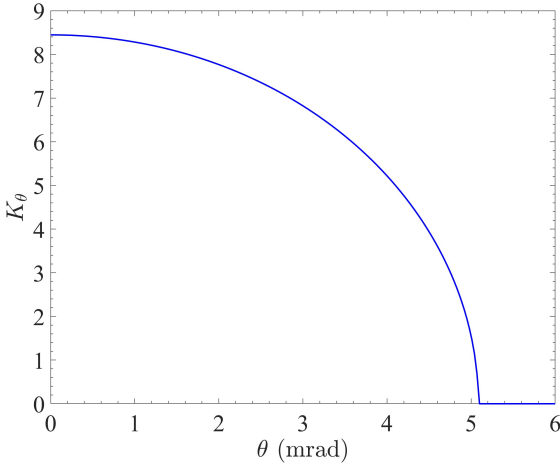


Fig. 8. Undulator parameter  $K_\theta$  vs.  $\theta$  with  $\lambda_u$  kept fixed. Parameters used:  $E_0 = 600$  MeV,  $\lambda_L = 1064$  nm,  $\lambda_u = 8$  cm.

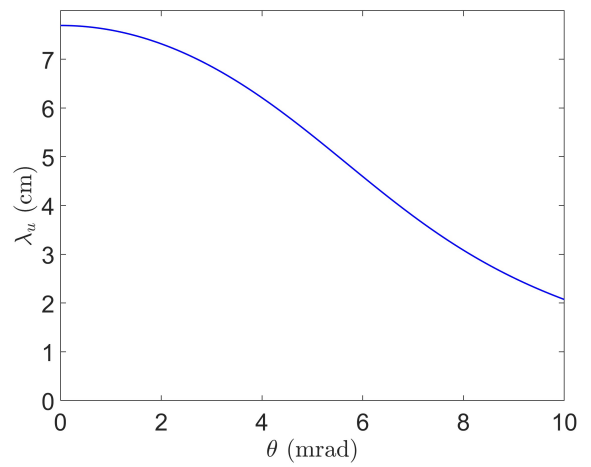


Fig. 10.  $\lambda_u$  vs.  $\theta$ , with  $B_0$  kept fixed. Parameters used:  $E_0 = 600$  MeV,  $\lambda_L = 1064$  nm,  $B_0 = 1.2$  T.

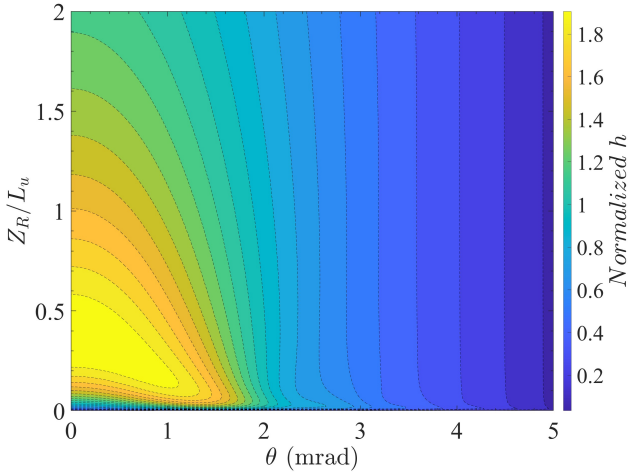


Fig. 9. Energy chirp strength  $h$  normalized by the largest energy chirp induced by a single normally incident laser, vs.  $\theta$  and  $Z_R/L_u$ . Keep  $\lambda_u$  fixed when changing  $\theta$ . Parameters used:  $E_0 = 600$  MeV,  $\lambda_L = 1064$  nm,  $\lambda_u = 0.08$  m,  $N_u = 10$ ,  $L_u = 0.8$  m.

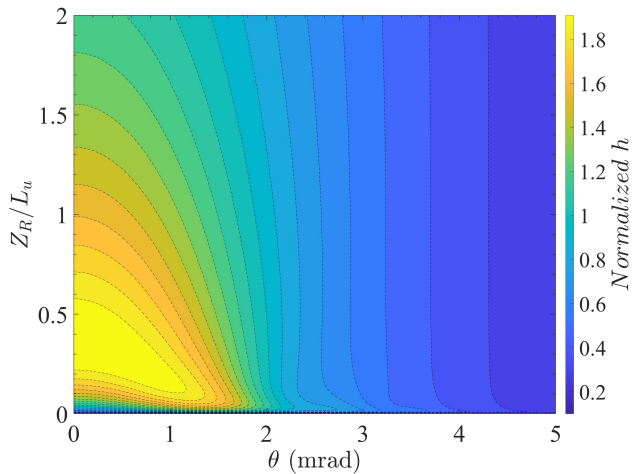


Fig. 11. Energy chirp strength  $h$  normalized by the largest energy chirp induced by a single normally incident laser, vs.  $\theta$  and  $Z_R/L_u$ . Keep  $B_0$  fixed when changing  $\theta$ . Parameters used:  $E_0 = 600$  MeV,  $\lambda_L = 1064$  nm,  $B_0 = 1.2$  T,  $L_u = 0.8$  m.

1670

### C. Realization Examples

1671 After the derivation of bunching factor and laser-induced 1672 modulation strengths, finally in this section we give some re- 1673 alization examples of microbunching schemes belonging to 1674 what we have analyzed. FEL seeding technique like phase- 1675 merging enhanced harmonic generation (PEHG) [37, 38], and 1676 angular dispersion-induced microbunching (ADM) [39] can 1677 be viewed as specific examples of our general definition of 1678 TLC-based microbunching schemes in Theorem One. More 1679 detailed discussion in this respect has been presented before 1680 in Ref. [33].

1681 Here we make a short comment about the relation between 1682 FEL seeding techniques like HGHG, PEGH, ADM and the 1683 storage ring schemes like LSF, GLSF discussed in this pa- 1684

1685 per. One is single-pass, and the other is multi-pass. One in- 1686 volves matrix multiplication or nonlinear transfer map once, 1687 and the other invokes eigen analysis or normal form analy- 1688 sis of the one-turn map. What they share is the bunch com- 1689 pression or harmonic generation mechanism. The relation 1690 between HGHG and LSF is similar to the relation between 1691 PEGH/ADM and GLSF.

1692 We also remind the readers that the GLSF SSMB scheme 1693 analyzed in this paper bears similarity to the approach dis- 1694 cussed in Ref. [40], in the transverse-longitudinal-coupling 1695 based microbunching and the modulation-demodulation pro- 1696 cesses. The difference is that here we aim for a true steady 1697 state in the context of storage ring dynamics and the electron 1698 beam pass the radiator turn by turn, while in Ref. [40] the 1699 radiator is placed at a bypass line and the ring is used to pre-

pare the electron beam which is sent to the bypass line every multiple revolutions in the ring. <sup>1710</sup> ultrasmall vertical emittance in a planar ring as explained before. The lumped laser-induced angular modulation is modeled as:

$$\begin{aligned} y' &= y' + A \sin(k_L z), \\ \delta &= \delta + A k_L y \cos(k_L z). \end{aligned} \quad (241)$$

## 1701 VII. ANGULAR MODULATION-BASED COUPLING 1702 SCHEMES

### 1703 A. Bunching Factor

1704 After investigating the energy modulation-based TLC mi-  
1705 crobunching schemes, now in this section we discuss angu-  
1706 lar modulation-based ones. The problem definition is similar  
1707 to that in the energy modulation-based schemes, only replac-  
1708 ing the energy modulation by angular modulation. We use  $y'$  <sup>1718</sup> Following the derivations in the section of energy  
1709 modulation as an example, since we will take advantage of the <sup>1719</sup> modulation-based schemes, the final form function in  
1710 this case is

$$\begin{aligned} \mathcal{F}(\mathbf{K}) &= \int \psi_f(\mathbf{X}) e^{-i\mathbf{K}\mathbf{X}} d\mathbf{X} \\ &= \int \psi_{m+}(\mathbf{X}) e^{-i\mathbf{K}\mathbf{R}\mathbf{X}} d\mathbf{X} \\ &= \int \psi_0(\mathbf{X}) e^{-i(\mathbf{K}\mathbf{R}\mathbf{X} + \mathbf{K}\mathbf{R}_{i4}A \sin(k_L z) + \mathbf{K}\mathbf{R}_{i6}A k_L y \cos(k_L z))} d\mathbf{X} \\ &= \sum_{p_1=-\infty}^{\infty} J_{p_1}(-\mathbf{K}\mathbf{R}_{i4}A) \int \psi_0(\mathbf{X}) e^{-i(\mathbf{K}\mathbf{R}\mathbf{X} - p_1 k_L z + \mathbf{K}\mathbf{R}_{i6}A k_L y \cos(k_L z))} d\mathbf{X} \\ &= \sum_{p_1=-\infty}^{\infty} J_{p_1}(-\mathbf{K}\mathbf{R}_{i4}A) \int \psi_0(\mathbf{X}) \sum_{p_2=-\infty}^{\infty} i^{p_2} J_{p_2}(-\mathbf{K}\mathbf{R}_{i6}A k_L y) e^{-i[\mathbf{K}\mathbf{R}\mathbf{X} - (p_1 + p_2)k_L z]} d\mathbf{X}. \end{aligned} \quad (243)$$

1722 The integration of the above result is given by generalized hypergeometric function. If  $\mathbf{K} = (0 \ 0 \ 0 \ 0 \ k_z \ 0)$  and  $R_{56} = 0$ ,  
1723 then  $\mathbf{K}\mathbf{R}_{i6} = 0$ , and the initial beam distribution is Gaussian as given in Eq. (190), then the 1D bunching factor is

$$\begin{aligned} b(k_z) &= \sum_{p=-\infty}^{\infty} J_p(-\mathbf{K}\mathbf{R}_{i4}A) \int \psi_0(\mathbf{X}) e^{-i(\mathbf{K}\mathbf{R}\mathbf{X} - p k_L z)} d\mathbf{X} \\ &= \sum_{p=-\infty}^{\infty} J_p(-k_z R_{54} A) \exp\left(-\frac{\mathbf{M}_p \Sigma_0 \mathbf{M}_p^T}{2}\right), \end{aligned} \quad (244)$$

1725 with  $\mathbf{M}_p$  given by Eq. (188).

1726 To appreciate the physical principle, instead of a general mathematical analysis, we use one specific case as an example. If  
1727  $R_{51} = 0$ ,  $R_{52} = 0$ ,  $R_{55} = 1$ ,  $R_{56} = 0$ , and the initial beam is transverse-longitudinal decoupled and has an upright distribution  
1728 in the longitudinal phase space, then

$$b(k_z) = \sum_{p=-\infty}^{\infty} J_p(-k_z R_{54} A) \exp\left(-\frac{k_z^2}{2} \left[ \epsilon_y (R_{53}^2 \beta_y - 2R_{53} R_{54} \alpha_y + R_{54}^2 \gamma_y) + \left(1 - \frac{p k_L}{k_z}\right)^2 \sigma_{z0}^2 \right]\right), \quad (245)$$

1730 with  $\alpha_y, \beta_y, \gamma_y$  being the Courant-Snyder functions before the modulation, and  $\sigma_{z0}$  being the initial RMS energy spread.

1732 If the initial bunch length is much longer than the laser wave-  
1733 length, the above exponential terms will be non-zero only  
1734 when  $1 - \frac{p k_L}{k_z} = 0$ , which means there is only bunching at <sup>1737</sup> at the  $n$ -th laser harmonic to be  
1735 the laser harmonics. In this case, we have the bunching factor

$$\begin{aligned} b_n &= b(k_z = n k_L) \\ &= J_n(-n k_L R_{54} A) \exp\left[-\frac{(n k_L)^2}{2} \epsilon_y \mathcal{H}_{yR}\right], \end{aligned} \quad (246)$$

1738 where  $\mathcal{H}_{yR} = R_{53}^2 \beta_y - 2R_{53}R_{54}\alpha_y + R_{54}^2 \gamma_y$ . One can appreciate the similarity of the above result with the bunching factor of the energy modulation-based TLC microbunching schemes, i.e., Eq. (206). The  $R_{54}$  here plays the role of  $R_{53}$  there. If further  $R_{53} = 0$ , then Eq. (246) reduces to

1739 can be viewed as partial transverse-longitudinal emittance exchanges at the optical laser wavelength range. They do not necessarily need to be a complete emittance exchanges since 1740 1757 1758 1759 1760 1761 1762

$$b_n = J_n(-nk_L R_{54} A) \exp \left[ -\frac{(nk_L R_{54} \sigma_{y'})^2}{2} \right], \quad (247)$$

1744 where  $\sigma_{y'}$  is the initial RMS beam angular divergence. So  
 1745  $R_{54}$  and  $\sigma_{y'}$  in this scheme play the role of  $R_{56}$  and  $\sigma_\delta$  in  
 1746 HGHG as shown in Eq. (195), respectively. In a planar un-  
 1747 coupled ring, the natural vertical emittance is quite small, thus  
 1748 also  $\sigma_{y'}$ . Therefore, using this scheme we can realize a high  
 1749 harmonic bunching in a storage ring, for example to generate  
 1750 ultrashort soft X-ray pulse.

1751 As can be seen from our analysis, both the energy 1769 After deriving the bunching factor, now we derive the laser-  
 1752 modulation-based and the angular modulation-based TLC mi- 1770 induced angular modulation strength for quantitative evalua-  
 1753 crobunching schemes share the same spirit, i.e., to take advan- 1771 tion. We start with the usual angular modulation proposal by  
 1754 tage of the small transverse emittance, the vertical emittance 1772 applying a  $TEM_{01}$  mode laser in an undulator [43]. The elec-  
 1755 in our case, to generate microbunching with a shallow mod- 1773 tric field of a Hermite-Gaussian  $TEM_{01}$  mode laser polarized  
 1756 ulation strength. These TLC-based microbunching schemes 1774 in the horizontal plane is [36]

1757 can be viewed as partial transverse-longitudinal emittance ex-  
1758 changes at the optical laser wavelength range. They do not  
1759 necessarily need to be a complete emittance exchanges since  
1760 for microbunching, the most important coordinate is  $z$ , and  $\delta$   
1761 is relatively less important. As we will show soon, although  
1762 the spirit is the same, given the same level of modulation laser  
1763 power, the physical realization of energy modulation-based  
1764 TLC microbunching schemes turn out to be more effective for  
1765 our SSMB application compared to the angular modulation-  
1766 based schemes.

## B. Modulation Strength

## 1. TEM01 Mode Laser-Induced Angular Modulation

$$\begin{pmatrix} E_x \\ E_y \\ E_z \\ cB_x \\ cB_y \\ cB_z \end{pmatrix} = E_{x0} e^{ik_L s - i\omega_L t} (-iZ_R Q)^2 \exp \left[ i \frac{k_L Q}{2} (x^2 + y^2) \right] \left( \frac{2\sqrt{2}}{w_0} \right) \begin{pmatrix} y \\ 0 \\ -Qxy \\ i \frac{Qx}{k_L} - Q^2 xy^2 \\ \left( Q^2 x^2 - \frac{iQ}{k_L} + 1 \right) y \\ \frac{i}{k_L} - Qy^2 \end{pmatrix}. \quad (248)$$

1776 The relation between  $E_{x0}$  and the laser peak power for a <sub>1790</sub>  $\sqrt{\frac{Z_R \lambda_L}{\pi}}$  we have  
 1777 TEM<sub>01</sub> mode laser is given by

$$P_L = \frac{E_{x0}^2 Z_R \lambda_L}{2 Z_0}. \quad (249)$$

1779 Note there is a factor of two difference in the above laser  
 1780 power formula compared to the case of a  $\text{TEM}_{00}$  mode laser.  
 1781 The electron wiggles in a horizontal planar undulator accord-  
 1782 ing to Eq. (210), and the laser-electron exchanges energy ac-  
 1783 cording to Eq. (218). Making the same assumption and fol-  
 1784 lowing similar procedures as before, we can get the integrated  
 1785 modulation voltage induced by a  $\text{TEM}_{01}$  mode laser in the  
 1786 undulator

$$(249)_{1791} \quad V_L = \frac{4K[JJ]}{\gamma} \frac{\sqrt{\pi P_L Z_0}}{\lambda_L} \frac{\frac{L_u}{2Z_R}}{1 + \left(\frac{L_u}{2Z_R}\right)^2} y. \quad (251)$$

1792 The induced energy modulation strength with respect to  $y$   
 1793 around the zero-crossing phase is then

1795 The symplecticity of the dynamical system will require that  
 1796 this formula also gives the linear angular chirp strength  
 1797 around the zero-crossing phase. It is interesting to note that,  
 1798 given the laser power, the modulation kick strength depends  
 1799 on the ratio between  $Z_R$  and  $L_u$ , instead of their absolute val-  
 1800 ues.

1801 One may wonder that when  $\frac{L_u}{2Z_R}$  is fixed, the induced angular chirp strength is independent of the modulator length  
 1802  $L_u$ . While in a  $\text{TEM}_{00}$  mode laser modulator, as given in  
 1803 Eq. (221), we have the energy modulation strength propor-  
 1804

1805 tional to  $\sqrt{L_u}$ . Mathematically this is because in the expres- 1829  
 1806 sion of a  $\text{TEM}_{01}$  mode laser field, there is a term  $(-iZ_R Q)^2$ ,  
 1807 while in a  $\text{TEM}_{00}$  mode laser, this term is  $(-iZ_R Q)$ . Phys-  
 1808 ically it means the on-axis power density of a  $\text{TEM}_{01}$  mode  
 1809 laser decays faster, compared to that of a  $\text{TEM}_{00}$  mode laser, 1830  
 1810 when we go away from the laser waist. This may not be sur- 1831  
 1811 prising if we keep in mind that the intensity peaks of a  $\text{TEM}_{01}$  1832  
 1812 mode laser are not on-axis. But we recognize there is a lower 1833  
 1813 limit of the modulator length, below which the laser waist 1834  
 1814 size is too small and our approximation of ignoring particle 1835  
 1815 transverse coordinate and wiggle motion on the modulation 1836  
 1816 breaks down.

1817 According to Eq. (252), the maximal modulation is realized 1837  
 1818 when  $Z_R = \frac{L_u}{2}$  and the value is

$$1819 g_{\max} = \frac{\partial \left( \frac{eV_L}{E_0} \right)}{\partial y} = \frac{ek_L K[JJ]}{\gamma^2 m_e c^2} \sqrt{\frac{P_L Z_0}{\pi}}. \quad (253)$$

1820 For example, if  $E_0 = 600$  MeV,  $\lambda_L = 1064$  nm,  $\lambda_u = 8$  cm

1821 ( $B_0 = 1.13$  T),  $L_u = 0.8$  m ( $N_u = 10$ ),  $Z_R = \frac{L_u}{2}$ , 1844  
 1822 then for  $P_L = 1$  MW the induced angular chirp strength is 1845  
 1823  $g = 0.55$  m $^{-1}$ . As a comparison, the energy chirp strength 1846  
 1824 induced by such a 1 MW  $\text{TEM}_{00}$  laser modulator as evaluated 1847  
 1825 before is  $h = 955$  m $^{-1}$ . So generally, a  $\text{TEM}_{01}$  mode laser is 1848  
 1826 not effective in imprinting angular modulation. Actually we 1849  
 1827 will see in the next section, even a dual-tilted-laser setup is 1850  
 1828 still not effective enough for our application.

## 2. Dual-Titled-Laser-Induced Angular Modulation

1829 Another way to imprint angular modulation on the electron  
 1830 beam is using a titled incident  $\text{TEM}_{00}$  mode laser to modulate  
 1831 the beam in an undulator. To further lower the required laser  
 1832 power, we can apply dual-tilted-laser (DTL) with a crossing  
 1833 configuration [44, 45]. Here in this paper, we focus on the an-  
 1834 gular modulation scheme based on the DTL setup. Note that  
 1835 if we want to use a DTL for energy modulation, the two lasers  
 1836 should be in phase to make the two laser induced energy mod-  
 1837 ulations add. While for angular modulation, they should be  
 1838  $\pi$ -phase shifted with respect to each other. This is because for  
 1839 angular modulation, the particle on the reference orbit should  
 1840 get zero energy kick. Only when the particle transverse co-  
 1841 ordinate is nonzero will it get an energy kick. So the energy  
 1842 modulations induced by the two lasers should cancel on axis.  
 1843

1844 To induce vertical angular modulation, we let the two lasers  
 1845 cross in  $y$ - $z$  plane and be polarized in the horizontal plane.  
 1846 The laser field of a normal incident  $\text{TEM}_{00}$  laser is given by  
 1847 Eq. (207). Assuming that the two lasers are  $\pi$ -phase-shifted  
 1848 with respect to each other and have the same amplitude. In  
 1849 addition, we assume that  $\theta_2 = -\theta_1 = -\theta$ , and the two lasers  
 1850 will have the same Rayleigh length. Then the superimposed field  
 1851 is

$$1852 \begin{pmatrix} E_x \\ E_y \\ E_z \end{pmatrix}_{\text{unrot}} = E_{x0} e^{ik_L(-y \sin \theta + s \cos \theta) - i\omega_L t} \frac{\exp \left[ -\frac{k_L(x^2 + (y \cos \theta + s \sin \theta)^2)}{2(Z_R + i(-y \sin \theta + s \cos \theta))} \right]}{1 + i \frac{(-y \sin \theta + s \cos \theta)}{Z_R}} \begin{pmatrix} 1 \\ -i \frac{x}{Z_R + i(-y \sin \theta + s \cos \theta)} \sin \theta \\ -i \frac{x}{Z_R + i(-y \sin \theta + s \cos \theta)} \cos \theta \end{pmatrix} \\ - E_{x0} e^{ik_L(y \sin \theta + s \cos \theta) - i\omega_L t} \frac{\exp \left[ -\frac{k_L(x^2 + (y \cos \theta - s \sin \theta)^2)}{2(Z_R + i(y \sin \theta + s \cos \theta))} \right]}{1 + i \frac{(y \sin \theta + s \cos \theta)}{Z_R}} \begin{pmatrix} 1 \\ i \frac{x}{Z_R + i(y \sin \theta + s \cos \theta)} \sin \theta \\ -i \frac{x}{Z_R + i(y \sin \theta + s \cos \theta)} \cos \theta \end{pmatrix}. \quad (254)$$

1853 As before, we will focus on the impact of  $E_x$  on the laser-electron interaction, and ignore the contribution from  $E_z$ . Note that  
 1854 if  $y = 0$ , then  $E_x = 0$ . We want to know  $\frac{\partial E_x}{\partial y}$  when  $y$  is close to zero. For this purpose, we do Taylor expansion of the above  
 1855 horizontal electric field with respect to  $\theta$  when  $\theta$  is small,

$$1856 E_x = E_{x0} \frac{Z_R (2isk_L Z_R + 2k_L Z_R^2 + x^2 k_L + y^2 k_L - 2Z_R - 2is) \exp \left[ -\frac{k_L(x^2 + y^2)}{2(Z_R + iz)} + ik_L s - i\omega_L t \right]}{(s - iZ_R)^3} \theta y. \quad (255)$$

1857 When  $x, y \ll Z_R, \lambda_L \ll Z_R$ , we have

$$1858 E_x \approx -i2k_L E_{x0} \frac{\exp \left[ -\frac{(x^2 + y^2)}{w_0^2 (1 + i \frac{s}{Z_R})} + ik_L s - i\omega_L t \right]}{\left( 1 + i \frac{s}{Z_R} \right)^2} \theta y. \quad (256)$$

1859 But note that when  $L_u \theta$  is comparable to  $w_0$ , the term  $s \sin \theta$  should be kept in the exponential term. Also for the laser phase,  
 1860 we should use the more accurate  $s \cos \theta$ . These arguments have been explained before also when we analyze the application of  
 1861 a DTL for energy modulation. So the more correct approximate expression of  $E_x$  is

$$1862 E_x \approx -i2k_L E_{x0} \frac{\exp \left( -\frac{s^2 \theta^2}{w_0^2 (1 + i \frac{s}{Z_R})} + ik_L s \cos \theta - i\omega_L t \right)}{\left( 1 + i \frac{s}{Z_R} \right)^2} \theta y. \quad (257)$$

Again taking the same notation as given in Eq. (233), the integrated modulation voltage induced by a DTL (two lasers  $\pi$ -phase-shifted with respect to each other) in a planar horizontal undulator can be calculated to be

$$V_L \approx \operatorname{Re} \left[ \int_{-\frac{L_u}{2}}^{\frac{L_u}{2}} v_x E_x \frac{ds}{c} \right] \approx k_L E_{x0} \frac{K[JJ]}{\gamma} \theta y Z_R \left[ \int_{-\frac{L_u}{2Z_R}}^{\frac{L_u}{2Z_R}} \frac{\exp\left(-v \frac{u^2}{(1+u^2)}\right)}{(1+u^2)^2} \left[ (1-u^2) \cos\left(v \frac{u^3}{(1+u^2)}\right) + 2u \sin\left(v \frac{u^3}{(1+u^2)}\right) \right] du \right] \sin \phi_0. \quad (258)$$

We choose  $\phi_0 = \frac{\pi}{2}$  to maximize  $V_L$ . Therefore, we get the maximum linear angular chirp strength as

$$g = \frac{\partial \left( \frac{eV_L}{E_0} \right)}{\partial y} = \frac{ek_L K[JJ]}{\gamma^2 m_e c^2} \sqrt{\frac{2P_L Z_R}{\lambda_L}} F_{\text{DTL-A}} \left( \frac{L_u}{2Z_R}, \frac{k_L Z_R \theta^2}{2} \right) \sqrt{L_u} \theta, \quad (259)$$

where

$$F_{\text{DTL-A}}(x, v) = \frac{1}{\sqrt{x}} \int_{-x}^x \frac{\exp\left(-v \frac{u^2}{(1+u^2)}\right)}{(1+u^2)^2} \left[ (1-u^2) \cos\left(v \frac{u^3}{(1+u^2)}\right) + 2u \sin\left(v \frac{u^3}{(1+u^2)}\right) \right] du. \quad (260)$$

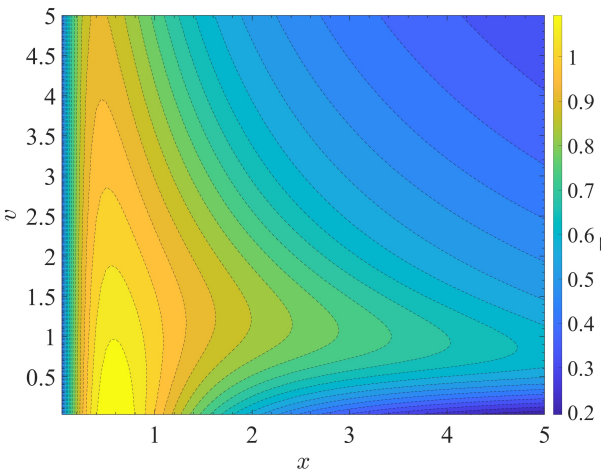


Fig. 12. Contour plot of  $F_{\text{DTL-A}}(x, v)$  given by Eq. (260).

A contour plot of  $F_{\text{DTL-A}}(x, v)$  is shown in Fig. 12.

Then the angular chirp strength introduced by a DTL compared to the energy chirp strength introduced by a single TEM<sub>00</sub> laser modulator, i.e., that given in Eq. (221), with the same laser parameters and undulator length can be expressed as

$$\frac{g}{h} = \xi \theta. \quad (261)$$

with

$$\xi = \frac{F_{\text{DTL-A}} \left( \frac{L_u}{2Z_R}, \frac{k_L Z_R \theta^2}{2} \right)}{\tan^{-1} \left( \frac{L_u}{2Z_R} \right)} \frac{K[JJ]}{K[JJ]|_{\theta=0}}. \quad (262)$$

Note that  $K[JJ]$  in the numerator is a function of  $\theta$  according to the off-axis resonance condition given in Eq. (230). Since  $\xi \sim 1$ , and  $\theta$  is usually in mrad level, given the same laser power, the DTL-induced angular chirp strength will be much smaller than the energy modulation strength induced by a TEM<sub>00</sub> mode laser. This observation has been supported by more quantitative calculation of the angular chirp strength induced by a DTL as shown in Figs. 13 and 14. As before, we have considered the case of keeping  $\lambda_u$  or  $B_0$  unchanged when we change the crossing angle  $\theta$ , respectively. In both cases, the maximal angular chirp strength induced with  $P_L = 1$  MW is about  $g \approx 1.7 \text{ m}^{-1}$ . While from the evaluation in Sec. VIB 1, at the same power level, a TEM<sub>00</sub> mode laser modulation can induce an energy chirp strength of  $h \sim 955 \text{ m}^{-1}$ . This as explained is because  $\theta$  is only 1 to 2 mrad.

So we can see that the DTL-induced angular chirp strength, although a factor of three larger than that induced by a single normally incident TEM<sub>01</sub> mode laser with the same laser power, is still generally quite small. There are two reasons why a DTL is not effective in imprinting angular modulation:

- The crossing angle between the laser and the electron propagating directions results in that they have a rather limited effective interaction region. For example, if the crossing angle is  $\theta = 5 \text{ mrad}$ , and the undulator length is  $L_u = 0.8 \text{ m}$ . Then the center of electron beam and center of laser beam at the undulator entrance and exit depart from each other with a distance of  $\frac{L_u}{2} \theta = 2 \text{ mm}$ , which is a large value compared to the laser beam waist  $w_0 = \sqrt{\frac{Z_R \lambda_L}{\pi}} \approx \sqrt{\frac{L_u \lambda_L}{2\pi}} = 368 \mu\text{m}$  and results in a very weak laser electric field felt by the electron there.
- The decrease of undulator parameter  $K$  with the increase of  $\theta$  to meet the off-axis resonance condition, as can be seen in Figs. 8 and 10.

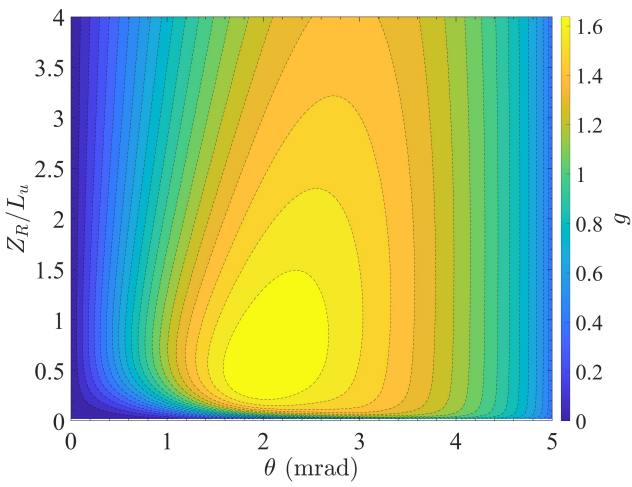


Fig. 13. Angular chirp strength  $g$  vs.  $\theta$  and  $Z_R/L_u$ , keep  $\lambda_u$  fixed when changing  $\theta$ . Parameters used:  $E_0 = 600$  MeV,  $\lambda_L = 1064$  nm,  $P_L = 1$  MW,  $\lambda_u = 0.08$  m,  $N_u = 10$ ,  $L_u = 0.8$  m.

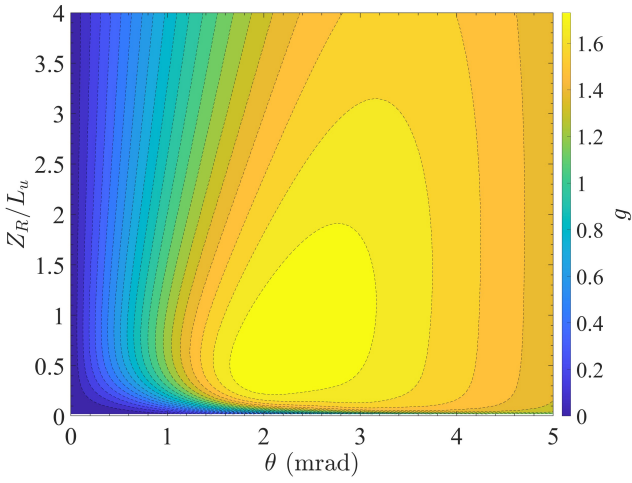


Fig. 14. Angular chirp strength  $g$  vs.  $\theta$  and  $Z_R/L_u$ , keep  $B_0$  fixed when changing  $\theta$ . Parameters used:  $E_0 = 600$  MeV,  $\lambda_L = 1064$  nm,  $P_L = 1$  MW,  $B_0 = 1.2$  T,  $L_u = 0.8$  m.

Since the angular chirp strength is small, then according to Theorem Two, the required vertical beta function at the modulator  $\beta_{yM}$  will be large. For example, if  $\epsilon_y = 4$  pm,  $\sigma_{zR} = \sqrt{\epsilon_y \mathcal{H}_{yR}} = 2$  nm, and  $g = 2 \text{ m}^{-1}$ , then we need  $\beta_{yM} = 2.5 \times 10^5$  m, which is too large to be used in practice in a storage ring. If we want to lower  $\beta_{yM}$ , it then means a higher modulation laser power is needed. This is the reason why we tend to use energy modulation-based coupling schemes for bunch compression or microbunching generation in GLSF SSMB. Our analysis and conclusion here is consistent with what reported in Ref. [49] when comparing energy and angular modulation microbunching schemes for laser plasma accelerator based light source.

Generally, when we compare the energy modulation-based

and DTL-induced angular modulation-based bunch compression schemes, from the Theorem One and Two, i.e., Eqs. (150) and (152), for the same modulation laser wavelength  $\lambda_L$  and power  $P_L$ , vertical emittance  $\epsilon_y$  and target linear bunch length at the radiator  $\sigma_{zR} = \sqrt{\epsilon_y \mathcal{H}_{yR}}$ , we have

$$\beta_{yM}(\text{Angular modulation}) \sim \frac{\mathcal{H}_{yM}(\text{Energy modulation})}{\theta^2}. \quad (263)$$

### C. Realization Examples

Similar to the section on energy modulation-based schemes, here we also introduce some realization examples of angular modulation-based microbunching. The first proposal of applying the angular modulated beam for harmonic generation to our knowledge is from Ref. [43]. Later an emittance exchange-based harmonic generation scheme is proposed in Ref. [46]. These two schemes apply the TEM<sub>01</sub> mode laser to induce angular modulation. Following these development, there are proposals to realize angular modulation using TEM<sub>00</sub> mode lasers, with Ref. [47] using an off-resonance laser, and Ref. [48] using a tilted incident laser. And later a dual-tilted-laser (DTL) modulation scheme is applied in emittance exchange at the optical laser wavelength range [44]. And most recently, the DTL scheme is proposed to compress the bunch length in SSMB and lower the requirement on the laser power by a factor of four compared to a single-tilted laser scheme [45]. Note that for these angular modulation-based harmonic or bunch compression schemes, we have the inequality given in Eq. (152), i.e., our Theorem Two.

## VIII. 1 KW GLSF SSMB EUV SOURCE

Our goal in this paper as stated is to find a solution for high-power EUV source based on SSMB, using parameters within the reach of present technology. According to our analysis, generalized longitudinal strong focusing (GLSF) turns out to be the most promising scenario, compared to the longitudinal weak focusing and longitudinal strong focusing. The key of a GLSF SSMB ring is the precision transverse-longitudinal coupling dynamics to utilize the ultrasmall natural vertical emittance in a planar electron storage ring for efficient microbunching formation. For our purpose we find energy modulation-based coupling schemes are preferred than angular modulation-based coupling ones, in lowering the required modulation laser power. So the conclusion is that we will use a TEM<sub>00</sub> laser induced energy modulation-based coupling scheme in a GLSF SSMB storage ring. In this section, we first present a solution of 1 kW-average-power EUV source based on GLSF SSMB. More detailed analyses to support our solution are then developed.

TABLE 2. An example parameter set of a GLSF SSMB ring for 1 kW-average-power EUV radiation generation.

Parameter	Value	Description
$E_0$	600 MeV	Beam energy
$C_0$	$\sim 200$ m	Circumference
$\eta$	$\sim 5 \times 10^{-3}$	Phase slippage factor
$I_P$	40 A	Peak current
$f_e$	0.5%	Electron beam filling factor
$I_A$	200 mA	Average current
$B_{\text{ring}}$	1.33 T	Bending magnet field in the ring
$\rho_{\text{ring}}$	1.5 m	Bending radius in the ring
$U_{0\text{dipoles}}$	7.7 keV	Radiation loss per particle per turn from ring dipoles
$B_{0w}$	6 T	Bending field of damping wiggler
$L_w$	40 m	Total length of $N_{wc}$ identical damping wigglers
$N_{wc}$	20	Number of identical damping wigglers
$\lambda_w$	$< 0.168$ m	Wiggler period length
$U_{0w}$	328 keV	Radiation loss per particle per turn from damping wiggler
$P_{R\text{beam}}$	68.3 kW	Total radiation loss power of the electron beam
$P_{RF}$	100 $\sim$ 200 kW	Total power consumption of the RF system
$\sigma_{\delta 0}$	$4.2 \times 10^{-4}$	Natural energy spread (without damping wiggler)
$\sigma_{\delta w}$	$8.2 \times 10^{-4}$	Natural energy spread (with damping wiggler)
$\sigma_{\delta\text{IBS}}$	$8.5 \times 10^{-4}$	Energy spread with IBS (with damping wiggler)
$\epsilon_x$	2 nm	Horizontal emittance
$\epsilon_y$	40 pm	Vertical emittance
$\tau_{y\text{RD}}$	2.38 ms	Vertical radiation damping time with damping wiggler
$\tau_{y\text{IBS}}$	7.11 ms	Vertical IBS diffusion time
$\lambda_L$	1064 nm	Modulation laser wavelength
$\sigma_{zR}$	2 nm	Linear bunch length at the radiator
$\mathcal{H}_{yR}$	0.1 $\mu$ m	$\mathcal{H}_y$ at the radiator
$\mathcal{H}_{yM}$	0.056 m	$\mathcal{H}_y$ at the modulator
$A = \frac{eV_L}{E_0}$	$2.3 \times 10^{-3}$	Modulator induced energy modulation strength
$h$	$1.33 \times 10^4$ m $^{-1}$	Modulator induced linear energy chirp strength
$\lambda_{uM}$	0.1 m	Modulator undulator period
$B_{0M}$	0.806 T	Modulator peak magnetic flux density
$K_{uM}$	7.53	$K$ of modulator undulator
$N_{uM}$	15	$N_u$ of modulator undulator
$L_{uM}$	1.5 m	Modulator length
$\Delta\epsilon_{yM}$	13.4 pm	Modulators' quantum excitation to vertical emittance
$Z_R$	$\sim \frac{L_{uM}}{3}$	Laser Rayleigh length
$P_{LP}$	130 MW	Peak modulation laser power
$f_L$	0.5%	Laser beam filling factor
$P_{LA}$	651 kW	Average modulation laser power
$\lambda_R = \frac{\lambda_L}{79}$	13.5 nm	Radiation wavelength
$b_{79}$	0.0675	Bunching factor
$\sigma_{\perp R}$	20 $\mu$ m	Effective transverse electron beam size at the radiator
$\lambda_{uR}$	1.8 cm	Radiator undulator period
$B_{0R}$	0.867 T	Radiator peak magnetic flux density
$N_{uR}$	$79 \times 4$	Number of undulator periods
$L_{uR}$	5.69 m	Radiator length
$P_{RP}$	224 kW	Peak radiation power
$P_{RA}$	1.12 kW	Average radiation power

1974

## A. A Solution of 1 kW EUV Source

1982

## B. Some Basic Considerations

1975 Based on what we have studied in previous sections and the 1983 Now we present the detailed considerations and calcula-  
 1976 various important physical effects to be discussed in this sec- 1984 tions to support our solution. First are some basic considera-  
 1977 tion, here we present an example parameter set of an 1 kW- 1985 tions on the parameter choice. As explained in the beginning  
 1978 average-power EUV light source based on GLSF SSMB as 1986 of Sec. IV, we will use a beam energy of  $E_0 = 600$  MeV  
 1979 shown in Tab. 2. All the parameter list should be doable from 1987 and a modulation laser wavelength of  $\lambda_L = 1064$  nm. In the  
 1980 an engineering viewpoint. Such a table summarizes our in- 1988 GLSF scheme, a small vertical emittance is crucial. We as-  
 1981 vestigations presented in this paper. 1989 sume that the vertical emittance used to accomplish our goal

stated above is  $\epsilon_y = 40$  pm. One may notice that the vertical emittance we use is actually not extremely small. This conservative choice is mainly a refection of consideration for intra-beam scattering (IBS) to be introduced soon. To realize significant coherent EUV generation, and considering that we may generate microbunching based on a coasting beam or RF bunched beam in the ring, which is much longer than the linear bunch length  $\sigma_{zR} = \sqrt{\epsilon_y \mathcal{H}_{yR}}$  to be as short as 2 nm. The bunching factor at 13.5 nm according to Eq. (206) is then 0.0675.

With  $\epsilon_y = 40$  pm, to get the desired linear bunch length 2 nm at the radiator, we need  $\mathcal{H}_{yR} = 0.1 \mu\text{m}$ . If  $\beta_y$  at the radiator is around 1 m, then the required control precision of dispersion and dispersion angle at the radiator is at the level of 0.3 mm and 0.3 mrad. Such a precise control of  $\mathcal{H}_{yR}$  is challenging but realizable using present technology. We remind the readers that the dispersion function is actually not well defined when the system is transverse-longitudinal coupled, and  $\mathcal{H}_y$  here should be replaced by the our defined generalized beta function  $\beta_{55}^{II}$ . But here we still use the classical definition of  $\mathcal{H}_y$  in getting the numbers for the above  $D_x$  and  $D'_x$  control

precision to give the readers a more concrete feeling. Following similar line of thought, we also need a precision control of  $\mathcal{H}_x$  or  $\beta_{55}^I$  at the radiator, since the horizontal emittance is even larger than the vertical one. Generally, we require a precision control of both  $D_{x,y}$  and  $D'_{x,y}$ . Besides, we also need to ensure the coupling of horizontal emittance  $\epsilon_x$  to the vertical plane to be less than 1% since our applied  $\epsilon_x = 2$  nm is about two orders of magnitude larger than  $\epsilon_y = 40$  pm.

Another important parameter is the beam current, both the average and peak ones. First we observe that given the same average beam current, the average radiation power will be higher with the decreasing of the beam filling factor  $f_e$ . This is because the peak power of the coherent radiation is proportional to the peak current squared  $P_{RP} \propto I_P^2 \propto I_A^2 f_e^{-2}$ , where  $I_P$  and  $I_A$  are the peak and average current, respectively, and  $f_e$  is the electron beam filling factor. The average radiation power is then  $P_{RA} = P_{RP} f_e \propto I_A^2 f_e^{-1}$ . So we tend to choose as high average current and as small filling factor as we can, as long as collective effects like IBS and coherent synchrotron radiation to be analyzed soon do not degrade the beam properties. We have applied a 40 A peak current and a 200 mA average current in our solution. Note that in the calculation of filling factor, for simplicity we have assumed the beam current is like square waves. The real beam distribution is more like a smooth curve, for example a Gaussian profile if there is only a single RF cavity in the ring. But this observation only results in some numerical factor adjustment and does not affect the core part of our analysis. So in Tab. 2 and below, we take this simplification of a square wave current distribution.

### C. Quantum Excitation Contribution to Vertical Emittance

After the general considerations, let us now take a closer look at the critical parameter  $\epsilon_y$ . It turns out the first con-

$$\Delta\epsilon_{yR} = C_q \frac{\gamma^2}{J_y} \frac{1}{I_2} \times \frac{\mathcal{H}_{yR}}{\rho_{0R}^3} \frac{4}{3\pi} L_{uR}, \quad (264)$$

where  $L_{uR}$  is the radiator undulator length,  $\rho_{0R}$  is the bending radius corresponds to the peak magnetic field of the radiator  $B_{0R}$ . Assuming that the radiation energy loss in the GLSF section is much less than that induced by the bending magnets in the ring, then we have  $I_2 \approx \frac{2\pi}{\rho_{\text{ring}}}$ . Taking the the approximation  $J_y \approx 1$ , in an easy-to-use form we have

$$\Delta\epsilon_{yR}[\text{nm}] = 8.9 B_{\text{ring}}^{-1}[\text{T}] B_{0R}^3[\text{T}] \mathcal{H}_{yR}[\text{m}] L_{uR}[\text{m}]. \quad (265)$$

For the parameters given in Tab. 2,  $B_{\text{ring}} = 1.33$  T,  $\lambda_{uR} = 1.8$  cm ( $B_{0R} = 0.867$  T),  $\mathcal{H}_{yR} = 0.1 \mu\text{m}$ ,  $L_{uR} = 5.69$  m ( $N_{uR} = 4 \times 79$ ), then  $\Delta\epsilon_{yR} = 2.5$  fm, which is much less than  $\epsilon_y$ . Generally, since  $\mathcal{H}_y$  at the radiator is quite small, the contribution of radiator to the vertical emittance is not the dominant one, compared to that from modulators and dipoles to be introduced.

Similar to the analysis for radiator, the contribution of two GLSF modulators to  $\epsilon_y$  is

$$\Delta\epsilon_{yM}[\text{nm}] = 17.8 B_{\text{ring}}^{-1}[\text{T}] B_{0M}^3[\text{T}] \mathcal{H}_{yM}[\text{m}] L_{uM}[\text{m}], \quad (266)$$

where  $B_{0M}$  and  $L_{uM}$  are the peak magnetic field and length of the modulator undulators, respectively. For the parameters given in Tab. 2,  $B_{\text{ring}} = 1.33$  T,  $B_{0M} = 0.806$  T,  $\mathcal{H}_{yM} = 0.056$  m,  $L_{uM} = 1.5$  m, then  $\Delta\epsilon_{yM} = 592$  pm, which is a quite large value compared to that contributed from the radiator. This is mainly due to the fact that  $\mathcal{H}_{yM} \gg \mathcal{H}_{yR}$ . As we will introduce soon, we can apply a horizontal planar damping wiggler to control this contribution by increasing the radiation damping rate.

In the above analysis, we have assumed  $\mathcal{H}_y$  is a constant value throughout an undulator. This strictly speaking is not true, since there will be intrinsic dispersion generated inside an undulator. We can refer to the transfer matrix of an undulator or laser modulator to study the evolution of  $\mathcal{H}_y$  in an undulator radiator and modulator, to get a more accurate evaluation of their quantum excitation contribution, as to be shown in Sec. VIII D 2. Our calculation shows that this will result in a significant difference for radiator's contribution to  $\epsilon_y$ , but not much difference for the modulators. However, since the radiator's contribution to  $\epsilon_y$  is negligible small compared to that of modulators, here we still use the simplified formula Eq. (266) in our following discussion.

There are also vertical bending magnets in the GLSF section for optics manipulation to fulfill the bunch compression

or harmonic generation condition. But in principle we can use weak dipoles to minimize their quantum excitation contribution to vertical emittance, and satisfy the symplectic optics requirement at the same time. Of course, the total length of these dipoles should not be too long. Therefore, in our present evaluation, we will assume that the quantum excitation contribution from the two modulators are the dominant source of  $\epsilon_y$  if we consider single-particle dynamics alone.

## D. Application of Damping Wigglers

### 1. To Speed Up Damping

It is desired that  $\Delta\epsilon_{yM}$  is only a small portion of our desired  $\epsilon_y$ , since then it provides room for other contribution of vertical emittance, like IBS and that from  $x$ - $y$  coupling. In principle, we can also use a weaker modulator field to weaken the quantum excitation, but this then means the laser-electron interaction will be less efficient, and a larger laser power is needed if we want to imprint the same energy modulation strength. Instead, the solution we choose is to increase the radiation damping rate per turn. To speed up damping, which is helpful in controlling the vertical emittance growth from both the quantum excitation and IBS, we may invoke one or multiple damping wigglers. We can put horizontal planar wigglers at dispersion-free locations. In such a way, the damping wiggler will contribute only damping and no excitation to the vertical emittance. Assuming that

$$U_{0w} = R_w U_{0\text{dipoles}}, \quad (267)$$

with  $U_{0\text{dipoles}} = C_\gamma E_0^4 / \rho_{\text{ring}}$  the radiation energy loss per particle per turn from the bending magnets in the ring,  $U_{0w}$  the radiation loss from all the damping wigglers in the ring, and

$$R_w = \frac{U_{0w}}{U_{0\text{dipoles}}} = \frac{1}{2} \left( \frac{B_{0w}}{B_{\text{ring}}} \right)^2 \frac{L_w}{2\pi\rho_{\text{ring}}}, \quad (268)$$

where  $B_{0w}$  and  $L_w$  are the peak magnetic field and total length of the damping wigglers, respectively. Since the damping rate is proportional to the radiation energy loss per turn, then the damping constant will be a factor of  $R_w$  larger by applying the damping wiggler

$$\alpha_V = (1 + R_w) \alpha_{V0}, \quad (269)$$

with  $\alpha_{V0}$  the natural vertical damping rate without the damping wigglers. Then the above evaluated emittance growth from radioastron modulators and dipoles will become  $\frac{1}{1+R_w}$  of the original value. For example for the modulators, we have

$$\Delta\epsilon_{yM}[\text{nm}] = \frac{17.8 B_{\text{ring}}^{-1} [\text{T}] B_{0M}^3 [\text{T}] \mathcal{H}_{yM} [\text{m}] L_{uM} [\text{m}]}{1 + R_w}. \quad (270)$$

Put the above relation in another way

$$L_{uM} [\text{m}] \approx 56.2 (1 + R_w) \frac{B_{\text{ring}} [\text{T}] \Delta\epsilon_{yM} [\text{pm}]}{\mathcal{H}_{yM} [\mu\text{m}] B_{0M}^3 [\text{T}]} \quad (271)$$

We will use a rather strong superconducting damping wiggler or damping wigglers to speed up damping to fight against the IBS diffusion and quantum excitation to maintain a small vertical emittance. For the parameters given in Tab. 2,  $B_{0\text{ring}} = 1.33 \text{ T}$ ,  $U_{0\text{dipoles}} = 7.7 \text{ keV}$ ,  $B_{0w} = 6 \text{ T}$  and  $L_w = 40 \text{ m}$ , then  $U_{0w} = 328 \text{ keV}$  and  $R_w = 42.9$ . By applying such strong damping wigglers, we now have  $\Delta\epsilon_{yM} = 13.4 \text{ pm}$ , which is a factor of three smaller than the desired  $\epsilon_y = 40 \text{ pm}$  and should be acceptable. Assuming the circumference of the ring is  $C_0 = 200 \text{ m}$ , the longitudinal and vertical radiation damping time are correspondingly

$$\tau_{\delta\text{RD}} = 1.19 \text{ ms}, \quad \tau_{y\text{RD}} = 2.38 \text{ ms}. \quad (272)$$

We will compare this radiation damping speed with that of IBS diffusion later.

### 2. Impact of Damping Wigglers on Energy Spread, Horizontal Emittance and Phase Slippage

Our primary goal of applying damping wiggler is to speed up radiation damping, but the damping wiggler also contributes to quantum excitation, thus may affect the energy spread and horizontal emittance. Let us investigate the energy spread first. Considering both the ring dipoles and damping wiggler, the new equilibrium energy spread is

$$\sigma_{\delta w} = \sigma_{\delta0} \sqrt{\frac{1 + \frac{4}{3\pi} \left( \frac{B_{0w}}{B_{\text{ring}}} \right)^3 \frac{L_w}{2\pi\rho_{\text{ring}}}}{1 + \frac{1}{2} \left( \frac{B_{0w}}{B_{\text{ring}}} \right)^2 \frac{L_w}{2\pi\rho_{\text{ring}}}}}, \quad (273)$$

where

$$\sigma_{\delta0} = \sqrt{\frac{C_q}{J_z} \frac{\gamma^2}{\rho_{\text{ring}}}} \quad (274)$$

is the natural energy spread if there is no damping wiggler. Nominally, we have the longitudinal damping partition  $J_z \approx 2$ . So

$$\sigma_{\delta0} \approx 4.69 \times 10^{-4} B_{\text{ring}}^{\frac{1}{2}} [\text{T}] E_0^{\frac{1}{2}} [\text{GeV}]. \quad (275)$$

For example, if  $B_{0w} = 1.33 \text{ T}$ , and  $E_0 = 600 \text{ MeV}$ , then

$$\sigma_{\delta0} = 4.2 \times 10^{-4}. \quad \text{When } \frac{1}{2} \left( \frac{B_{0w}}{B_{\text{ring}}} \right)^2 \frac{L_w}{2\pi\rho_{\text{ring}}} \gg 1 \text{ and}$$

$\frac{4}{3\pi} \left( \frac{B_{0w}}{B_{\text{ring}}} \right)^3 \frac{L_w}{2\pi\rho_{\text{ring}}} \gg 1$ , which means the energy spread is dominant by the damping wigglers, we have

$$\sigma_{\delta w} \approx \sigma_{\delta0} \sqrt{\frac{8}{3\pi} \frac{B_{0w}}{B_{\text{ring}}}} \approx 4.32 \times 10^{-4} B_{0w}^{\frac{1}{2}} [\text{T}] E_0^{\frac{1}{2}} [\text{GeV}]. \quad (276)$$

So given the beam energy, the new equilibrium energy spread will depends solely on the peak magnetic field of the damping wiggler  $B_{0w}$ . For example, if  $E_0 = 600 \text{ MeV}$  and  $B_{0w} = 6 \text{ T}$ , then the asymptotic energy spread is  $\sigma_{\delta w} = 8.2 \times 10^{-4}$ .

2137 2138 2139 2140 2141 2142 2143 2144 2145 2146 2147 2148 2149 2150 2151 2152 2153 2154 2155 2156 2157 2158 2159 2160 2161 2162 2163 2164 2165 2166 2167 2168 2169 2170 2171 2172 2173 2174 2175 2176 2177

2178 This energy spread can affect coherent EUV radiation power 2190 Usually the central part of the wiggler has a sinusoidal field  
2179 in a long radiator as will be studied in Sec. VIII I. 2191 strength pattern along the longitudinal axis. We set the origin  
2192 of the global path length coordinate  $s = 0$  to be the location  
2193 of the peak magnetic field closest to the wiggler center. Note

2180 Now let us look at the impact on horizontal emittance. We 2194 that this choice of origin location has a correspondence to the  
2181 just said that we can place the damping wigglers at horizon- 2195 transfer matrix of wiggler to be given soon. Then the vertical  
2182 tally dispersion-free locations to minimize their quantum ex- 2196 magnetic field of a horizontal planar wiggler is

2183 citation on  $\epsilon_x$ . But there will be some intrinsic horizontal dis-

2184 persion and dispersion angle and thus  $\mathcal{H}_x$  generated inside the 2197

2185 wigglers and the strong field strength raises the concern that

2186 the quantum excitation of the damping wigglers may result in 2198 with  $B_{0w}$  the peak magnetic field and  $k_w = 2\pi/\lambda_w$  the  
2187 horizontal emittance growth. Now we present a quantitative 2199 wavenumber of wiggler, and  $k_x^2 + k_y^2 = k_w^2$ . The linear trans-  
2188 evaluation of this. Part of the content in this section can also 2200 fer matrix of  $\mathbf{X}$  from  $s = 0$  to  $s \in [-\frac{L_w}{2}, \frac{L_w}{2}]$  with  $L_w$  the  
2189 be found in Ref. [50] 2201 wiggler length is then [51]

$$B_y = B_{0w} \cosh(k_x x) \cosh(k_y y) \cos(k_w s), \quad (277)$$

2202

$$\mathbf{W}(s|0) = \begin{pmatrix} 1 & s & 0 & 0 & 0 & -\frac{K}{\gamma k_w} [1 - \cos(k_w s)] \\ 0 & 1 & 0 & 0 & 0 & -\frac{K}{\gamma} \sin(k_w s) \\ 0 & 0 & \cos(k_y s) & \frac{\sin(k_y s)}{k_y} & 0 & 0 \\ 0 & 0 & -k_y \sin(k_y s) & \cos(k_y s) & 0 & 0 \\ W_{51} & W_{52} & 0 & 0 & 1 & W_{56} \\ 0 & 0 & 0 & 0 & 0 & 1 \end{pmatrix}, \quad (278)$$

2203 where  $W_{51} = -W_{26}$ ,  $W_{52} = -sW_{26} + W_{16}$  and

2204

$$W_{56} = \frac{2\lambda_0}{\lambda_w} s + \frac{K^2}{\gamma^2} \left[ \frac{\sin(2k_w s) - 4\sin(k_w s)}{4k_w} \right], \quad (279)$$

2205 with  $\lambda_0 = \frac{1+K^2/2}{2\gamma^2} \lambda_w$  being the fundamental on-axis reso-  
2206 nant wavelength.

2207 In a planar uncoupled ring, the normalized eigenvector of  
2208 the storage ring one-turn map corresponding to the horizontal  
2209 eigenmode at  $s = 0$  can be expressed as the first vector in  
2210 Eq. (50). We assume  $\alpha_{x0}, \beta_{x0}$  are the Courant-Snyder func-

2211 tions and  $D_{x0}, D'_{x0}$  are the dispersion and dispersion angle  
2212 corresponding to the horizontal plane at  $s = 0$ , respectively.

2213 Then the horizontal chromatic function  $\mathcal{H}_{x0}$  at  $s = 0$  is

$$\begin{aligned} \mathcal{H}_{x0} &\equiv \beta_{55}^I(0) = 2|E_{I5}(0)|^2 \\ &= \frac{D_{x0}^2 + (\alpha_{x0}D_{x0} + \beta_{x0}D'_{x0})^2}{\beta_{x0}}. \end{aligned} \quad (280)$$

2214 The evolution of  $\mathcal{H}_x$  from  $s = 0$  to  $s \in [-\frac{L_w}{2}, \frac{L_w}{2}]$  is

2216

$$\begin{aligned} \mathcal{H}_x(s) &\equiv \beta_{55}^I(s) = 2|E_{I5}(s)|^2 = 2|(\mathbf{W}(s|0)\mathbf{E}_I(0))_5|^2 \\ &= \frac{(D_{x0} + W_{16} - W_{26}s)^2 + [\alpha_{x0}(D_{x0} + W_{16} - W_{26}s) + \beta_{x0}(D'_{x0} + W_{26})]^2}{\beta_{x0}}, \end{aligned} \quad (281)$$

2217 where  $W_{ij}$  means the  $i$ -th row and  $j$ -th column matrix term of  $\mathbf{W}(s|0)$ . Put in the explicit expression of the wiggler matrix  
2218 terms, we have

2219

$$\begin{aligned} \mathcal{H}_x(s) &= \frac{1}{\rho_w^2 k_w^4 \beta_{x0}} \{ [D_{x0} \rho_w k_w^2 + \sin(k_w s) k_w s + \cos(k_w s) - 1]^2 \\ &\quad + [\beta_{x0} k_w (\rho_w k_w D'_{x0} - \sin(k_w s)) + \alpha_{x0} (D_{x0} \rho_w k_w^2 + \sin(k_w s) k_w s + \cos(k_w s) - 1)]^2 \}. \end{aligned} \quad (282)$$

2220 We assume that the quantum excitation contribution from 2224 Then the quantum excitation of a wiggler to the horizontal  
2221 the entrance and exit region of the wiggler, where the field 2225 beam emittance can be evaluated by the integral  
2222 strength in reality deviates from the ideal sinusoidal pattern,  
2223 is much smaller than that of the central sinusoidal field region.

$$I_{5w} = \int_{-\frac{L_w}{2}}^{\frac{L_w}{2}} \frac{\mathcal{H}_x(s)}{|\rho(s)|^3} ds = \frac{1}{\rho_w^3} \int_{-\frac{L_w}{2}}^{\frac{L_w}{2}} \mathcal{H}_x(s) |\cos(k_w s)|^3 ds, \quad (283)$$

where  $\rho_w = \frac{\gamma m_e \beta c}{e B_{0w}}$  corresponds to the bending radius at the location of peak magnetic field  $B_{0w}$ , with  $\beta = \sqrt{1 - \frac{1}{\gamma^2}}$ . Put Eq. (282) in, we have

$$I_{5w} = \frac{4}{15\pi} \frac{L_w}{\rho_w^5 k_w^2} \left[ \beta_{x0} + \gamma_{x0} L_w^2 \mathcal{R} + 5\rho_w^2 k_w^2 \mathcal{H}_{x0} - \left( 10 + \frac{15\pi}{8} \right) \frac{\rho_w (D_{x0} + \alpha_{x0} D_{x0} + \beta_{x0} D'_{x0})}{\beta_{x0}} \right], \quad (284)$$

where  $\gamma_{x0} = \frac{1+\alpha_{x0}^2}{\beta_{x0}}$  and

$$\mathcal{R} = \frac{15}{32\pi^2} \frac{1}{N_w^3} \int_{-N_w\pi}^{N_w\pi} [\sin(x) x + \cos(x) - 1]^2 |\cos(x)|^3 dx, \quad (285)$$

with  $N_w = L_w/\lambda_w$  being the number of wiggler period which is assumed to be an integer. Equation (284) above is the exact formula for wiggler's contribution to the radiation integral  $I_{5x}$  in an electron storage ring.

Given a specific  $N_w$ ,  $\mathcal{R}$  can be straightforwardly obtained by integration in Eq. (285). When  $N_w \gg 1$ , we have  $\mathcal{R} \approx \frac{1}{12}$ , and

$$I_{5w} \approx \frac{4}{15\pi} \frac{L_w}{\rho_w^5 k_w^2} \left[ \langle \beta_x \rangle_w + 5\rho_w^2 k_w^2 \mathcal{H}_{x0} - \left( 10 + \frac{15\pi}{8} \right) \frac{\rho_w (D_{x0} + \alpha_{x0} D_{x0} + \beta_{x0} D'_{x0})}{\beta_{x0}} \right], \quad (286)$$

where  $\langle \beta_x \rangle_w$  is the average value of  $\beta_x$  along the wiggler

$$\langle \beta_x \rangle_w = \frac{1}{L_w} \int_{-\frac{L_w}{2}}^{\frac{L_w}{2}} \beta_x(s) ds = \beta_{x0} + \frac{\gamma_{x0} L_w^2}{12}. \quad (287)$$

Denote  $\chi_{x0} = \text{Arg} \left( \frac{E_{I5}(0)}{E_{I1}(0)} \right)$ , where  $E_{I5}(0)$  and  $E_{I1}(0)$

represent the fifth and first term of the first eigenvector in Eq. (50) and  $\text{Arg}()$  means the angle of a complex number, then Eq. (286) can be written as

$$I_{5w} \approx \frac{4}{15\pi} \frac{L_w}{\rho_w^5 k_w^2} \left[ \langle \beta_x \rangle_w + 5\rho_w^2 k_w^2 \mathcal{H}_{x0} - \left( 10 + \frac{15\pi}{8} \right) \rho_w \sqrt{\frac{2\mathcal{H}_{x0}}{\beta_{x0}}} \sin \left( \chi_{x0} - \frac{\pi}{4} \right) \right]. \quad (288)$$

The first term in the above bracket corresponds to the approximated formula found in literature

$$I_{5w,\text{intrinsic}} \approx \frac{4}{15\pi} \frac{L_w \langle \beta_x \rangle_w}{\rho_w^5 k_w^2}. \quad (289)$$

It can be viewed as the intrinsic contribution of a wiggler to the radiation integral  $I_{5x}$ , since there will be intrinsic dispersion and dispersion angle generated inside the wiggler even if  $D_{x0} = 0$  and  $D'_{x0} = 0$  as can be seen from the matrix term  $W_{16}$  and  $W_{26}$  of the wiggler. The second and third terms in the bracket arise from a nonzero  $\mathcal{H}_{x0}$ . When  $D'_{x0}$  or  $\frac{D_{x0}}{\beta_{x0}}$  is of the order  $\frac{K}{\gamma} = \frac{1}{\rho_w k_w}$ , which can easily be the case in a real lattice, the contribution from this nonzero  $\mathcal{H}_{x0}$  in the bracket could be comparable or even larger than the first term and cannot be neglected. The more accurate formula derived here should then be invoked to calculate the wiggler's quantum excitation of beam emittance. When the third term is much smaller than the second term, i.e., roughly when  $\mathcal{H}_{x0} \beta_{x0} \gg \left( \frac{K}{\gamma} \lambda_w \right)^2$ , Eq. (288) can be further approx-

$$I_{5w} \approx \frac{4}{15\pi} \frac{L_w \langle \beta_x \rangle_w}{\rho_w^5 k_w^2} + \frac{4}{3\pi} \frac{L_w \mathcal{H}_{x0}}{\rho_w^3}, \quad (290)$$

where the first term accounts for the intrinsic contribution, and the second term for the nonzero  $\mathcal{H}_{x0}$ .

From the above analysis, we can see that the minimum  $I_{5w}$  is realized when

$$\alpha_{x0} = 0, \beta_{x0} = \frac{L_w}{2\sqrt{3}}, D_{x0} = 0, D'_{x0} = 0, (\mathcal{H}_{x0} = 0), \quad (291)$$

and the minimal value is

$$I_{5w,\text{min}} \approx \frac{4}{15\sqrt{3}\pi} \frac{L_w^2}{\rho_w^5 k_w^2}. \quad (292)$$

Now we can evaluate the impact of the damping wigglers on the equilibrium horizontal emittance to make sure the desired  $\epsilon_x = 2 \text{ nm}$  can be realized. From Eq. (53), the equilib-

rium emittance with the damping wiggler is given by

$$\epsilon_{xw} = C_q \frac{\gamma^2}{J_x} \frac{I_{50} + I_{5w}}{I_{20} + I_{2w}}, \quad (293)$$

where  $I_{20}$  and  $I_{50}$  are the radiation integrals of the ring without the damping wiggler. Note that the natural emittance without the damping wiggler is given by

$$\epsilon_{x0} = C_q \frac{\gamma^2}{J_x} \frac{I_{50}}{I_{20}}. \quad (294)$$

If we want  $\epsilon_{xw} \leq \epsilon_{x0}$ , then we need  $C_q \frac{\gamma^2}{J_x} \frac{I_{5w}}{I_{2w}} \leq \epsilon_{x0}$ . Using  $I_{2w} \approx \frac{L_w}{2\rho_w^2}$  and Eq. (292), we then have

$$\lambda_w \leq 2\pi \sqrt{\frac{15\sqrt{3}\pi J_x \epsilon_{x0} \rho_w^3}{8C_q \gamma^2 L_w}}. \quad (295)$$

According to the above scaling, a longer wiggler length requires a shorter wiggler period to control the quantum excitation contribution to the horizontal emittance. This is because the average values of  $\beta_x$  and  $\mathcal{H}_x$  in the wiggler are linearly proportional to  $L_w$ . But note that the above analysis assumes there is only a single wiggler. If we split the wiggler into  $N_{wc}$  identical cells with the total length fixed, we can make the contribution of the wiggler to  $I_{5w}$  and thus quantum excitation to horizontal emittance becomes a factor of  $N_{wc}$  smaller, while the contribution to  $I_{2w}$  and thus the effect on radiation damping is unchanged. Then the tolerance of  $\lambda_w$  can be a factor of  $\sqrt{N_{wc}}$  larger. Put in the numerical numbers, we have a more useful scaling

$$\lambda_w [\text{m}] \leq 3.19 \sqrt{\frac{N_{wc} J_x E_0 [\text{GeV}] \epsilon_{x0} [\text{nm}]}{B_{0w}^3 [\text{T}] L_w [\text{m}]}}. \quad (296)$$

Nominally  $J_x \approx 1$ . For our example parameters given in Tab. 2,  $E_0 = 600 \text{ MeV}$ ,  $\epsilon_{x0} = 2 \text{ nm}$ ,  $B_{0w} = 6 \text{ T}$ ,  $L_w = 40 \text{ m}$ ,  $N_{wc} = 20$  which means each small wiggler has a length of 2 m, we then to realize  $\epsilon_{xw} \leq \epsilon_{x0}$  we need

$$\lambda_w \leq 0.168 \text{ m}. \quad (297)$$

A wiggler with a period length of 10 to 15 cm and a peak field of 6 T is doable using superconducting magnet technology. We recognize the impact of such a long (total length) damping wiggler on beam dynamics, single-particle nonlinear dynamics and collective instabilities need further in-depth study, especially considering the fact the gap of such a wiggler is small to realize such a strong field strength. Actually another practical reason to split the wiggler into shorter sections is to avoid the synchrotron radiation generated by itself heating the magnet poles. We also recognize it may take some efforts in the lattice design to make the optimal conditions given by Eq. (291) fulfilled in practice.

Apart from the quantum excitation, the damping wiggler also contributes to the phase slippage. If  $B_w = 6 \text{ T}$ ,  $\lambda_w = 0.1 \text{ m}$ ,  $L_w = 40$  which means a total wiggler period number  $N_w = 400$ , then the wiggler undulator parameter is  $K_w = 0.934 \times 6 \times 10 = 56.04$ , then the fundamental resonance wavelength of the wiggler is  $\lambda_{rw} = 2346$

$\frac{1+K_w^2/2}{2\gamma^2} \lambda_w = 57 \mu\text{m}$ . The  $R_{56}$  of the whole damping wiggler is twice the fundamental frequency radiation slippage length  $R_{w,56} = 2N_w \lambda_{rw} = 45.6 \text{ mm}$  [17]. Since the total  $R_{56}$  of the ring used in Tab. 2 is about 1 m, then the contribution of the damping wiggler to  $R_{56}$  is acceptable.

## E. Intra-beam Scattering

We mentioned that our conservative choice of  $\epsilon_y = 40 \text{ pm}$  is mainly out of the consideration for IBS. Now this can be understood with more quantitative calculations. We will see that IBS turns out to be the most fundamental obstacle in obtaining the ultrasmall vertical emittance in GLSF SSMB. This is partially because our choice of beam energy is not too high. In addition, to realize high EUV power, we need a high peak current which means a high charge density in phase space.

We use Bane's high-energy approximation [52] to calculate the IBS diffusion rate

$$\begin{aligned} \frac{1}{T_\delta} &\approx \frac{r_e^2 c N L_c}{16\gamma^3 \epsilon_x^{\frac{3}{4}} \epsilon_y^{\frac{3}{4}} \sigma_z \sigma_\delta^3} \left\langle \sigma_H g_{\text{Bane}} \left( \frac{a}{b} \right) (\beta_x \beta_y)^{-\frac{1}{4}} \right\rangle, \\ \frac{1}{T_{x,y}} &= \frac{\sigma_\delta^2 \langle \mathcal{H}_{x,y} \rangle}{\epsilon_{x,y}} \frac{1}{T_\delta}, \\ \frac{1}{\sigma_H^2} &= \frac{1}{\sigma_\delta^2} + \frac{\mathcal{H}_x}{\epsilon_x} + \frac{\mathcal{H}_y}{\epsilon_y}, \\ g_{\text{Bane}}(\alpha) &= \frac{2\sqrt{\alpha}}{\pi} \int_0^\infty \frac{du}{\sqrt{1+u^2\sqrt{\alpha^2+u^2}}}, \\ a &= \frac{\sigma_H}{\gamma} \sqrt{\frac{\beta_x}{\epsilon_x}}, \quad b = \frac{\sigma_H}{\gamma} \sqrt{\frac{\beta_y}{\epsilon_y}}. \end{aligned} \quad (298)$$

where  $r_e = 2.818 \times 10^{-15} \text{ m}$  is the classical electron radius and  $L_c = \ln \left( \frac{b_{\max}}{b_{\min}} \right)$  is the Coulomb Log factor, with  $b_{\max}$  and  $b_{\min}$  being the maximum and minimal impact factor for the scattering process, respectively. Typically  $L_c$  is in the range of 10 to 20.  $N$  is the number of electrons in the bunch. For a coasting beam, we need to replace  $\sigma_z \rightarrow L/(2\sqrt{\pi})$  where  $L$  is the bunch length. Note that  $\frac{eN}{L/c} = I_P$  according to our definition, where  $I_P$  is the peak current.

Now we put in some example numbers to do an estimation for the IBS diffusion rate in a GLSF EUV SSMB ring:

$$\begin{aligned} E_0 &= 600 \text{ MeV}, \quad I_P = 40 \text{ A}, \quad \sigma_\delta = 8.5 \times 10^{-4}, \\ \epsilon_x &= 2 \text{ nm}, \quad \epsilon_y = 40 \text{ pm}, \quad \langle \sigma_H \rangle = 4 \times 10^{-5}, \\ \frac{a}{b} &= \frac{1}{10}, \quad g_{\text{Bane}} \left( \frac{1}{10} \right) = 0.744, \quad \langle (\beta_x \beta_y)^{-\frac{1}{4}} \rangle = 0.32, \\ \langle \mathcal{H}_y \rangle &= \frac{2 \times 1.6 \times 0.056 \text{ m}}{200} = 0.9 \text{ mm}, \quad L_c = 10. \end{aligned} \quad (299)$$

Note that in Tab. 2 we have  $\mathcal{H}_y = 0.056 \text{ m}$  at the two modulators, whose length are both 1.6 m. In evaluating  $\langle \mathcal{H}_y \rangle$  we have only considered the contribution from the two modulators, where  $\mathcal{H}_y$  reach the its maximum value. This is a

2351 simplification, but should give a correct order of magnitude 2361  
 2352 estimation. Putting in the example numbers, we then have

2353  $\tau_{\delta\text{IBS}} = 113 \text{ ms}, \tau_{y\text{IBS}} = 7.11 \text{ ms}.$

2362 Now we want to evaluate if the peak current of 40 A we apply  
 2363 in the above example is doable. One of the main limitation  
 2364 of peak current is the microwave instability induced by coher-  
 2365 ent synchrotron radiation (CSR). According to Ref. [53], the  
 2366 CSR-induced microwave instability threshold is

2367 
$$(S_{\text{CSR}})_{\text{th}} = 0.5 + 0.12\Pi, \quad (301)$$

2354 Compared with the radiation damping times given in 2368 with  
 2355 Eq. (272), we can see that even for the vertical dimension, the  
 2356 IBS diffusion is more than three times slower than the radia-  
 2357 tion damping. Therefore, the IBS diffusion can now be con-  
 2358 trolled by the strong damping induced by the damping wig-  
 2359 glers. This calculation also justifies the necessity or benefit of 2370 and  $2g$  is the separation between the two plates. So the thresh-  
 2360 applying the damping wiggler. 2371 old peak current is

2372 
$$I_{\text{th,peak}} = \frac{eN_b}{\sqrt{2\pi}\sigma_{z0}/c} = \frac{1}{2\sqrt{2\pi}} I_{\text{Alf}} \gamma \left( 1 + 0.24 \frac{\sigma_{\delta0} |R_{56}|^{1/2} \rho^{1/2}}{|h_{RF}|^{1/2} g^{3/2}} \right) \frac{\sigma_{\delta0}^{4/3} |R_{56}|^{2/3} |h_{RF}|^{1/3}}{\rho^{1/3}}, \quad (303)$$

2373 with  $I_{\text{Alf}} = \frac{ec}{r_e} = 17 \text{ kA}$  being the Alven current. The  $R_{56} =$  2405 EUV radiation [17, 55]. What we need is  $|R_{56}| \sim 1 \text{ m}$ , and  
 2374  $-\eta C_0$  is that of the whole ring.  $h_{RF} = \frac{eV_{RF} \cos \phi_s}{E_0} k_{RF}$  is the 2406 at the same time  $\epsilon_x \lesssim 2 \text{ nm}$ , and some optimization may be  
 2375 linear energy chirp strength around the synchronous RF phase 2407 required realize such a goal.

2376 Putting in some typical parameters for the EUV SSMB: 2408 Now we check if the required RF system in the above ex-  
 2377  $E_0 = 600 \text{ MeV}$ ,  $B_0 = 1.33 \text{ T}$ ,  $\rho = 1.5 \text{ m}$ ,  $|R_{56}| = 1 \text{ m}$ , 2409 ample calculation is feasible. The longitudinal beta function  
 2378  $\sigma_{\delta0} = 8.5 \times 10^{-4}$ ,  $g = 4 \text{ cm}$ ,  $h_{RF} = 0.01 \text{ m}^{-1}$ , then 2410 at the RF cavity is  $\beta_z \approx \sqrt{\eta C_0/h_{RF}} = 10 \text{ m}$ , then the RMS  
 2411 bunch length is  $\sigma_z = \sigma_{\delta0} \beta_z = 8.5 \text{ mm}$ . To get a beam filling  
 2412 factor of 0.5%, roughly we need an RF wavelength of 1.7 m,  
 2413 which means an RF frequency of 176.5 MHz. Then the re-  
 2414 quired energy chirp strength of  $h_{RF} = 0.01 \text{ m}^{-1}$  means the  
 2415 required RF voltage is 1.62 MV. Such an RF voltage should  
 2416 be doable at this frequency range. Multiple cavities can be  
 2417 invoked if it is too demanding for a single cavity to reach the  
 2418 desired voltage.

2379  $I_{\text{th,peak}} = 60.3 \times (1 + 0.31) \text{ A} = 79 \text{ A}. \quad (304)$

2380 So our application of a peak current of 40 A should be safe  
 2381 from microwave instability.

2382 The astute readers may notice that one of the main reasons  
 2383 we have a large threshold current here is the large phase slip-  
 2384 page or  $R_{56}$  that we applied for the ring. To avoid confusion,  
 2385 first we need to make clear that in this example GLSF SSMB  
 2386 EUV source, the electron bunch in the ring can be a coasting  
 2387 beam or an RF-bunched beam, and microbunching appears  
 2388 only at the radiator, due to the phase space manipulation of  
 2389 electron beam in the GLSF section. Actually in our setup, we  
 2390 have used an RF-bunched beam in the ring. Therefore, the  
 2391 phase slippage factor of the ring does not need to be small,  
 2392 while this is required in a LWF SSMB ring. Then the question  
 2393 becomes whether the required large phase slippage is doable  
 2394 and what beam dynamics effects it may have. As a reference,  
 2395 the Metrology Light Source storage ring [54] in standard user  
 2396 mode has an  $|R_{56}| \approx 1.6 \text{ m}$ , which means a phase slippage  
 2397 factor of  $3.3 \times 10^{-2}$  given a circumference of 48 m. Therefore  
 2398 we believe our application of  $|R_{56}| = 1 \text{ m}$  is realizable. But 2428

2399 we recognize that such a large  $R_{56}$  requires large horizontal 2429 especially that induced by the strong damping wiggler, need  
 2400 dispersion  $D_x$  at the dipoles, since  $-R_{56} = \eta C_0 \approx 2\pi \langle D_x \rangle_\rho$  2430 to be compensated. Here we present some preliminary anal-  
 2401 where  $\langle \rangle_\rho$  means average around the dipoles in the ring. A 2431 ysis on the requirement of the energy compensation system  
 2402 large  $D_x$  may result in a large  $\mathcal{H}_x$ , and then the quantum ex- 2432 of such an GLSF SSMB EUV light source. From Tab. 2, the  
 2403 citation of dipoles to the horizontal emittance  $\epsilon_x$  should be 2433 total radiation loss per particle per turn is  $U_0 = U_{0\text{dipoles}} +$   
 2404 carefully evaluated. A too large  $\epsilon_x$  will degrade the coherent 2434  $U_{0w} + U_{0R} = 341.3 \text{ keV}$ , where the three terms on the right

## F. Microwave Instability

2367 
$$(S_{\text{CSR}})_{\text{th}} = 0.5 + 0.12\Pi, \quad (301)$$

## G. Energy Compensation System

2362 The large radiation loss of the electron beam in the ring,  
 2363 especially that induced by the strong damping wiggler, need  
 2364 to be compensated. Here we present some preliminary anal-  
 2365 ysis on the requirement of the energy compensation system  
 2366 of such an GLSF SSMB EUV light source. From Tab. 2, the  
 2367 total radiation loss per particle per turn is  $U_0 = U_{0\text{dipoles}} +$   
 2368  $U_{0w} + U_{0R} = 341.3 \text{ keV}$ , where the three terms on the right

hand side represent the radiation loss in dipoles, damping with the power consumption of the other systems like electric wiggler and radiator, respectively. So the synchronous acceleration phase corresponds to an acceleration voltage of  $V_{\text{acc}} = 341.3$  kV. Such a high voltage is not easy to be realized using an induction linac, considering the required repetition rate is at the MHz level. So we use conventional RF cavities to supply the radiation loss. Following the discussion of last section, and assuming we have used an RF frequency of 166.6 MHz (RF wavelength 1.8 m), then we need an RF voltage of 1.72 MV to realize an energy chirp strength of  $h_{RF} = 0.01$  m $^{-1}$ . Under this parameter set, and consider  $V_{RF} \gg V_{\text{acc}}$ , the RF bucket half-height is [17]

$$\hat{d}_{\frac{1}{2}} = \frac{2}{\beta_z k_{RF}} = \frac{\lambda_{RF}}{\pi} \sqrt{\frac{h}{\eta C_0}} = 5.73 \times 10^{-2}, \quad (305)$$

which is  $67.4\sigma_{\delta 0}$  with the energy spread  $\sigma_{\delta 0} = 8.5 \times 10^{-4}$ . So the bucket half-height should be large enough to ensure the beam quantum lifetime and Touschek lifetime.

To relieve the burden on the RF cavities, we may use three RF cavities to achieve the total RF voltage, with each cavity having a voltage of 573 kV. To minimize the power dissipated on the cavity, we need a large shunt impedance of each cavity which here we assume to be  $R_s = 20$  M $\Omega$ , then the total power dissipated on the three cavity walls is

$$P_{\text{diss}} = \frac{1}{3} \frac{V_{RF}^2}{R_s} = 49.2 \text{ kW.} \quad (306)$$

The power delivered to the 200 mA-average current beam is

$$P_b = I_A \frac{U_0}{e} = 68.3 \text{ kW.} \quad (307)$$

So the power dissipated on the cavity walls is at the same level as that delivered to the beam. We recognize the large shunt impedance may take efforts to realize in practice. If the shunt impedance is lower than the assumed value, then the power consumption on the wall will be correspondingly larger. Superconducting RF cavities can be used to lower the power dissipation on the wall.

Generally, the total power consumption of the RF system of an SSMB ring is at 100 kW to 200 kW level. Together

tromagnets, superconducting damping wiggler, vacuum and water cooling system, the overall power consumption of such an SSMB storage ring is at the level of several hundred kW. In principle, an SSMB ring can accommodate multiple GLSF in-

sertions and therefore multiple radiators, but here we consider the case of only one radiator in the ring. So for such an GLSF SSMB storage ring, it takes a couple of 100 kW electricity power to generate 1 kW EUV light. Such a large power consumption may raise the question on the advantage of such an SSMB-EUV source compared to the superconducting RF-based high-repetition rate FEL-EUV source, in particular, the energy recovery linac-based FEL-EUV source. As a

comparison, according to Ref. [56], it takes 7 MW overall power consumption to generate 10 kW EUV light in an ERL-FEL EUV source, which means 700 kW electricity power per 1 kW EUV light. So the overall power efficiency from electricity to EUV light for an SSMB-EUV source and an ERL-FEL EUV source is comparable. But we remind the readers that these numbers are only rough estimation, and it requires more indepth study to reach a concrete conclusion. Another side comment is that the radiation emitted by the damping wiggler may also be useful.

## H. Modulation Laser Power

Now we evaluate the modulation laser power required. Given the laser wavelength, modulator undulator parameters and the required energy chirp strength, we can use Eq. (221) to calculate the required laser power

$$P_L = \frac{\lambda_L}{4Z_0 Z_R} \left( h \frac{1}{\frac{eK[JJ]}{\gamma^2 m_e c^2} \tan^{-1} \left( \frac{L_u}{2Z_R} \right) k_L} \right)^2. \quad (308)$$

$$P_L \approx \frac{1}{1 + R_w} \frac{\epsilon_y}{\Delta \epsilon_{yM}} \frac{1}{(K[JJ])^2} \frac{\lambda_L^3}{3\pi^3 Z_0} \frac{55}{48\sqrt{3}} \frac{\alpha_F c^2 \lambda_e^2 \gamma^7 B_{0M}^3}{C_\gamma E_0^3 B_{\text{ring}}} \frac{1}{\sigma_{zR}^2} \frac{\frac{L_u}{2Z_R}}{\left[ \tan^{-1} \left( \frac{L_u}{2Z_R} \right) \right]^2}, \quad (309)$$

where  $\alpha_F = \frac{1}{137}$  is the fine structure constant, and  $R_w$  is given by Eq. (268). In the above derivation we have used the

electron momentum  $P_0 = \gamma m_e c$  and approximation  $E_0 \approx P_0 c$ . Now we try to derive more useful scaling laws to offer guidance in our parameter choice for a GLSF SSMB storage ring. As shown in Fig. 6, to maximize the energy modulation, we need  $\frac{Z_R}{L_u} = 0.359 \approx \frac{1}{3}$ . When  $K > \sqrt{2}$ , we approximate

2509

2510

2511

2512

2513

2514

2515

2516

2517

2518

2519

2520

2521

2522

2523

2524

2525

2526

2527

2528

2529

2530

2531

2532

2533

2534

2535

2536

2537

2538

2539

2540

2541

2542

2543

2544

2545

2546

2547

2548

2549

2550

2551

2552

2553

2554

2555

2556

2557

2558

2559

2560

2561

2562

2563

2564

2565

2566

2567

2568

2569

2570

2571

2572

2573

2574

2575

2576

2577

2578

2579

2580

2581

2582

2583

2584

2585

2586

2587

2588

2589

2590

2591

2592

2593

2594

2595

2596

2597

2598

2599

2600

2601

2602

2603

2604

2605

2606

2607

2608

2609

2610

2611

2612

2613

2614

2615

2616

2617

2618

2619

2620

2621

2622

2623

2624

2625

2626

2627

2628

2629

2630

2631

2632

2633

2634

2635

2636

2637

2638

2639

2640

2641

2642

2643

2644

2645

2646

2647

2648

2649

2650

2651

2652

2653

2654

2655

2656

2657

2658

2659

2660

2661

2662

2663

2664

2665

2666

2667

2668

2669

2670

2671

2672

2673

2674

2675

2676

2677

2678

2679

2680

2681

2682

2683

2684

2685

2686

2687

2688

2689

2690

2691

2692

2693

2694

2695

2696

2697

2698

2699

2700

2701

2702

2703

2704

2705

2706

2707

2708

2709

2710

2711

2712

2713

2714

2715

2716

2717

2718

2719

2720

2721

2722

2723

2724

2725

2726

2727

2728

2729

2730

2731

2732

2733

2734

2735

2736

$$P_L \propto \frac{1}{1+R_w} \frac{\epsilon_y}{\Delta\epsilon_{yM}} \frac{\lambda_L^3}{K^2} \frac{\gamma^4 B_{0M}^3}{B_{\text{ring}}} \frac{1}{\sigma_{zR}^2}$$

$$\propto \frac{1}{1+R_w} \frac{\epsilon_y}{\Delta\epsilon_{yM}} \frac{\lambda_L^{\frac{7}{3}} \gamma^{\frac{8}{3}} B_{0M}^{\frac{7}{3}}}{B_{\text{ring}}} \frac{1}{\sigma_{zR}^2}.$$

Putting in the numbers for the constants, we obtain the quantitative expressions of the above scalings for practical use

$$P_L[\text{kW}] \approx 5.7 \frac{1}{1+R_w} \frac{\epsilon_y}{\Delta\epsilon_{yM}} \frac{\lambda_L^{\frac{7}{3}} [\text{nm}] E_0^{\frac{8}{3}} [\text{GeV}] B_{0M}^{\frac{7}{3}} [\text{T}]}{\sigma_{zR}^2 [\text{nm}] B_{\text{ring}} [\text{T}]}.$$

The above scaling laws are accurate when  $K > \sqrt{2}$ , and it should be noted that the calculated power refers to the peak power of the laser. For completeness, here we give also the modulator length scaling

$$L_{uM}[\text{m}] \approx 56.2 (1+R_w) \frac{B_{\text{ring}}[\text{T}] \Delta\epsilon_{yM}[\text{pm}]}{\mathcal{H}_{yM}[\mu\text{m}] B_{0M}^3[\text{T}]}.$$

Therefore, to lower the required modulation laser power, we can apply a large  $R_w$ , which means strong damping wigglers. A low beam energy and short laser wavelength are also preferred. But their choices should take more factors into account, for example IBS and engineering experience of optical enhancement cavity as explained in Sec. IV. A strong bending magnet field in the ring is also desired. Concerning the modulator field strength, a weaker one is favored to lower the required laser power. But note that the required modulator length may be longer, if we keep the quantum excitation contribution of modulators to vertical emittance  $\Delta\epsilon_{yM}$  unchanged in this process.

## I. Radiation Power

Having formed the microbunching, now comes the radiation generation. We will use a planar undulator as the radiator. Coherent undulator radiation power at the odd- $H$ -th harmonic from a transversely-round electron beam is [17, 55]

$$P_{H,\text{peak}}[\text{kW}] = 1.183 N_u H \chi [JJ]_H^2 F F_{\perp}(S) |b_{z,H}|^2 I_P^2 [\text{A}],$$

where  $N_u$  is the number of undulator periods,

$$[JJ]_H^2 = \left[ J_{\frac{H-1}{2}}(H\chi) - J_{\frac{H+1}{2}}(H\chi) \right]^2,$$

with  $\chi = \frac{K^2}{4+2K^2}$ , and the transverse form factor is

$$F F_{\perp}(S) = \frac{2}{\pi} \left[ \tan^{-1} \left( \frac{1}{2S} \right) + S \ln \left( \frac{(2S)^2}{(2S)^2 + 1} \right) \right],$$

with  $S = \frac{\sigma_{\perp}^2 \omega}{L_u}$  and  $\sigma_{\perp}$  the RMS transverse electron beam size,  $b_{z,H}$  is the bunching factor at the  $H$ -th harmonic determined by the longitudinal current distribution, and  $I_P$  is the peak current.

The above formula is derived by assuming that the longitudinal and transverse distribution of the electron beam do

not change much in the radiator. Actually the energy spread of electron beam can lead to current distribution change inside the undulator, considering that the undulator has an  $R_{56} = 2N_u \lambda_0$ , where  $\lambda_0$  is the fundamental on-axis resonant wavelength of the undulator. If we consider the impact of the energy spread on coherent radiation, and assuming that the microbunching length reach its minimum at the radiator center, there will be a correction or reduction factor multiplied to the radiation power given by Eq. (314)

$$\mathcal{C} = \frac{\sqrt{\pi}}{2} \frac{\text{erf}(\frac{\omega}{c} \sigma_{\delta} N_u \lambda_0)}{\frac{\omega}{c} \sigma_{\delta} N_u \lambda_0}.$$

The above scaling laws are accurate when  $K > \sqrt{2}$ , and it should be noted that the calculated power refers to the peak power of the laser. For completeness, here we give also the modulator length scaling

Therefore, to lower the required modulation laser power, we can apply a large  $R_w$ , which means strong damping wigglers. A low beam energy and short laser wavelength are also preferred. But their choices should take more factors into account, for example IBS and engineering experience of optical enhancement cavity as explained in Sec. IV. A strong bending magnet field in the ring is also desired. Concerning the modulator field strength, a weaker one is favored to lower the required laser power. But note that the required modulator length may be longer, if we keep the quantum excitation contribution of modulators to vertical emittance  $\Delta\epsilon_{yM}$  unchanged in this process.

## IX. SUMMARY

This paper is about our efforts in obtaining a solution for 1 kW EUV light source based on SSMB. Here we give a short summary of this endeavor. We start by presenting the generalized Courant-Snyder formalism to build the theoretical framework for the following investigations. Based on the formalism we conducted theoretical minimum emittance analysis in an electron storage ring, from which we know that to get small longitudinal emittance, we need to decrease the bending angle of each bending magnet which means increasing the number of bending magnets in the ring. In principle we can get as small longitudinal emittance and as short bunch length as we want along this line. But there is actually practical limitation. To get short bunch length, we need not only to increase the bending magnet number, but also to lower the phase slippage factor of the ring. Using present realizable phase slippage, which at minimum is in the order of  $1 \times 10^{-6}$ , a bunch length of a couple of 10 nm is

the lower limit if we apply the longitudinal weak focusing regime. To compress the bunch length further, longitudinal strong focusing regime can be invoked, not unlike its transverse counterpart in the final focus of a collider, to compress the longitudinal beta function thus the bunch length at the radiator significantly. This scheme can realize a bunch length of nm level, thus allowing coherent EUV radiation generation.

However, since the compression of longitudinal beta function requires a strong energy chirp of the electron beam, which is similar to a strong quadrupole focusing strength in the transverse dimension, the modulation laser power required is at GW level, making the optical enhancement cavity of SSMB can only work in a low duty cycle pulsed mode, and thus limits the filling factor of the microbunched beam in the ring,

and thus the average output EUV power. This then leads us to the generalized longitudinal strong focusing (GLSF) regime, which is the focus of this paper. The basic idea of GSF is to exploit the ultrasmall natural vertical emittance in a planar section to the vertical emittance, the application of damping electron storage ring and apply partial transverse-longitudinal wiggler to speed up damping and its impact on the transverse emittance exchange to compress the bunch length or generate high-harmonic bunching with a shallow energy modulation strength, thus lowering the requirement on the modulation laser power. The backbone of such a scheme is the transverse-longitudinal phase space coupling. To find a solution based on the GSF scheme, we first conduct some formal mathematical analysis of transverse-longitudinal coupling (TLC)-based bunch compression and harmonic generation schemes, and prove three related theorems which are useful in the later choice of parameters and evaluation of laser power. We then go into the details of different specific coupling schemes, grouping them into two categories, i.e., energy modulation-based coupling schemes and angular modulation-based coupling schemes. We derive the formulas of bunching factor and laser-induced modulation strength in each case, and use them

for quantitative calculations and comparisons. Our conclusion from these analyses is that the commonly used TEM<sub>00</sub> mode laser-induced energy modulation-based schemes are favored for our application in SSMB, as its requirement on the modulation laser power is lower than that in the angular coupling schemes. We thank Chao Feng, Ji Li and Yujie Lu for helpful discussions on storage ring-based coherent light source, tilted laser modulation schemes, and the issue of quantum excitation contribution of damping wiggler to the horizontal beam emittance. Many helpful discussions with our colleagues in Tsinghua and other institutes are also much appreciated.

## ACKNOWLEDGMENTS

---

[1] D. F. Ratner, A. W. Chao. Steady-state microbunching in a storage ring for generating coherent radiation. *Phys. Rev. Lett.* **105**, 154801 (2010). [doi: 10.1103/PhysRevLett.105.154801](https://doi.org/10.1103/PhysRevLett.105.154801)

[2] Y. Jiao, D. F. Ratner, A. W. Chao, Terahertz coherent radiation from steady-state microbunching in storage rings with X-band radio-frequency system. *Phys. Rev. ST Accel. Beams* **14**, 110702 (2011). [doi: 10.1103/PhysRevSTAB.14.110702](https://doi.org/10.1103/PhysRevSTAB.14.110702)

[3] A. Chao, E. Granados, X. Huang, et al. High Power Radiation Sources using the Steady-state Microbunching Mechanism. The 7th International Particle Accelerator Conference, Busan. 2016. p. 1048.

[4] C. Tang, X. Deng, A. Chao, et al. An overview of the progress on SSMB. The 60th ICFA advanced beam dynamics workshop on future light sources, Shanghai. 2018. p. 166 [doi: 10.18429/JACoW-FLS2018-THP2WB02](https://doi.org/10.18429/JACoW-FLS2018-THP2WB02)

[5] X. J. Deng, A. W. Chao, W. H. Huang, et al., Single-particle dynamics of microbunching. *Phys. Rev. Accel. Beams* **23**, 044002 (2020). [doi: 10.1103/PhysRevAccelBeams.23.044002](https://doi.org/10.1103/PhysRevAccelBeams.23.044002)

[6] X. J. Deng, R. Klein, A. W. Chao, et al., Widening and distortion of the particle energy distribution by chromaticity in quasi-isochronous rings. *Phys. Rev. Accel. Beams* **23**, 044001 (2020). [doi: 10.1103/PhysRevAccelBeams.23.044001](https://doi.org/10.1103/PhysRevAccelBeams.23.044001)

[7] Y. Zhang, X. J. Deng, Z. L. Pan, et al., Ultralow longitudinal emittance storage rings. *Phys. Rev. Accel. Beams* **24**, 090701 (2021). [doi: 10.1103/PhysRevAccelBeams.24.090701](https://doi.org/10.1103/PhysRevAccelBeams.24.090701)

[8] X. J. Deng, A. W. Chao, W. H. Huang, et al., Courant-Snyder formalism of longitudinal dynamics. *Phys. Rev. Accel. Beams* **24**, 094001 (2021). [doi: 10.1103/PhysRevAccelBeams.24.094001](https://doi.org/10.1103/PhysRevAccelBeams.24.094001)

[9] Z. Li, X. Deng, Z. Pan, et al., Generalized longitudinal strong focusing in a steady-state microbunching storage ring. *Phys. Rev. Accel. Beams* **26**, 110701 (2023). [doi: 10.1103/PhysRevAccelBeams.26.110701](https://doi.org/10.1103/PhysRevAccelBeams.26.110701)

[10] C.-Y. Tsai, A. W. Chao, Y. Jiao, et al., Coherent-radiation-induced longitudinal single-pass beam breakup instability of a steady-state microbunch train in an undulator. *Phys. Rev. Accel. Beams* **24**, 114401 (2021). [doi: 10.1103/PhysRevAccelBeams.24.114401](https://doi.org/10.1103/PhysRevAccelBeams.24.114401)

[11] C.-Y. Tsai, Theoretical formulation of multiturn collective dynamics in a laser cavity modulator with comparison to Robinson and high-gain free-electron laser instability. *Phys. Rev. Accel. Beams* **25**, 064401 (2022). [doi: 10.1103/PhysRevAccelBeams.25.064401](https://doi.org/10.1103/PhysRevAccelBeams.25.064401)

[12] C.-Y. Tsai, Longitudinal single-bunch instabilities driven by coherent undulator radiation in the cavity modulator of a steady-state microbunching storage ring. *Nucl. Instrum. Methods Phys. Res. A* **1042**, 167454 (2022). [doi: 10.1016/j.nima.2022.167454](https://doi.org/10.1016/j.nima.2022.167454)

[13] Z. Zhao, N. Wang, H. Xu, et al., Calculations of space-charge tune shifts in storage rings with extremely short bunches and small bunch spacing. *Phys. Rev. Accel. Beams* **27**, 094201 (2024). [doi: 10.1103/PhysRevAccelBeams.27.094201](https://doi.org/10.1103/PhysRevAccelBeams.27.094201)

[14] X. Deng, A. Chao, J. Feikes, et al., Experimental demonstration of the mechanism of steady-state microbunching. *Nature* **590**, 576 (2021). [doi: 10.1038/s41586-021-03203-0](https://doi.org/10.1038/s41586-021-03203-0)

[15] A. Kruschniski, X. Deng, J. Feikes, et al., Confirming the theoretical foundation of steady-state microbunching. *Commun. Phys.* **7**, 160 (2024). [doi: 10.1038/s42005-024-01657-y](https://doi.org/10.1038/s42005-024-01657-y)

[16] Z. Pan, Research on optimization and design of advanced laser-driving storage ring. PhD thesis, Tsinghua University, Beijing, 2020.

2710 [17] X. Deng, *Theoretical and experimental studies on steady-state 2775  
2711 microbunching*. (Springer Nature, 2024). doi: [10.1007/978-2776  
2713](https://doi.org/10.1007/978-2776<br/>2712 981-99-5800-9)

2714 [18] Y. Zhang, Research on longitudinal strong focusing SSMB 2778  
2715 ring. PhD Thesis, Tsinghua University, Beijing, 2022. 2779

2716 [19] C. X. Tang, X. J. Deng, Steady-state micro-bunching ac- 2780  
2717 celerator light source. *Acta Phys. Sin.* **71**, 152901 (2022). 2781  
2718 doi: [10.7498/aps.71.20220486](https://doi.org/10.7498/aps.71.20220486) 2782

2719 [20] R. Bonifacio, C. Pellegrini, L. M. Narducci, Collective in- 2783  
2720 stabilities and high-gain regime in a free electron laser. *Op- 2784  
2721 tics Communications* **50**, 373 (1984). doi: [10.1016/0030-4018\(84\)90105-6](https://doi.org/10.1016/0030-4018(84)90105-6) 2785

2722 [21] A. W. Chao, Evaluation of beam distribution parameters in 2787  
2723 an electron storage ring. *J. Appl. Phys.* **50**, 595 (1979). 2788  
2724 doi: [10.1063/1.326070](https://doi.org/10.1063/1.326070) 2789

2725 [22] M. C. Wang, G. E. Uhlenbeck, On the theory of the 2790  
2726 Brownian motion II. *Rev. Mod. Phys.* **17**, 323 (1945). 2791  
2727 doi: [10.1103/RevModPhys.17.32](https://doi.org/10.1103/RevModPhys.17.32) 2792

2728 [23] N. Campbell, The study of discontinuous phenomena. *Proc. 2793  
2729 Cambridge Philos. Soc.* **15**, 117 (1909). 2794

2730 [24] M. Sands, Synchrotron Oscillations Induced by Radiation 2795  
2731 Fluctuations. *Phys. Rev.* **97**, 470 (1955). doi: [10.1103/PhysRev.97.470](https://doi.org/10.1103/PhysRev.97.470) 2796

2733 [25] K. W. Robinson, Radiation Effects in Circular Electron Ac- 2798  
2734 celerators. *Phys. Rev.* **111**, 373 (1958). doi: [10.1103/PhysRev.111.373](https://doi.org/10.1103/PhysRev.111.373) 2799

2736 [26] E. D. Courant, H. S. Snyder, Theory of the alternating- 2801  
2737 gradient synchrotron. *Ann. Phys. (N.Y.)* **3**, 1 (1958). 2802  
2738 doi: [10.1006/aphy.2000.6012](https://doi.org/10.1006/aphy.2000.6012) 2803

2739 [27] M. Sands, The Physics of Electron Storage Rings: An Intro- 2804  
2740 duction. SLAC report SLAC-121, 1970. 2805

2741 [28] X. Deng, Optical Stochastic Cooling in a General Coupled 2806  
2742 Lattice. in Proceedings of the 67th ICFA Adv. Beam Dyn. 2807  
2743 Workshop Future Light Sources, Luzern, Switzerland (JA- 2808  
2744 CoW, Geneva, 2023), p. 143. doi: [10.18429/JACoW-FLS2023-TU4P30](https://doi.org/10.18429/JACoW-FLS2023-TU4P30) 2809

2746 [29] L. C. Teng, Minimum emittance lattice for synchrotron radi- 2811  
2747 ation storage rings. *Argonne National Laboratory Technical 2812  
2748 Note. No. ANL-LS-17*. 1985. 2813

2749 [30] X. J. Deng, A. W. Chao, J. Feikes, et al., Breakdown of 2814  
2750 classical bunch length and energy spread formula in a quasi- 2815  
2751 isochronous electron storage ring. *Phys. Rev. Accel. Beams* **26**, 2816  
2752 054001 (2023). doi: [10.1103/PhysRevAccelBeams.26.054001](https://doi.org/10.1103/PhysRevAccelBeams.26.054001) 2817

2753 [31] X.-Y. Lu, R. Chiche, K. Dupraz, et al., 710 kW stable average 2818  
2754 power in a 45,000 finesse two-mirror optical cavity. *Opt. Lett.* 2819  
2755 **49**, 6884 (2024). doi: [10.1364/OL.543388](https://doi.org/10.1364/OL.543388) 2820

2756 [32] D. Ratner, A. Chao, Reversible seeding in storage rings. 2821  
2757 Proc. of the 33th International Free-electron Laser Conference. 2822  
2758 Shanghai, 2011. p. 57. 2823

2759 [33] X. J. Deng, W. H. Huang, Z. Z. Li, et al., Harmonic genera- 2824  
2760 tion and bunch compression based on transverse-longitudinal 2825  
2761 coupling. *Nucl. Instrum. Methods Phys. Res. A* **1019**, 165859 2826  
2762 (2021). doi: [10.1016/j.nima.2021.165859](https://doi.org/10.1016/j.nima.2021.165859) 2827

2763 [34] Dragt, Alex J. *Lie methods for nonlinear dynamics with appli- 2828  
2764 cations to accelerator physics* University of Maryland (2020). 2829

2765 [35] L. H. Yu, Generation of intense uv radiation by subharmon- 2830  
2766 ically seeded single-pass free-electron lasers. *Phys. Rev. A* 2831  
2767 **44**, 5178 (1991). doi: [10.1103/PhysRevA.44.5178](https://doi.org/10.1103/PhysRevA.44.5178) 2832

2768 [36] A. W. Chao, Focused laser. Unpublished Note. 2023. 2833

2769 [37] H. Deng, C. Feng, Using off-resonance laser modula- 2834  
2770 tion for beam-energy-spread cooling in generation of short- 2835  
2771 wavelength radiation. *Phys. Rev. Lett.* **111**, 084801 (2013). 2836  
2772 doi: [10.1103/PhysRevLett.111.084801](https://doi.org/10.1103/PhysRevLett.111.084801) 2837

2773 [38] C. Feng, H. Deng, D. Wang, et al., Phase-merging enhanced 2838  
2774 harmonic generation free-electron laser. *New J. Phys.* **16**, 043021 (2014). doi: [10.1088/1367-2630/16/4/043021](https://doi.org/10.1088/1367-2630/16/4/043021) 2839

[39] C. Feng, Z. Zhao, A storage ring based free-electron laser for 2775  
2776 generating ultrashort coherent EUV and X-ray radiation. *Sci. 2777  
2778 Rep* **7**, 4724 (2017). doi: [10.1038/s41598-017-04962-5](https://doi.org/10.1038/s41598-017-04962-5)

[40] B. Jiang, C. Feng, C. Li, et al., A synchrotron-based kilowatt- 2779  
2780 level radiation source for EUV lithography. *Sci. Rep.* **12**, 3325 2781  
2782 (2022). doi: [10.1038/s41598-022-07323-z](https://doi.org/10.1038/s41598-022-07323-z)

[41] C.-Y. Tsai, Analytical study of higher harmonic bunching and 2783  
2784 matrix formalism in linear high-gain free-electron laser model. 2785  
2786 *Nucl. Instrum. Methods Phys. Res. A* **1048**, 167974 (2023). 2787  
2788 doi: [10.1016/j.nima.2022.167974](https://doi.org/10.1016/j.nima.2022.167974)

[42] A. W. Chao, *Physics of collective beam instabilities in high 2789  
2790 energy accelerators*. (Wiley, 1993).

[43] D. Xiang, W. Wan, Generating ultrashort coherent soft 2791  
2792 X-ray radiation in storage rings using angular-modulated 2793  
2794 electron beams. *Phys. Rev. Lett.* **104**, 084803 (2010). 2795  
2796 doi: [10.1103/PhysRevLett.104.084803](https://doi.org/10.1103/PhysRevLett.104.084803)

[44] X. Wang, C. Feng, C. Yang, et al., Transverse-to-longitudinal 2797  
2798 emittance-exchange in optical wavelength. *New J. Phys.* **22**, 2799  
2800 063034 (2020). doi: [10.1088/1367-2630/ab8e5d](https://doi.org/10.1088/1367-2630/ab8e5d)

[45] Y. Lu, X. Wang, X. Deng, et al., Methods for enhancing the 2801  
2802 steady-state microbunching in storage rings. *Results Phys* **40**, 2803  
2804 105849 (2022). doi: [10.1016/j.rinp.2022.105849](https://doi.org/10.1016/j.rinp.2022.105849)

[46] B. Jiang, J. G. Power, R. Lindberg, et al., Emittance-exchange- 2805  
2806 based high harmonic generation scheme for a short-wavelength 2807  
2808 free electron laser. *Phys. Rev. Lett.* **106**, 114801 (2011). 2809  
2810 doi: [10.1103/PhysRevLett.106.114801](https://doi.org/10.1103/PhysRevLett.106.114801)

[47] K. Feng, C. Yu, J. Liu, et al., Coherent X-ray source generation 2811  
2812 with off-resonance laser modulation. *Opt. Express* **26**, 19067 2813  
2814 (2018). doi: [10.1364/OE.26.019067](https://doi.org/10.1364/OE.26.019067)

[48] X. Wang, C. Feng, C.-Y. Tsai, et al., Obliquely incident laser 2815  
2816 and electron beam interaction in an undulator. *Phys. Rev. Accel. 2817  
2818 Beams* **22**, 070701 (2019). doi: [10.1103/PhysRevAccelBeams.22.070701](https://doi.org/10.1103/PhysRevAccelBeams.22.070701)

[49] W. Liu, C. Feng, Y. Jiao, et al., A coherent harmonic generation 2819  
2820 method for producing femtosecond coherent radiation in a laser 2821  
2822 plasma accelerator based light source. *J. Synchrotron Rad.* **28**, 2823  
2824 669 (2021). doi: [10.1107/S1600577521002745](https://doi.org/10.1107/S1600577521002745)

[50] X. Deng, J. Li, Y. Lu, Contribution of Wiggler to Radiation 2825  
2826 Integral in an Electron Storage Ring. arXiv 2410.12863 (2024). 2827  
2828 doi: [10.48550/arXiv.2410.12863](https://doi.org/10.48550/arXiv.2410.12863)

[51] J. Zhao, Undulator in SLIM. Unpublished Note. Oct. 2023.

[52] K. Bane, A simplified model of intrabeam scattering, in Proceedings of the 8th European Particle Accelerator Conference, Paris, France, 2002 (EPS-IGA and CERN, Geneva, 2002), p. 1443.

[53] K. F. Bane, Y. Cai, G. Stupakov, Threshold studies of the 2829  
2830 microwave instability in electron storage rings. *Phys. Rev. ST Accel. Beams* **13**, 104402 (2010). doi: [10.1103/PhysRevSTAB.13.104402](https://doi.org/10.1103/PhysRevSTAB.13.104402)

[54] J. Feikes, M. von Hartrott, M. Ries, et al., Metrology Light 2831  
2832 Source: The first electron storage ring optimized for generating 2833  
2834 coherent THz radiation. *Phys. Rev. ST Accel. Beams* **14**, 030705 (2011). doi: [10.1103/PhysRevSTAB.14.030705](https://doi.org/10.1103/PhysRevSTAB.14.030705)

[55] X. J. Deng, Y. Zhang, Z. L. Pan, et al., Average and 2835  
2836 statistical properties of coherent radiation from steady-state 2837  
2838 microbunching. *J. Synchrotron Radiat.* **30**, 35 (2023). 2839  
2840 doi: [10.1107/S1600577522009973](https://doi.org/10.1107/S1600577522009973)

[56] N. Nakamura, R. Kato, H. Sakai et al., High-power EUV free- 2841  
2842 electron laser for future lithography. *Jpn. J. Appl. Phys.* **62**, 2843  
2844 SG0809 (2023). doi: [10.35848/1347-4065/acc18c](https://doi.org/10.35848/1347-4065/acc18c)